Performance Characterization of a Dye-Sensitized Photovoltaic Module under Tropical Weather Conditions: The Case of Nairobi, Kenya

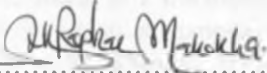Raphael Venson Makokha Otakwa, B.Sc. (Hons., Nairobi)
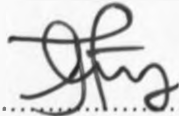
Department of Physics, University of Nairobi.

August, 2012.

Declaration

This thesis is my own work. It has not been examined or submitted for examination in any other University:

Signed:..

Raphael Venson Makokha Otakwa: Reg. No. 156/62923/2010

Dated:.........15TH AUGUST, 2012...................................

This thesis has been submitted for examination with our approval as supervisors:

Signed: Supervisor..

Dr. Justus Simiyu

Department of Physics, University of Nairobi, Kenya

Dated................15/8/2012...........................

Signed: Supervisor..

Dr. Sebastian M. Waita

Department of Physics, University of Nairobi, Kenya

Dated......................15/8/2012.........................

Signed: Supervisor..

Prof. Dr. Julius M. Mwabora

Department of Physics, University of Nairobi, Kenya

Dated.........15.8.2012...........................

- ii -

Dedication

'I remember one morning when I discovered a cocoon in
the bark of a tree, just as the butterfly was making a hole in
its case and preparing to come out. I waited a while, but it
was too long appearing and I was impatient. I bent over it
and breathed on it to warm it. I warmed it as quickly as I
could and the miracle began to happen before my eyes,
faster than life. The case opened, the butterfly started
slowly crawling out and I shall never forget my horror
when I saw how its wings were folded back and crumpled;
the wretched butterfly tried with its whole trembling body
to unfold them. Bending over it, I tried to help it with my
breath. In vain. It needed to be hatched out patiently and
the unfolding of the wings should be a gradual process in
the sun. Now it was too late. My breath had forced the
butterfly to appear, all crumpled, before its time. It
struggled desperately and, a few seconds later, died in the
palm of my hand.'

Nikos Kazantzakis

Just as *Nikos Kazantzakis* and his butterfly, I desired to finish this M.Sc. work faster, but

encounters proliferated and slowed me along the way. During such times, I found forte in

the inspiration from my cherished family! To this end, I am delighted to dedicate this work

to Joan Emonyangwa, Olive Nyangasi, Peris Baraka, Fredrick Ndikolo, Josephine Ikhuyo

and Lynn Muhonja for their resilience, patience and invaluable support.

Acknowledgements

Abstract

The performance of a Dye-Sensitized Solar Module (DSSM) of active area 175.12 cm^2 has been investigated at a tropical climate area at co-ordinates 35.81° East, 1.28° South. Investigation of the DSSM's performance parameters; short circuit current density (J_{sc}), open circuit voltage (V_{oc}), fill factor (FF) and solar-to-electricity conversion efficiency (η) has been carried out under different values of air mass (AM), irradiance intensities, and the DSSM's surface temperature. As AM increased from 1 to 1.09, V_{oc} reduced linearly by 2.05% from 8.31 V to 8.14 V. J_{sc} also reduced linearly but by 26.06%, from 1.04x10^{-3} Acm^{-2} to 7.69x10^{-4} Acm^{-2}. FF increased linearly by 19.05% from 0.51 to 0.63, while η increased by 27.68% from 1.77% to 2.26% as AM increased from 1 to 1.04, and then reduced to 1.27% at AM1.05, followed by an increase of 1.06% at AM 1.08 before increasing to 1.19% at AM 1.09. The good response of the DSSM to short wavelength radiation made it perform well at increased AM values as compared to what is reported of Amorphous Silicon (a-Si) photovoltaic (PV) devices.

As irradiance intensity increased from 653 Wm^{-2} to 805 Wm^{-2}, V_{oc} increased linearly by 11.94% from 7.12 V to 8.07 V. J_{sc} also increased linearly, but by 64.41% from 5.92x10^{-4} Acm^{-2} to 9.66x10^{-4} Acm^{-2} as irradiance intensity increased from 653 Wm^{-2} to 997 Wm^{-2}. FF decreased linearly by 20.55% from 0.73 to 0.58 as irradiance intensity increased from 653 Wm^{-2} to 1095.7 Wm^{-2}, while η increased linearly by 5.74% from 4.70% to 4.90% as irradiance intensity increased from 653 Wm^{-2} to 747 Wm^{-2}. The DSSM performed better compared to what is reported of a-Si PV devices under irradiance-dependence. From temperature-dependence studies, V_{oc} decreased linearly by 41.22% from 9.80 V to 5.76 V as the DSSM's surface temperature increased from 31.6°C to 43.8°C. J_{sc} also decreased linearly but by 3.26% from 7.98x10^{-4} Acm^{-2} to 7.92x10^{-4} Acm^{-2} while FF and η linearly increased and decreased by 14.04% from 0.57 to 0.65 and by 33.50 % from 5.95 % to 3.95 % respectively as the DSSM's surface temperature increased from 31.6°C to 43.8°C. Better performance for the DSSM was observed compared to what is reported of a-Si PV devices.

The DSSM's overall performance was found to be better than what is reported of a-Si PV devices under the limiting conditions of AM, irradiance intensity and device surface temperature. The results are useful in respect of PV sizing, especially in the area of Building Integrated Photovoltaics (BIPV) in Kenya and the tropics.

Abstract

The performance of a Dye-Sensitized Solar Module (DSSM) of active area 175.12 cm^2 has been investigated at a tropical climate area at co-ordinates 35.81° East, 1.28° South. Investigation of the DSSM's performance parameters; short circuit current density (J_{sc}), open circuit voltage (V_{oc}), fill factor (*FF*) and solar-to-electricity conversion efficiency (η) has been carried out under different values of air mass (*AM*), irradiance intensities, and the DSSM's surface temperature. As *AM* increased from 1 to 1.09, V_{oc} reduced linearly by 2.05% from 8.31 V to 8.14 V. J_{sc} also reduced linearly but by 26.06%, from 1.04×10^{-3} Acm^{-2} to 7.69×10^{-4} Acm^{-2}. *FF* increased linearly by 19.05% from 0.51 to 0.63, while η increased by 27.68% from 1.77% to 2.26% as *AM* increased from 1 to 1.04, and then reduced to 1.27% at *AM*1.05, followed by an increase of 1.06% at *AM* 1.08 before increasing to 1.19% at *AM* 1.09. The good response of the DSSM to short wavelength radiation made it perform well at increased *AM* values as compared to what is reported of Amorphous Silicon (a-Si) photovoltaic (PV) devices.

As irradiance intensity increased from 653 Wm^{-2} to 805 Wm^{-2}, V_{oc} increased linearly by 11.94% from 7.12 V to 8.07 V. J_{sc} also increased linearly, but by 64.41% from 5.92×10^{-4} Acm^{-2} to 9.66×10^{-4} Acm^{-2} as irradiance intensity increased from 653 Wm^{-2} to 997 Wm^{-2}. *FF* decreased linearly by 20.55% from 0.73 to 0.58 as irradiance intensity increased from 653 Wm^{-2} to 1095.7 Wm^{-2}, while η increased linearly by 5.74% from 4.70% to 4.90% as irradiance intensity increased from 653 Wm^{-2} to 747 Wm^{-2}. The DSSM performed better compared to what is reported of a-Si PV devices under irradiance-dependence. From temperature-dependence studies, V_{oc} decreased linearly by 41.22% from 9.80 V to 5.76 V as the DSSM's surface temperature increased from 31.6°C to 43.8°C. J_{sc} also decreased linearly but by 3.26% from 7.98×10^{-4} Acm^{-2} to 7.92×10^{-4} Acm^{-2} while *FF* and η linearly increased and decreased by 14.04% from 0.57 to 0.65 and by 33.50 % from 5.95 % to 3.95 % respectively as the DSSM's surface temperature increased from 31.6°C to 43.8°C. Better performance for the DSSM was observed compared to what is reported of a-Si PV devices.

The DSSM's overall performance was found to be better than what is reported of a-Si PV devices under the limiting conditions of *AM*, irradiance intensity and device surface temperature. The results are useful in respect of PV sizing, especially in the area of Building Integrated Photovoltaics (BIPV) in Kenya and the tropics.

Table of Contents

List of Symbols

A	Cross-sectional area
CB_{TiO2}	The conduction band of TiO_2
dx	Distance across the p-n junction
dV_o	Change in potential difference across the p-n junction
e^-	The electron
e_{CB}^-	The electron injected into the conduction band
E	Band gap energy
E_c	Conduction band energy
E_F	Fermi energy
E_g	Band gap energy
E_{HOMO}	Energy of the Highest Occupied Molecular Orbital
E_{LUMO}	Energy of the Least Unoccupied Molecular Orbital
E_o	The internal electric field across the p-n junction plane
E_v	Valence band energy
f_{FD}	Fermi distribution function
h	Height of the vertical post
$h\nu$	Photon energy
I	Current
I_D	Current passing through the diode
I_s	Saturation current
I_{sc}	Short circuit current
J_L	Current density from the source
J	The ideal current density
J_D	Current density flowing through the diode
J_{dark}	Dark current density
J_s	Saturation current density
J_{sc}	Short circuit current density
J_{sh}	Current density flowing through the shunt resistor
J_{ph}	Photo-generated current density
J_{mp}	Maximum power current density
$J(V)$	Voltage-dependent total current

J-V	Current density-voltage
k	Boltzmann constant
m	Metres
m	Ideality factor
N_A	Acceptor carrier concentration
N_D	Donor carrier concentration
n_t	Intrinsic carrier concentration of electrons
$n_p(o)$	Equilibrium electron densities on the p-region
$p_n(o)$	Equilibrium hole densities on the n-region
p	Holes in the valence band
P_{in}	Power of the incident radiation
P_m	Maximum power
P_{mp}	Maximum power point
P_T	Theoretical power
P-V	Power-Voltage
q	Elementary charge (hole or electron)
R_s	Series resistance
R_{sh}	Shunt resistance
s	Shadow length of the vertical post
S	Ground state of the dye
S_{HOMO}	Ground state of the dye molecule's highest occupied molecular orbital
S^+	Oxidized state of the dye
$S^{\bullet}$	Excited state of the dye
$S^{\bullet}_{LUMO}$	Excited state of the Least Unoccupied Molecular Orbital of the dye molecule
T	Absolute temperature
V	Voltage
V_F	Forward bias voltage
V_{mp}	Maximum power voltage
V_o	Contact or built-in potential difference/voltage
V_{oc}	Open circuit voltage
V_R	Reverse bias voltage
V_T	Thermal voltage

ΔE	Difference in energy
Δh	Change in enthalpy
$\Delta \mu$	Change in chemical potential
ΔV_o	Change in the potential difference across the p-n junction
W	Watts
β	The inverse of the product of Boltzmann constant and the absolute temperature
μ	Chemical potential
μ_c	Chemical potential of the conduction band
μ_{HOMO}	Chemical potential of the Highest Occupied Molecular Orbital
μ_{LUMO}	Chemical potential of the Least Unoccupied Molecular Orbital
μm	Micrometre
μ_v	Chemical potential of the valence band
°C	Degrees centigrade
η	Solar to electricity conversion efficiency
θ	Angle from the vertical/zenith
Ω	Ohm
σ	Shunt conductance
%	Percentage

List of Abbreviations

ACTS	African Centre for Technology Studies
AEI	American Enterprise Institute
AIST	Advanced Industrial Science and Technology
ALCVD	Atomic Layer Chemical Vapour Deposition
AM	Air Mass
APC	African PRIDE Centre
ASCII	American Standard Code for Information Interchange
ASHRAE	American Society of Heating, Refrigeration and Air conditioning Engineers
a-Si	Amorphous Silicon
ASME	American Society of Mechanical Engineers
BIPV	Building Integrated Photovoltaics
B.Sc.	Bachelor of Science
CB	Conduction Band
CE	Counter Electrode
CIGS	Copper Indium Gallium Diselenide
CIS	Copper Indium Diselenide
cm	Centimetres
CRI	Copenhagen Resource Institute
c-Si	Crystalline Silicon
DC	Direct Current
Dr.	Doctor
DSC	Dye Sensitized Cell
DSSCs	Dye-Sensitized Solar Cells
DSSM	Dye-Sensitized Solar Module
et al.	And Others
EOLSS	Encyclopaedia of Life Support Systems
eV	Electron Volt
FF	Fill Factor
GEF	Global Environmental Facility
G24i	G24 Innovations Limited

GPIB	General Purpose Interface Bus
GSFC	Goddard Space Flight Center
GTZ	Geutshe Gesellschaft für Technische Zusammenarbeit
HOMO	Highest Occupied Molecular Orbital
Hons.	Honours
HP	Hewlett Packard
Hrs.	Hours
IEEE	Institute of Electrical and Electronics Engineers
Inc.	Incorporated
ICTP	International Centre for Theoretical Physics
ICRSD	International Conference on Remote Sensing Data
IEA	International Energy Agency
IPCC	Intergovernmental Panel on Climate Change
IR	Infra-Red
ISES	International Solar Energy Society
ITO	Indium Tin Oxide
ISO	International Standards Organization
KenGen	Kenya Electricity Generating Company
KDM	Kenya Meteorological Department
kWh	Kilowatt Hour
KIPPRA	Kenya Institute of Public Policy Research
LabVIEW^{TM}	Laboratory Virtual Instruments Electronics Workbench Trade Mark
LLC	Limited Liability Company
LUMO	Least Unoccupied Molecular Orbital
$mAcm^{-2}$	Milliamperes per Square Centimetre
M-B	Maxwell Boltzman
M.Sc.	Master of Science
MOE	Ministry of Energy
MOCVD	Metalorganic Chemical Vapour Deposition
MRSEC	Materials Research Science and Engineering Centres
mV	Millivolts
NASA	National Space Aeronautics and Space Administration
NHE	Normal Hydrogen Electrode

NSF	National Science Foundation
NI	National Instruments
No.	Number
NREL	National Resource Ecology Laboratory
n-type	Negative Type
NZE	Net Zero Energy
oc	Open Circuit
Ph.D.	Doctor of Philosophy
p-n	Positive-Negative
PRIDE	Perennial Revival of Innovative Developments in Education
Prof.	Professor
p-type	Positive Type
PV	Photovoltaic
REQE	Radiative External Quantum Efficiency
RCPV	Research Centre for Photovoltaics
Red/Ox	Reduced State/Oxidised State
Reg.	Registration
RI	Resnick Institute
sc	Short Circuit
SHSs	Solar Home Systems
SPEEC	Social, Political, Economic, Environmental and Cultural
SWE	Staebler Wronski Effect
TBC	Text Book Centre
TCO	Transparent Conducting Oxide
TM	Trade Mark
UK	United Kingdom
USA	United States of America
UV	Ultra-Violet
VIS	Visible
WE	Working Electrode
Wm^{-2}	Watts per square metre

List of Chemical Formulae

Al	Alluminium
As	Arsenide
B	Boron
$CdSe$	Cadmium Selenide
$CdTe$	Cadmium Telluride
$Co^{(II/III)}$	Cobalt (II/III)
$Cu(In,Ga)Se_2$	Copper Indium or Gallium Di-Selenide
CO_2	Carbon dioxide
$F:SnO_2$	Fluorine-doped Tin Oxide
$GaInAsP$	Gallium Indium Arsenide Phosphide
$GaAlAs$	Gallium Aluminium Arsenide
$GaAs$	Gallium Arsenide
H_2O	Water
I^-	Iodide
I_3^-	Triiodide
In	Indium
$InAs$	Indium Arsenide
$InSb$	Indium Antimonide
InP	Indium Phosphide
Nb	Niobium
Ni	Nickel
$NiCr$	Nickel Chromium
N_2	Nitrogen
O_2	Oxygen
O_3	Ozone
P	Phosphorus
Pt	Platinum
Si	Silicon
SnO_2	Tin Oxide
TiO_2	Titanium Dioxide
ZnO	Zinc Oxide

List of Figures

List of Tables

CHAPTER ONE
INTRODUCTION

1.1 Renewable Energy

The need to switch to the use of renewable energy is ever increasing world over. Fossil fuel reserves that have been depended upon to provide the world's energy needs are rapidly diminishing [Leng, 2005; Aleklett, 2007; Murray and King, 2012]. This decline has led to volatility in energy prices [Timmer, 2012], fanned by the high costs of fossil fuel exploration and mining [Leng, 2005]. The sensitive geopolitical issues experienced by countries with fossil fuel reserves [Hahn, *et al.*, 2007], e.g., national security and conflicts, have further compounded the grim situation. The ensuing escalations in energy costs have denied many people access to energy, with those at the bottom of the economic pyramid being the most affected [Barnes and Toman, 2006].

The over-reliance upon fossil fuels by the world [Heymann, 2011] is associated with environmental effects such as upturns in acid rains, greenhouse gases and the depletion of the ozone layer [Dincar, 2003]. Upsurge in greenhouse gases is in turn linked to environmental impacts, like global warming [Intergovernmental Panel on Climate Change (IPCC), 2007; International Energy Agency (IEA), 2007]. These impacts have adversely affected life on earth [Muoghalu, 2003], with frequent occurrences of floods and droughts that destroy ecosystems and life on earth. Adoption of energy sources that are alternative to fossil fuels is therefore imperative. Renewable energy sources offer the most sustainable way forward [Bárd, 2012].

Renewable energy sources include biomass, geothermal, tidal or wave power, water cycle or hydro, wind as well as solar radiation. They are a result of the earth's inherent heat, gravitational perturbations by the moon and sun, and solar radiation [Kuhbrodt, *et*

al., 2006]. The most abundant and fairly distributed of these is solar radiation. About 3.9×10^{24} joules of solar energy reach the earth annually [Quaschning, 2005]. Apart from being abundant in supply, solar energy can, through the solar thermal conversion pathway, be used to produce heat for direct use or for further conversion to electricity [Lewis and Crabtree, 2007]. It can also yield chemical fuel through natural photosynthesis in green plants or through artificial photosynthesis in human-engineered systems. Solar energy can also be converted directly to electricity through the solar photovoltaic (PV) conversion pathway by exciting electrons in a solar cell. The PV conversion pathway is the most espoused [Rabah, *et al.*, 1999].

Though prices of PV systems are currently still high [Bakas, 2011], investing in solar PV assures free energy after a reasonable payback period. This makes electricity from solar PV both cost effective and economical in the long run [Krugmann, 2011]. Solar PV is also environmentally friendly [Gunerhan, *et al.*, 2009], and can be availed even to the remotest parts of the world. This is due to the minimal incidences of wear and tear of solar PV systems [Whitney, 2010], as they do not comprise of heavy moving parts. Generating electricity from the sun's radiation through the PV conversion pathway does not interfere with people's ways of life, because solar PV systems can be integrated in existing structures like houses – thus not requiring additional land where they can be installed. Displacement of populations, which is a norm during fossil fuel exploration and exploitation and during the development of hydro and geothermal sources of electricity, does not happen with PV electricity generation. The PV conversion pathway also provides an opportunity for individuals, households, communities and nations to redeem their ecological footprints. These considerations make solar PV a socially, politically, economically, environmentally and culturally (SPEEC) attractive method of enhancing access to electricity for all.

1.2 Reducing the cost of solar PV electricity

Reduction in the prices of solar PV modules has been pursued through two strategies. The first has been the high efficiency strategy [Torcellini, *et al.*, 2006]. Fabrication costs for conventional silicon PV modules are high, which calls for high solar cell efficiencies [Saga, 2010]. Solar cell efficiencies can however only be increased to a certain extent, mainly through re-inventing manufacturing methods, developing new materials and through informed device engineering [American Society of Mechanical Engineers (ASME), 2010].

However, as solar PV technologies keep maturing, it becomes increasingly expensive to raise their efficiencies further [Kalowekamo and Baker, 2009]. In fact, it reaches a certain point when corresponding increases in cell efficiency may not adequately cover PV cells' total fabrication costs. This has been the case with silicon solar cells. Reduction in the costs for such cells can therefore be practical only through economies of scale. Alternative technologies have nonetheless opened up ways of attaining significantly higher solar cell efficiencies. They include tandem or multi-junction cells and concentrating systems [Haneman, 2006]. High efficiency PV conversion principles like multiple electron-hole pair cells, multi-band and impurity cells [Green, 2001] have also been explored. Solar cells based on these technologies are however expensive to fabricate [Yastrebova, 2007] and still remain at theoretical levels.

The second strategy in reducing the prices of solar PV modules has been the low fabrication-cost strategy. It is not practical to achieve high solar cell efficiencies if their resultant performance/price ratio will not guarantee sustainable energy supply. The attention accorded to research in thin films [Mwabora, 1999; Wronski, *et al.*, 2002; Naghavi, *et al.*, 2003; Saga, 2010; Aliyu, *et al.*, 2012; Chun, 2012], among others, has been inspired by this strategy. Silicon solar cell materials have been vastly studied under

- 3 -

this strategy both at thin film and wafer levels. Studies on a-Si PV devices, which currently dominate most PV markets due to their affordability, have however reported mixed performance under varying air mass (*AM*) values [King, *et al.*, 2000; Ugwoke, 2012], irradiance intensities [Hishikawa and Okamoto, 1994; Katrine, 2008; Ghoneim, *et al.*, 2011; Ugwoke, 2012], and module surface temperatures [Carlson, 1977; Carlson, *et al.*, 2000; Meneses-Rodriguez, *et al.*, 2005; Katrine, 2008; Katherine, 2010]; with reduced performance under these limiting weather conditions dominating the findings.

While silicon solar panels are assembled from individual cells processed from about 100 cm^2 silicon wafers [Antoniadis, 2011], thin film semiconductor materials can be deposited onto large surfaces [Ling and Bao, 2004]. This is beneficial for mass production. Thin films from the direct band gap group III/IV semiconductor materials have been preferred in thin film development as compared to silicon. This is because group III/IV semiconductor materials have a much higher absorption coefficient than silicon, and therefore, less than 1 μm thick semiconductor layers are required, which is 100 to 1000 times less than what would be required of silicon [Halme, 2002]. The cost of group III/IV semiconductor materials is however prohibitive.

Reduction in the cost of solar cells can, therefore, be practically achieved through using cheaper fabrication materials [Simiyu, 2010] and making advances in solar cell technologies [Yu, *et* al., 2012; Qingjiang, *et al.*, 2012]. This is one of the reasons why research in Dye-Sensitized Solar Cells (DSSCs) has been extensive [Nwanya, *et al.*, 2011], with promising advances involving local materials being reported [Ozuomba, *et al.*, 2011]. Apart from using cheaper fabrication materials, DSSCs also promise cheaper electricity because they can be fabricated under less stringent conditions compared to silicon-based solar cells [O'Regan and Grätzel, 1991]. Despite these accolades in respect

- 4 -

of the DSSC technology, its adaptation to the field operating weather conditions in developing countries like Kenya has been wanting.

1.3 Photovoltaics in Kenya

Kenya receives a large amount of solar radiation, estimated at 4.5 kWh per square metre per day [Ministry of Energy (MOE), 2010]. This is because of its location within the 15° north and 15° south parallel bands around the earth, where the greatest amount of solar energy is found [Rabah, *et. al.*, 1995]. It is therefore an ideal candidate for solar energy utilization. Sadly, solar PV accounts for only 0.32% of the overall amount of electricity used in Kenya [Kenya Institute of Public Policy Research (KIPPRA), 2010]. Kenya is however reported to be one of the best solar PV users in Africa [GTZ, 2009a; World Bank, 2010]; which demonstrates how solar PV has inadequately penetrated Africa.

Kenya's electricity demand growth rate is estimated at 6-10% per year [Kenya Electricity Generating Company (KenGen), 2010]. As the country moves towards becoming a middle income economy by the year 2030, solar PV can play a pivotal role if Vision 2030 [Kenya. Ministry of Planning and National Development, Kenya. National Economic and Social Council, 2007] flagship projects like the Konza City [http://www.konzacity.co.ke, 2012] can embrace solar energy utilization, and help move the country towards Net Zero Energy (NZE) status. The history of solar PV in Kenya dates back to the late 1970s [Duke, *et al.*, 2002], punctuated by a remarkable increase in solar PV uptake that has been linked by some experts to increased sales to institutions [Kenya Institute of Public Policy Research (KIPPRA), 2010].

Other experts have however credited the Solar Home Systems (SHSs) segment as the major driver of Kenya's solar PV market [Martinot, *et al.*, 2000; Jacobsen, 2004; Bailis, *et al.*, 2006; GTZ, 2009b]. In both cases, however, the cost factor has played a critical

role in influencing uptake [Duke, *et al.*, 2002]. Amorphous silicon (a-Si) PV modules have therefore been preferred in Kenya due to their affordability [Karekezi and Kithyoma, 2003]. Low performance has however been reported about a-Si modules [Duke, *et. al.*, 2002]. These concerns have a tendency of choking solar PV penetration [Charron and Athienitis, 2006]. They therefore have the potential of negatively influencing solar PV uptake in Kenya in spite of the existence of increased opportunities through sectors like housing, agriculture, community systems and hybrid power sources in isolated mini-grids [Carlo, 2008; GTZ, 2009c; GTZ, 2009b].

Since affordability and performance are fundamental in inspiring solar PV uptake, DSSC PV devices stand a very good chance of taking up a large share of the solar PV opportunities that exist in Kenya. This is because DSSCs are cheaper source of electrical power compared to their silicon-based counterparts [O'Regan and Grätzel, 1991] and have been reported to perform well under limiting weather conditions [Gavin, 2011]. Considerable research work spanning over a decade has been going on in Kenya on DSSC technologies. Studies on Anthocyanin sensitized TiO_2 photoelectrochemical solar cells have been carried out [Simiyu, 2010] and TiO_2 DSSCs with a hole transport material investigated [Ogacho, 2010]. Effects of the concentration of dopant states in the photo-activity in Niobium (Nb) doped TiO_2 are currently being investigated [Ajuoga, 2009]. Theoretical approaches to the temperature effect on the mobility and transport of photo-injected electrons in DSSCs have been considered [Kahuthu, 2009; Olwendo, 2008].

DSSCs fabricated from obliquely DC sputtered TiO_2 films have also been investigated [Waita, 2008] and the effects of nitration on pressed TiO_2 photoelectrodes for DSSCs studied [Wafula, 2006]. Elsewhere in Tropical Africa, dye from local banana leaves has been used to fabricate DSSCs [Ozuomba, *et al.*, 2011]. DSSCs from these studies and

- 6 -

many others carried out around the world have neither been characterized under the field operating weather conditions in the tropics nor a comparison of their performance with what is reported of a-Si PV devices carried out. The focus on a-Si PV devices besides dye sensitized PV devices in this study is because a-Si PV devices are reported to be preferred by the Kenyan PV market [Karekezi and Kithyoma, 2003].

1.4 Problem Statement

Enormous research work has been carried out on DSSCs in Kenya, in the tropics and world over. The work attests to DSSCs' vast merits, and enhances their chances of taking up large portions of the solar PV market in Kenya. Performances of the already fabricated DSSCs, including those from which the DSSMs that are currently on the PV market have not been investigated under the field operating weather conditions in Kenya. This has links to the nonexistence of DSSMs in the field of solar PV applications in Kenya despite the DSSC technology's relevance to the country.

1.5 Rationale and Significance of the Study

The need to move to NZE status in Kenya is beckoning. Conscious of Kenya's ecological footprint, especially as it embarks on extracting the recently found oil and coal deposits, adopting green energy is imperative. Increased use of solar PV will be helpful in this endeavour. However, the high costs of crystalline silicon (c-Si) PV modules and the performance concerns of the a-Si PV modules available on the Kenyan PV market choke solar PV electricity penetration in the country. DSSCs' potentially inexpensive manufacturing technologies promise cheaper solar PV electricity.

This gives DSSCs an exceptional chance of taking up a large portion of the solar PV market in Kenya, and presents an opportunity to increase solar PV penetration. Investigating the DSSM's open circuit voltage (V_{oc}), (J_{sc}), fill factor (FF)and efficiency

(η) under the field operating weather conditions in Kenya and comparing the results with what is reported of a-Si PV modules will provide scientific information necessary to ascertain the effectiveness of the two technologies in respect of the operating weather conditions in Kenya. It will also provide critical scientific knowledge significant for both the fabrication and field application of DSSCs and a-Si PV devices for use in Kenya.

1.6 Objectives of the Study

This study seeks to investigate how a DSSM performs under the field operating weather conditions in Nairobi, Kenya, and to compare it with what is reported of a-Si modules under similar operating weather conditions.

The specific objectives are:

1. To study the effect of irradiance intensity on the performance parameters of a DSSM operating under the weather conditions of Nairobi, Kenya. These performance parameters are: J_{sc}, V_{oc}, FF and η,

2. To study the effect of temperature on the photoelectric conversion of a DSSM operating under the field weather conditions of Nairobi, Kenya, and

3. To compare the performance of the DSSM in in respect of objectives (1) and (2) above with what is reported of a-Si modules operating under similar operating weather conditions.

- 8 -

CHAPTER TWO
LITERATURE REVIEW

2.1 Introduction

In this chapter, a review of the theory on semiconductors, and on the *p-n* junction diode is presented. The ideal solar cell is described and the various categories of solar cells and their achieved in-laboratory efficiencies presented. A review of the DSSC semiconductor electrochemistry, the history, and the reported research advances on DSSCs is also presented. Current density-voltage (*J-V*) characterization of a solar cell is introduced and the atmospheric refraction of solar radiation described. Further, reviews of the history and reported research advances on the DSSC technology, and studies on the performance of a-Si PV devices under different *AM* values, irradiance intensities and temperature variations have also been presented. Though few published scholarly articles exist in the area of field application of DSSCs, a review of the work that has been done in this area has also been presented.

2.2 Semiconductor Theory

At absolute zero temperature, Maxwell-Boltzmann (M-B) distribution function predicts that all atoms in a solid are in ground state [Tolman, 1938]. The distribution of electrons at various energy levels in the atom is governed by the Fermi-Dirac distribution function [Kittel, 1958]:

$$f_{FD}(E, T, E_F) = \frac{1}{\exp\left[\beta(E - E_F)\right] + 1} \qquad (2.1)$$

where $f_{FD}(E, T, E_F)$ is the Fermi-Dirac distribution function, E represents the band gap energy, T represents the absolute temperature, E_F represents the Fermi level energy and β is the inverse of the product of Boltzmann constant and the absolute temperature, i.e., [Kittel, 1958]:

$$\beta = \frac{1}{kT}$$

(2.2)

where k and T represent the Boltzmann constant and the absolute temperature respectively.

Equation (2.1) computes the probability that a given energy level, E will be occupied when the absolute temperature is T and the Fermi energy (or Fermi level) is E_F. The Fermi energy is the highest energy level occupied when temperature is zero. The energy (E) in the exponential factor in equation (2.1) shows how the band gap is very important in semiconductor theory. When temperature is increased from zero, more atoms get into excited states [Clement and Quinnel, 1952], which describes the temperature-dependence of resistivity of semiconductors. Only those electrons with sufficient energy to jump from the valence band (VB) into the conduction band (CB) are available to participate in the conduction process of the semiconductor. When electrons move into the CB, they leave behind vacancies in the VB. These vacancies are called holes. They represent the absence of negative charges and are thought of as positive charges. During conduction, electrons move in a direction opposite to the applied electric field while holes move in the direction of the electric field [Masters, 2004].

Fine-tuning intrinsic semiconductors (semiconductors with a net balance in the number of electrons in the CB and holes in the VB) through doping improves their conductivity [Millman and Halkins, 1972]. Doping a semiconductor with an impurity element with more electrons in its outermost shell than those in the host semiconductor, e.g., doping Si with Arsenic (As) creates a negative-type (n-type) semiconductor. Doping a semiconductor with an impurity element with fewer electrons in the outermost shell than those in the host semiconductor, e.g., doping Si with Boron (B) creates a positive-type (p-type) semiconductor [Neaman, 1997].

The p-n Junction Diode

The p-n junction diode consists of two harmonized regions of a p-type and an n-type material, separated by a region of depletion, which is assumed to be thin. The depletion region forms instantaneously across the p-n junction. The p-type material is usually doped with an acceptor impurity, like B, which results in the presence of holes as the dominant or majority carriers. Similarly, doping of Si with a donor impurity, like Phosphorus (P) or As creates an n-type material, where electrons are the majority carriers. Aluminium (Al) contacts are normally preferred to provide access to the p-terminal and n-terminal of the abrupt or step junction because they provide a low-transition potential between the semiconductor and the metal [Berkeley, 2003]. The principal characteristic of a p-n junction diode is that it allows current to flow easily in one direction but not at all in the other [Shockley, 1949].

A one-dimensional simplification of the p-n junction, illustrated in figure 3.1, helps in understanding the p-n junction diode behaviour. A large carrier concentration gradient results at the boundary when the p-type and n-type materials are brought together. The electron concentration changes from a high value in the n-type material to a very small value in the p-type material. The converse happens for the hole concentration. This gradient causes electrons to diffuse from the n-region to the p-region and holes from the p-region to the n-region. When the holes migrate from the p-type material, they leave behind immobile acceptor ions, which are negatively charged. Consequently, the p-type material is negatively charged in the vicinity of the p-n-boundary [Masters, 2004].
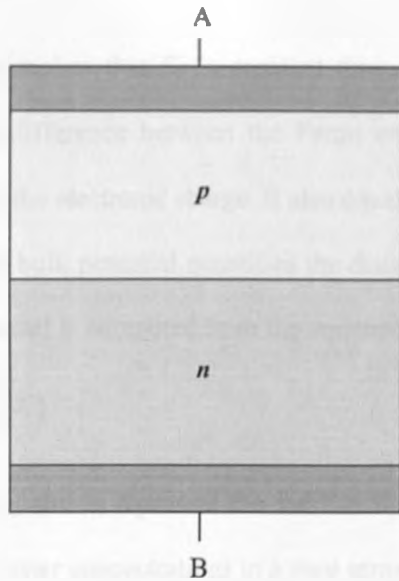
Figure 2.1: A one-dimensional representation of the *p-n* junction.

Similarly, a positive charge builds up on the *n*-side of the boundary as the diffusing electrons leave behind positively charged donor ions. The region at the junction, where the majority carriers have migrated from, leaving behind the fixed acceptor and donor ions, is called the depletion or space-charge region [Shockley, 1949]. The acceptor and donor charges create an electric field across junction the boundary, which is directed from the *n*-region to the *p*-region. This field counteracts the diffusion of holes and electrons, as it causes electrons to drift from the *p*-region to the *n*-region and holes from the *n*-region to the *p*-region. Under equilibrium, the depletion charge sets up an electric field such that drift currents are equal and opposite of diffusion currents, resulting in a zero net current flow.

Figure 2.2 presents a plot of the current directions, the current density, the electric field and the electrostatic field of an abrupt *p-n* junction under zero-bias conditions. Every open *p-n* junction has a contact or built-in potential difference, V_o across it that maintains an equilibrium [Millman and Halkins, 1972; Neaman, 1997]. Built-in voltage is equivalent to the potential across the depletion region during thermal equilibrium. Since

thermal equilibrium implies that E_F is constant throughout the p-n diode, the built-in potential equals the difference between the Fermi energies of the p-type and n-type materials, divided by the electronic charge. It also equals the sum of the bulk potential of each region since the bulk potential quantifies the distance between E_F and the intrinsic energy. Built-in potential is computed from the equation [Lundstrom, 1995]:

$$V_o = V_T \ln \left[\frac{N_A N_D}{n_i^2} \right]$$

(2.3)

where V_o, V_T, N_A, N_D and n_i represent the built-in voltage, thermal voltage, acceptor, donor and intrinsic carrier concentrations in a pure semiconductor sample respectively.

Thermal voltage (V_T) in equation (2.3) is obtained from the equation [Berkeley, 2003]:

$$V_T = \frac{kT}{q}$$

(2.4)

where V_T, k, T and q represent the thermal voltage, Boltzmann constant, the absolute temperature and the elementary charge (electron or hole), respectively.
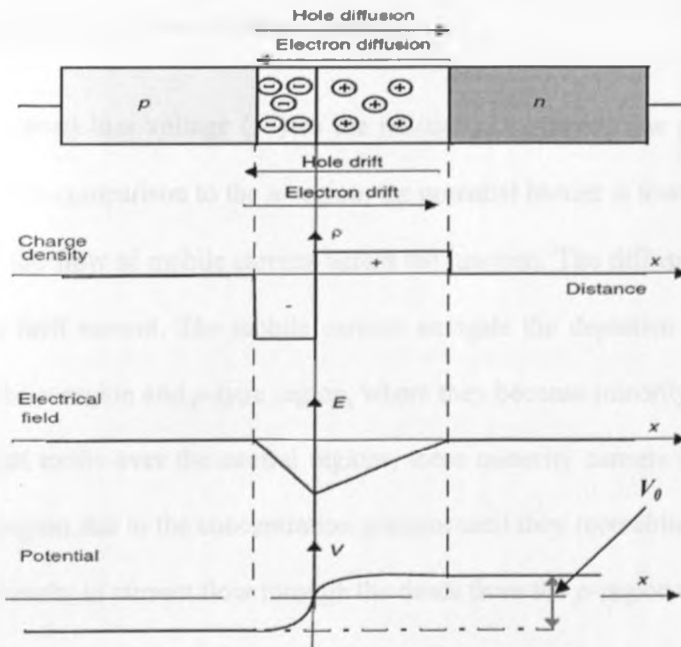
Figure 2.2: Diagrammatic representation of the electrostatic variables of an abrupt p-n junction with the p-side heavily doped compared to the n-side under equilibrium conditions [Berkeley, 2003].

Related to the built-in potential difference is the internal electric field, (E_o) that appears across the junction plane [Halliday, *et. al.*, 2009]:

$$E_o = - \frac{dV_o}{dx}$$

(2.5)

where E_o, dV_o and dx represent the internal electric field across the junction, change in potential difference across the junction and the distance across the junction respectively.

This field exerts a force on the electrons that opposes their diffusion. Therefore, for an electron to move from the *n*-region to the *p*-region or vice versa, it must be sufficiently energetic to overcome the potential barrier (ΔV_o). Although the electric field acts to retard the motion of these majority carriers, for minority carriers, it is usually a downhill drift. By thermal agitation however, an electron that is close to the junction plane can be raised from the VB to the CB of the *p*-type material, so that it easily drifts across the junction plane, aided along by the electric field. Likewise, if a hole is created in the *n*-type material, it drifts across to the other side of the junction plane. These processes leave the depletion region free of charge carriers.

Applying a forward bias voltage (V_F) to the junction, i.e., having the potential of the *p*-region raised in comparison to the *n*-region, the potential barrier is lowered, leading to an increase in the flow of mobile carriers across the junction. The diffusion current then dominates the drift current. The mobile carriers navigate the depletion region and get injected into the *n*-region and *p*-type region, where they become minority carriers. If no voltage gradient exists over the neutral regions, these minority carriers diffuse through the depletion region due to the concentration gradient until they recombine with majority carriers. This results in current flow through the diode from the *p*-region to the *n*-region, which depends exponentially on the applied bias voltage.

applying a reverse-bias voltage (V_R) on the other hand raises the potential barrier. The ideal diode equation (2.6) [Shockley, 1949] predicts that the diode current (I_D) approaches negative saturation current for $V \gg V_T$.

$$I = I_s[\exp\left(\frac{V}{mV_T}\right) - 1] \tag{2.6}$$

where I, I_s, V, m and V_T represent the total current produced by the PV device (from the electron and hole contributions), the saturation current, voltage across the terminals of the PV device, the ideality factor (=1 for ideal PV devices and $\neq$ 1 for non-ideal PV devices) and the thermal voltage respectively.

In practical cases, current is evaluated as passing through a given cross sectional area (A), hence throughout the rest of this thesis, we will refer to current density (J), which is determined by,

$$J = \frac{I}{A} \tag{2.7}$$

where J and I represent the ideal current density and current flowing through an area A of the PV device respectively.

Voltage (potential difference) across the terminals of a *p-n* junction (V) is computed from the equation [Lundstorm, 1995]:

$$V = V_o - V_F \tag{2.8}$$

where V, V_o and V_F represent the voltage across the terminals of the p-n junction, the contact or built in voltage and forward-bias voltage respectively.

From the law of the junctions (the number of electrons or holes crossing from the *n*-side to the *p*-side or *p*-side to the *n*-side respectively, increases exponentially as a function of the forward bias voltage (equations 3.9 and 3.10)), application of external voltage

increases the number of electrons or holes crossing over the potential barrier to the p – side or the n-side respectively by an exponential factor [Pota, 2004]:

$$n_p(o) = \exp\left(\frac{V}{kT}\right)$$

(2.9)

$$p_n(o) = \exp\left(\frac{V}{kT}\right)$$

(2.10)

where $p_n(o)$, $n_p(o)$, V, k and T represent the equilibrium electron densities on the p-region, equilibrium hole densities on the n-region, voltage across the p-n junction, Boltzmann constant and the absolute or junction temperature respectively.

2.4 Solar Cells

2.4.1 An Ideal Solar Cell

An ideal solar cell is modelled with a current source in parallel with a diode. Figure 2.3 is the equivalent circuit of a practical solar cell. It shows the shunt and series resistances. Shunt resistances (R_{sh}) are due to leakages of current across the p-n junction around the edge of the solar cell. Series resistances (R_s) arise from the bulk resistance of the semiconductor material and the resistance of the contacts of the cells [Mwabora, 1999]. Current flowing through solar cell components is governed by the voltages across them. The ideal current density of a solar cell (J) is equal to that from the source (J_L) minus that which is flowing through the diode (J_D) and the shunt resistor (J_{sh}) [Streetman, 1993]:

$$J = J_L - J_D - J_{sh}$$

(2.11)

where J, J_L, J_D and J_{sh} represent the ideal current density, current density from the source, and current density flowing through the diode and the shunt resistor respectively.
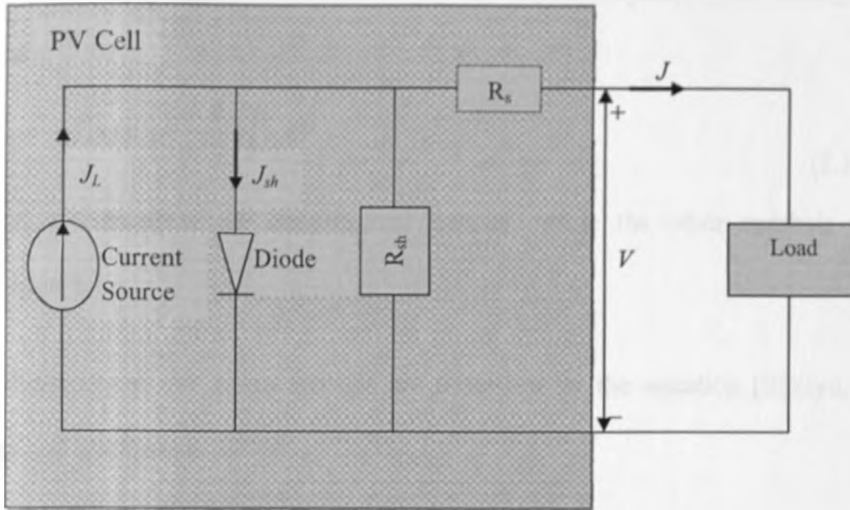
Figure 2.3: An equivalent circuit for a solar cell showing the series resistance, shunt resistance, current from the source, current flowing through the diode, current flowing through the shunt resistor, ideal current density of the solar cell and the voltage across the solar cell terminals. The shaded rectangle represents the equivalent circuit of the inner part a solar cell to which the external contacts are connected.

2.4.2 *J-V Characterization of Solar Cells*

The response of a PV device is determined by its *J-V* characteristics both in the dark and under illumination. *J-V* characteristics are modelled according to the ideal diode equation (2.6), which for practical cases, is modified to take into account the shunt and series resistances [Hedegus and Shafarman, 2004]:

$$J = J_l - J_e \exp\left[\frac{V + R_s J}{m V_T}\right] - \sigma V \tag{2.12}$$

where J, J_L, J_s, V, m, V_T, R_s, and σ represent the ideal current density, current density from the source (in this work, it is the photo-generated current density, J_{ph} and will be referred to as such), saturation current density, voltage across the PV terminals, the ideality factor, thermal voltage, series resistance and shunt conductance respectively.

In the dark, an applied voltage (known also as the bias voltage) generates current density in the direction opposite to that which is generated by light. This is known as

dark current density and is computed from the equation [Sze, 1981; Hedegus and Shafarman, 2004]:

$$J_{dark} = -J_s \exp\left[\frac{V + R_s J}{m V_T}\right] - \sigma V \qquad (2.13)$$

where J_{dark} represents the dark current density, while the other symbols are as described in 2.12.

Under illumination, J-V characteristics are described by the equation [Simiyu, 2010; Hedegus and Shafarman, 2004]:

$$J = J_{ph} - J_s \exp\left[\frac{V + R_s J}{m V_T}\right] - \sigma V \qquad (2.14)$$

where J_{ph} represents the photo-generated current density, while the other symbols are as described in 2.12.

Setting of the ideality factor in equation (2.6) to one relates to an ideal case, which assumes that all recombinations in the PV device occur via the band to band or the bulk areas of the PV device only but not in the junction. The ideality factor therefore describes how closely the PV device follows the ideal case scenario. In practical cases however, PV devices are non-ideal since recombinations occur in other ways and areas of the devices other than through band to band or in the bulk area of the devices. Non-ideal devices therefore yield ideality factors that deviate from the ideal.

From equations (2.13) and (2.14), the dark current density and photo-generated current density (respectively) can be plotted as functions of the applied bias voltage. This results in a curve typically known as the current density-voltage (J-V) characteristic curve. Figure 2.4 presents a J-V curve and the related P-V curve.
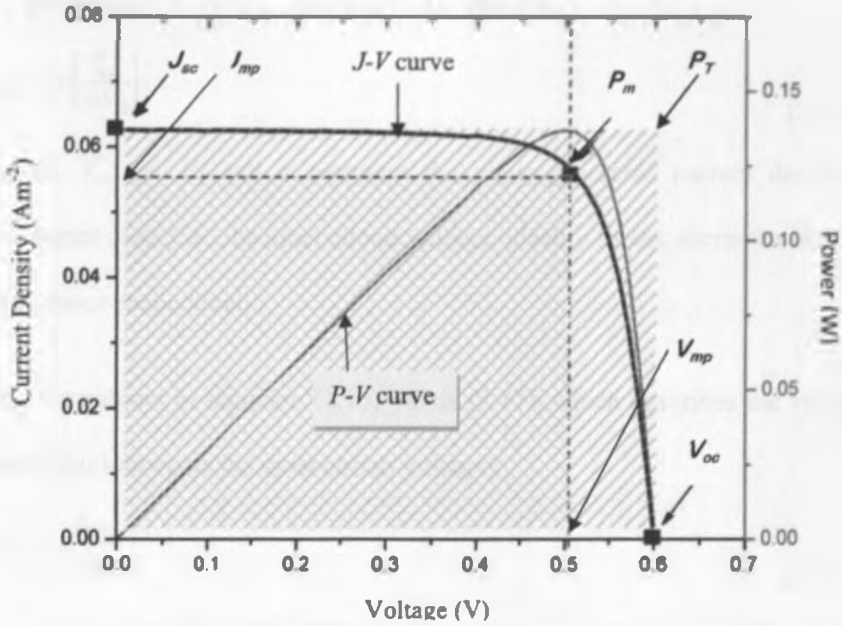
Figure 2.4: Diagram of the *J-V* and *P-V* characteristics showing J_{sc}, V_{oc}, J_{mp}, V_{mp}, P_m and P_T [Newport Corporation, 2011].

From the *J-V* curve, key performance and device parameters; V_{oc}, J_{sc}, J_s, FF, R_s, R_{sh} can be extracted and, *m* and η computed. V_{oc} is the voltage measured when the terminals of a PV device are isolated. This relates to the condition when the potential difference is at its maximum value. At this point, dark current density and short circuit photo-current densities exactly cancel out and no flow of current is observed between the PV terminals. Setting *J* = 0 in equation (2.14), and rearranging yields equation (2.15) that can be used to compute the photo-generated current density.

$$J_{ph} = J_s \exp\left[\frac{V}{mV_T}\right] \qquad (2.15)$$

where J_{ph}, J_s, *V*, *m*, and V_T represent the photo-generated current density, saturation current density, the voltage across the PV device's terminals, the ideality factor and thermal voltage respectively.

hen V is maximum, i.e., $V=V_{oc}$, equation (2.15) leads to:

$$J_{ph} = J_s \exp\left[\frac{V_{oc}}{mV_T}\right]$$

(2.16)

where J_{ph}, J_s, V_{oc}, m, V_T and σ represent the photo-generated current density, the saturation current densities, the open circuit voltage, ideality factor, thermal voltage and shunt conductance respectively.

Making V_{oc} the subject in equation (2.16) yields (2.17), which describes the voltage at zero current (also known as the open circuit voltage):

$$V_{oc} = mV_T \ln\frac{J_{ph}}{J_s}$$

(2.17)

where J_{ph}, J_s, V_{oc}, m and V_T represent the photo-generated current density, the saturation current density, the open circuit voltage, the ideality factor and thermal voltage respectively.

J_{sc} describes the photo-generated charge carriers. It corresponds to the condition when the circuit is shorted and both the load and power are zero [Simiyu, 2010], leading to low impedance [National Instruments, 2009]. It is calculated at the point when the applied voltage is zero. If we set the applied voltage, V to zero and J to J_{sc} in equation (2.14), we obtain:

$$J_{sc} = J_{ph} - J_s$$

(2.18)

where J_{sc}, J_{ph}, and J_s represent the short circuit, photo-generated and saturation current densities respectively.

Since J_s in equation 2.18 remains relatively unchanged for a given solar cell as it depends on the semiconductor used in the fabrication of the device,

- 20 -

$$J_{sc} \equiv J_{ph} \qquad\qquad\qquad\qquad\qquad\qquad (2.19)$$

where J_{sc} and J_{ph} represent the short circuit and the photo-generated current densities respectively.

The actual current that flows out of a solar PV device is the ideal current, i.e., the short-circuit current density, minus the current that flows through the diode or dark current density, J_{dark}:

$$J = J_{sc} - J_{dark} \qquad\qquad\qquad\qquad\qquad (2.20)$$

where J, J_{sc} and J_{dark} represent the ideal, short circuit and dark current densities respectively.

FF is generally influenced by R_s and R_{sh}. It is a measure of the quality of the PV device. The closer to a square for a PV device's J-V characteristics points to a FF that is closer to unity, hence the quality of the PV device. FF is calculated by comparing the maximum power (P_m) to the theoretical power (P_T) that would be output at both V_{oc} and J_{sc}. This is determined from the equation [Simiyu, 2010]:

$$FF = \frac{P_m}{V_{oc}J_{sc}} = \frac{J_{mp}V_{mp}}{V_{oc}J_{sc}} \qquad\qquad\qquad (2.21)$$

where FF, P_m, V_{oc}, J_{sc}, J_{mp} and V_{mp} represent the fill factor, the maximum power density, the open circuit voltage, the short circuit current density, the maximum power current density and the maximum power voltage respectively.

The units for P_m are Watts (W) - in terms of electromagnetism, one watt is the rate at which work is done when one ampere (A) of current flows through an electrical potential difference of one volt (V). Since the units for J_{mp} and J_{sc} are Am^{-2} and those for V_{mp} and V_{oc} are volts (V), FF is therefore a ratio of the product of J_{mp} and V_{mp}, i.e., P_m and the product of V_{oc} and J_{sc}. Decreasing R_{sh} and increasing R_s decreases FF and P_m.

- 21 -

There exists a certain potential between the J_{sc} and V_{oc} on the J-V curve where P_m is found. At this point, the PV device delivers the highest power output. Voltage at this point is V_{mp}, while the current density at this point is J_{mp}. P_m, V_{mp}, J_{mp} can also be computed as shown in equations (2.22), (2.23) and (2.24). Figure 2.4 also presents a plot of the power generated by a PV device at various voltages, i.e., the P-V curve. From the P-V curve, the PV device's P_m, J_{mp} and V_{mp} can be extracted.

$$P_m = FFV_{oc}J_s \quad (2.22)$$

$$V_{mp} = \frac{FFV_{oc}J_{sc}}{J_{mp}} \quad (2.23)$$

$$J_{mp} = \frac{FFV_{oc}J_{sc}}{V_{mp}} \quad (2.24)$$

where P_m, FF, V_{oc}, J_{sc}, J_{mp} and V_{mp} represent the maximum power, the fill factor, the open circuit voltage, the short circuit current density, the current density at maximum power and the voltage at maximum power respectively.

η is associated with the overall performance of a PV device. It is defined as the ratio of P_m to the power of incident radiation (P_{in}), which is given by the equation [Hedegus and Shafarman, 2004]:

$$\eta = \frac{P_m}{P_{in}} = \frac{J_{mp}V_{mp}}{P_{in}} = \frac{V_{oc}J_{sc}FF}{P_{in}} \times 100\% \quad (2.25)$$

where η, P_m, J_{mp}, V_{mp}, V_{oc}, J_{sc} FF, and P_{in} represent the efficiency, maximum power, maximum power current density, maximum power voltage, open circuit voltage, short circuit current density, fill factor and the power of the incident light respectively.

2.4.3 Categories of Solar Cells

Solar cells are categorized as first, second or third generation [Walton, 2010] depending on the time or period when they emerged along the PV development roadmap [Nelson, 2010]. First generation solar cells are based on silicon *p-n* junction semiconductors

[Lobato, 2007]. They were first demonstrated by Chapin, Fuller and Pearson at the Bell Laboratories [Chaplin, *et al.*, 1954] and are reported to have a 31% theoretical efficiency limit (also known as the Shockely-Queissner limit) [Shockley and Queissner, 1961; Abrams, *et al.*, 2011]. Their current operational efficiencies range from 12% to 16%. This is less than half the limit that has been theoretically established of these cells [Tiedje, *et al.*, 1984]. It implies that although they have not reached their theoretically established limit, they only have a gain in efficiency of about 50% that can be realized from their current established values.

First generation solar cells have an economic viability challenge mainly due to the costly fabrication processes and low working lifetimes associated with them [Boucher, 2008]. To surmount this, cheaper fabrication processes as well as studies to increase their working lifetimes have been ongoing [He, *et al.*, 2012; Crain, *et al.*, 2012]. First generation solar cell devices nonetheless dominate the world PV market currently [Pizzini, *et al.*, 2005]. They come in three types; the single crystal or mono-crystalline, the polycrystalline and the amorphous [Proulx, 2011]. Each type has its own strategic market niche, with a-Si receiving significant attention because of its lower cost when compared to the other first generation PV devices. In the area of field applications, extensive focus has been directed towards investigating the performance of a-Si PV devices under various weather conditions around the world. Studies on the effect of *AM* on the performance of a-Si PV modules have shown slight increases in V_{oc} and reductions in J_{sc}, *FF* and η as *AM* increased [King, *et al.*, 2000; Ugwoke, 2012].

Under varying irradiance intensities, V_{oc} for a-Si PV modules has been reported to decrease while J_{sc} has been reported to significantly increase as irradiance intensities increased [Hishikawa and Okamoto, 1994; Katrine, 2008; Ugwoke, 2012]. An increase in *FF* and η at irradiance intensities of about 0.5 Sun, followed by decreases thereafter

have been observed [Ghonein, *et al.*, 2011; Ugwoke, 2012]. Other studies have reported a linear decrease in V_{oc} as a-Si module surface temperatures increased [Katherine, 2010], and a constant J_{sc} as module surface temperatures increased [Katrine, 2008]. On the temperature-dependence of *FF*, both a positive temperature-dependence [Katherine, 2010] and a negative temperature-dependence [Katrine, 2008] have been reported. On the area of applications, a-Si solar cells have been reported to be largely used in low-power cheap consumer electronic devices [Mulvaney, *et al.*, 2009].

Other silicon solar cell categories include, the high-grade single crystal or mono-crystalline, which are mainly used in the space industry [Iles, 2001], and the Polycrystalline silicon solar cells, which are also used in low-power consumer electronic goods. The fabrication costs of polycrystalline solar cells have however been nominal compared to mono-crystalline silicon solar cells [Ruby, 2011]. Polycrystalline solar cells are nonetheless fraught with lower efficiencies [Meng, *et al.*, 2000]. This can be attributed to recombinations at their grain boundaries. Reduction in the fabrication costs of silicon solar cells has been a key research goal with notable gains having been reported through the making of ribbon silicon in a process that circumvents the sawing of crystal ingots. This leads to 40% wastage elimination in the fabrication processes [Green, 2003].

The use of group III/IV direct band gap semiconductor materials like Gallium Arsenide (*GaAs*), Gallium Aluminium Arsenide (*GaAlAs*), Gallium Indium Arsenide Phosphide (*GaInAsP*), Indium Arsenide (*InAs*), Indium Antimonide (*InSb*) and Indium Phosphide (*InP*) has also been explored. These materials have been preferred in areas like the space industry, where efficiency is the prime objective over cost [Lobato, 2007]. This is because whereas about 100 µm thickness is required for 90% light absorption in silicon, only 1 µm of GaAs would be required for the same absorption [Rotman, 2012]. This is

because the excitation of an electron in a direct band gap material does not require the aid of a phonon for momentum transfer [Sigrist, 2010]. These considerations have made group III/IV semiconductor materials to be preferred at thin film levels, where they are more effective when compared to silicon. They are however very costly for the majority of solar PV applications.

The Arab oil embargo of 1973 – 1974 [Lillich, 1975] stirred increased interest in and funding for alternative sources of energy [Birkmire and Eser, 1997]. Two main variants in PVs were explored. These are; Copper Indium Di-Selenide ($CuInSe_2$) [Kazmerski, et. al., 1976] and Cadmium Telluride ($CdTe$), [Cusano, 1963]. Both were coupled with n-type Cadmium Selenide ($CdSe$) to create p-n heterojunctions. Since CdSe has a large band gap of 2.4 electron volts (eV) [Purnima, et al., 2011], it was used as a window layer to the p-n junction. This is because being a direct band gap semiconductor, only a thin film of about 10 µm is required for complete light absorption [Patel, et al., 2009]. Solar cells developed following the 1973 – 1974 energy crisis are categorized as second generation solar cells [Halme, 2002].

Laboratory results for $CuInSe_2$-based solar cells have been very promising. The techniques for their fabrication however remain complex [Kao, et al., 2012]. The up-scaling phase is also faced with challenges that include the need to have very low reaction temperatures, and to reduce the thickness of the cells [Mwabora, 1999]. These challenges have made the technology less cost-effective. There is also debate on the validity of using rare elements such as Indium (In) [Resnick Institute (RI), 2011]. These concerns, coupled with the high performance/price ratio of second generation solar cells, has led to their unfavourable rating and inspired further research that led to third generation solar cells.

Third generation solar cells are solar cells that do not fall into the first and second generation categories. They endeavour to circumvent the 31% Shockley-Queissner limit [Shockley and Queissner, 1961] by concentrating light from sources. This has been achieved mainly through the use of tandem cells with multiple band gaps [Lantratov, *et. al.*, 2007] and by means of multiple carrier excitation [Luque and Hedegus, 2003; Conibeer, 2007]. Tandem solar cells and the solar cells that are based on multiple carrier excitation are however complex to fabricate, making them costly. Cheaper third generation alternatives have nonetheless been explored. These are; the DSSCs [O'Regan and Grätzel, 1991] and the organic heterojunctions [Benanti and Venkataraman, 2006].

In organic heterojunction solar cells, the photo-generated electron-hole pairs are tightly bound, forming excitons [Hadipour, *et al.*, 2011]. Charge separation therefore occurs at the electron donor and acceptor organic polymers or at selected contacts [Thompson and Fréchet, 2008]. The heterojunctions come in two different structures. These are; the bi-layer heterojunction and the bulk heterojunction [Tada, *et al.*, 2011]. The bi-layer heterojunction is akin to the *p-n* heterojunction, while the bulk heterojunction seeks to maximize the *p-n* interface through intertwining the *n*-type and *p*-type polymers. Efficiencies in these systems are at best 7.9% [Nelson, 2010]. They are however still in their infancy stages with enormous potential due to the many organic compounds that can be synthesized.

2.5 Dye-Sensitized Solar Cells (DSSCs)

2.5.1 The Design

DSSCs architecturally consist of two layers of transparent conducting oxide (TCO) glass substrates between which the other materials used in their fabrication are sandwiched. The substrates are normally fluorine-doped tin oxide ($F:SnO_2$) or indium tin oxide (ITO). On the first layer of TCO glass substrate that serves as the working electrode

(WE), a film of nanometre-sized particles of porous titanium dioxide (TiO_2) are deposited by sputtering, pressing or screen printing. The film thickness, and hence performance, are determined by the deposition technique chosen. On the surface of the TiO_2, a light-harvesting monolayer of dye is adsorbed [Hu, *et. al.*, 2007; Chen, *et. al.*, 2007].

On the second layer of the TCO glass substrate, which is the counter electrode (CE), a thin catalytic layer of platinum (Pt) is applied. This improves the short-circuit current (I_{sc}) through the catalytic reduction of the tri-iodide in the redox electrolyte. The CE should be efficient in transferring electrons to the electrolyte. In between the TiO_2 nanoparticles and Pt, a redox electrolyte (usually a mixture of iodine and iodide in an organic solvent) is filled to penetrate the porous layers of TiO_2. The porous TiO_2 nanoparticles provide a large surface per projected area so that when the dye is attached to their surfaces, the area through which light can be captured is greatly increased.

DSSCs capture optical energy from the sun and convert it into electrical energy with no net chemical change in the system. All this is performed in a closed chemical circuit [Grätzel and Durrant, 2008]. They remain 'top runners' among third generation solar cells due to their low cost and easy fabrication using environmentally benign materials [Grätzel, 2009]. Their scalable, self-assembled and bottom-up fabrication processes are economical and ecological, making them attractive and credible alternatives to the conventional solar PV systems [Yum, *et al.*, 2010]. Figure 2.5 illustrates the principle of operation and energy level scheme for DSSCs.
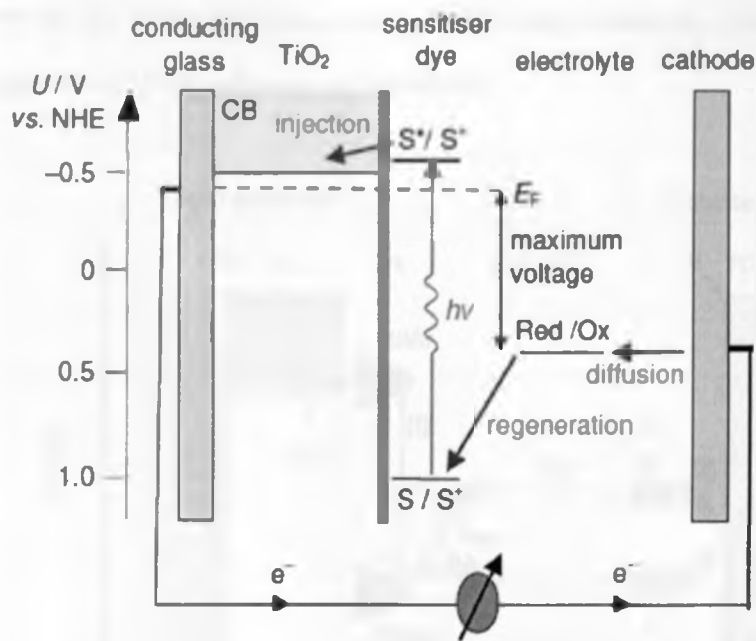
Figure 2.5: Diagrammatic presentation showing the processes that an electron goes through during the operation of a DSSC [Ferber, *et. al.,* 1998].

2.5.2 The DSSC Semiconductor Electrochemistry

While conventional PV principles rely on the work functions of interfacing materials, in DSSCs, the semiconductor electrochemistry is critical in the physical and chemical processes that take place during photo-generation. In terms of energy levels, the electronic excitation in the dye, achieved through light absorption, promotes the system into a high energy state that is associated with the Lowest Unoccupied Molecular Orbital (LUMO). This simultaneously creates an electron deficiency on the low energy state – the Highest Occupied Molecular Orbital (HOMO). Figure 2.6 presents the operation scheme of a DSSC.

Electrons in the LUMO and HOMO states are separated by a change in enthalpy (Δh) as follows [Bisquert, *et al.*, 2004]:

$$\Delta h = \Delta E = E_{LUMO} - E_{HOMO} \tag{2.26}$$

where Δh, ΔE, E_{LUMO} and E_{HOMO} represent the change in enthalpy, difference in energy, energy of the LUMO and energy of the HOMO.
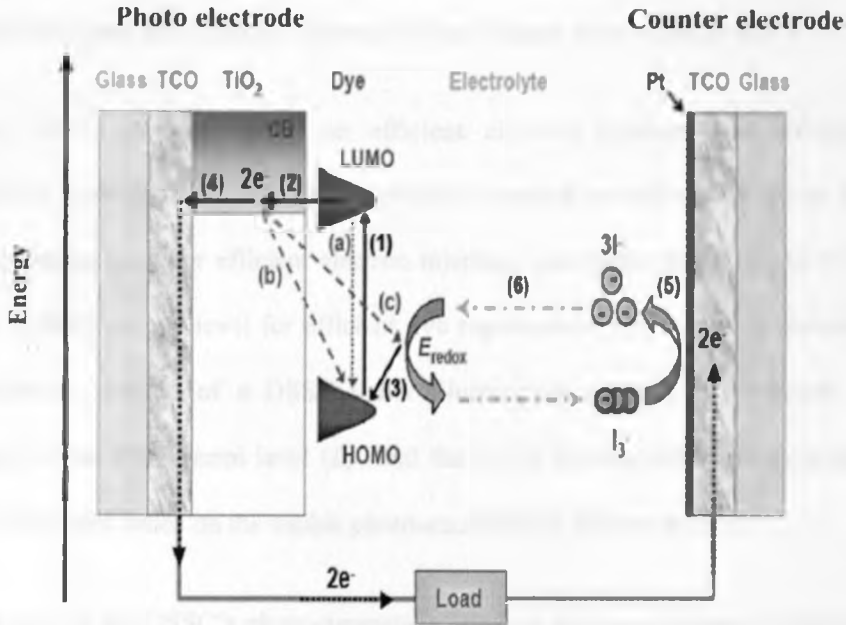
Figure 2.6: Diagram illustration of the operation scheme of a DSSC [Halme, 2002].

Equation (2.26) compares to equation (2.27) in semiconductors,

$$\Delta E = E_c - E_v \tag{2.27}$$

where ΔE, E_c and E_v represent the energy difference, the conduction band energy and the valence band energy respectively.

The departure of the states from their thermal equilibrium values implies that there is a difference in their chemical potentials (μ) as follows:

$$\Delta \mu = \mu_{LUMO} - \mu_{HOMO} \tag{2.28}$$

where $\Delta \mu$, μ_{LUMO} and μ_{HOMO} represent the change in chemical potential, the chemical potential of the LUMO and the chemical potential of the HOMO respectively.

Equation (2.27) compares to equation (2.28) in semiconductors,

$$\Delta\mu = \mu_c - \mu_v \qquad (2.29)$$

where $\Delta\mu$, μ_c, and μ_v represent the change in chemical potential, the chemical potential of the conduction band and chemical potential of the valence band respectively.

Efficient DSSC operation relies on efficient electron injection and efficient dye regeneration. Further, the LUMO energy of the dye should be sufficiently higher than the TiO_2 conduction band for efficient electron injection. $\Delta\mu$ of the redox should be higher than the HOMO energy level for efficient dye regeneration and sustained photocurrent. The maximum voltage of a DSSC under illumination normally corresponds to the difference of the TiO_2 Fermi level (E_F) and the $\Delta\mu$ of the electrolyte. Nonetheless, the basic PV principle relies on the visible photo-excitation of the dye molecule.

The first step in the DSSC's photo-generation involves photo-excitation of electrons the HOMO level to the LUMO level of the dye molecules as illustrated by step (1) in figure 2.6, and by equation (2.30):

$$TiO_2/S + h\nu \leftrightarrow TiO_2/S^{\bullet}_{LUMO} \qquad (2.30)$$

where TiO_2, S, $h\nu$, and $S^{\bullet}_{LUMO}$ represent the titanium dioxide, the ground state of the dye molecules, the photon energy and the excited state of the least unoccupied molecular orbital of the dye molecule respectively.

The electron is then ejected from the excited dye molecules injected into the conduction band of the TiO_2 as demonstrated by step (2) in figure 2.6, and by equation (2.31):

$$S^{\bullet}_{LUMO} + CB_{TiO_2} \rightarrow TiO_2/S^+ + e_{CB}^- \qquad (2.31)$$
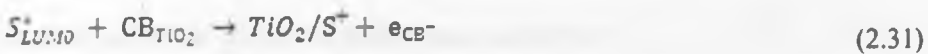
where $S^{\bullet}_{LUMO}$, CB_{TiO2}, TiO_2, S^+ and e_{CB} represent the excited state of the LUMO of the dye molecule, the conduction band of the TiO_2, the titanium dioxide, the oxidized dye molecule and the electron injected into the conduction band respectively.

The electron then migrates through the TiO_2 nanoparticle network as illustrated by step (4) in figure 2.6 towards the transparent conducting oxide (TCO) substrate. The physics of charge transfer and transport in molecular and organic materials during these processes is dominated by charge localization resulting from polarization of the medium and relaxation of the molecular ions. The kinetics behind the catalytic reaction at the CE must guarantee fast generation of the redox couple as illustrated by step (5) in figure 2.6, and by equation 2.32 [Kalaignan and Kang, 2006],

$$Pt + [I_3]^- \rightarrow 3I^-$$ (2.32)

where Pt, I_3^- and $3I^-$ represent the Platinum, Iodide and the Iodine ions respectively.

The electron injection rate must be faster than the decay rate so as to achieve an efficient cell operation. The S^+ must be regenerated by the redox couple at the speed of nanoseconds so as to kinetically compete with the metal oxide's electrons for the subsequent electron injection as well as prevent recombinations. This is because recombinations depend on the kinetics at the metal oxide/dye/electrolyte interface [Thavasi, et al., 2009]. Also, the rate of reduction of S^+ by the electron donor in the electrolyte, as demonstrated by step (3) in figure 2.6 and by equation (2.33) must be higher than the rate of back reaction of the injected electrons with the dye oxidation in equation (2.35) as well as the rate of injected electrons in the electron acceptor in the electrolyte as illustrated by step (6) in figure 2.5 and by equation (2.32):
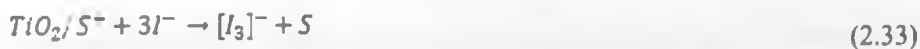
$$TiO_2/S^+ + 3I^- \rightarrow [I_3]^- + S$$ (2.33)

where TiO_2, S^+, $3I^-$, I_3^- and S represent the titanium dioxide nanoparticles, the oxidized dye molecules, and the iodine and iodide ions respectively.

During these processes, some electrons are not successfully injected into the TiO_2 conduction band due to inadequate energy and drop back to the HOMO level as

- 31 -

illustrated in step (a) in figure 2.6. Some electrons already injected into the conduction band of the TiO_2 migrate back to the HOMO level of the dye or electrolyte as demonstrated by steps (b) and (c) due to electron trapping defects. These result in electron recombinations described by equations (2.34) and (2.35), which decrease the performance of the cell.

$$e_{CB^-} - S_{HOMO} \rightarrow S + CB_{TiO_2}$$
(2.34)

$$e_{CB^-} + [I_3]^- \rightarrow 3I^- + CB_{TiO_2}$$
(2.35)
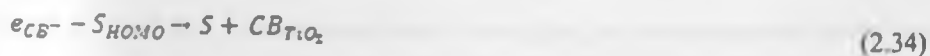
where e_{CB^-}, S_{HOMO}, S, I_3^-, $3I^-$ and CB_{TiO2} represent the electron in the conduction band, the ground state of the dye molecule's highest occupied molecular orbital, the ground state of the dye molecule, the iodine and iodide redox couple and the conduction band of the titanium dioxide nanoparticles.

Discoveries like the PV effect [Becquerel, 1848] and the capturing of the first photographic image onto a mirror-polished surface that had a coating of silver halide particles [Daguerre, 1839] stimulated early work on DSSCs. The halides used in Daguerre's work had band gaps of 2.7 electron volts (eV) to 3.2 eV. They were hence not photoactive to light of energy less than 2.7 eV that corresponds to wavelengths of greater than 450 nm. An improvement on Daguerre's work was achieved by sensitizing silver halide emulsions with a dye, which led to an extension in the photo-response of the emulsions into the red and infra-red radiation spectrum [Vogel, 1873]. Understanding the operating mechanisms of electron injection from dye molecules into the conduction band of an n-type semiconductor substrate was however not realized until the 1960s [Williams, 1960]. Another discovery that enhanced work on DSSCs was the observed reactions by excited chlorophyll molecules at TiO_2 electrodes. This was found to compare with photosynthesis [Tributsch, 1971].

Early DSSCs however had electrical resistances due to their characteristic thick dye layers and poor dye-anchorage, which led to their low conversion efficiencies [Simiyu, 2010]. The discovery of ruthenium complex dyes and black dyes as sensitizers has however helped push DSSC efficiencies well above 10% [Gao, et al., 2008]. With regard to semiconductors, TiO_2, Zinc Oxide (ZnO) and Tin Oxide (SnO_2) have been used in the fabrication of DSSCs. In the present era of ecological and environmental consciousness, preferences are for inert, non-toxic compounds with TiO_2 adequately meeting these requirements [Kalyanasundaram and Grätzel, 1998; Kay and Grätzel, 1999]. TiO_2 has also been preferred because its electrodes are stable upon irradiation [Fujishima and Honda 1971] and is transparent in the visible region [Pulka, 1984]. This has made it the semiconductor of choice in the fabrication of DSSCs [Grätzel, 2003].

The challenge of dye-adsorption onto the TiO_2 semiconductor in DSSCs has been addressed through using dispersed TiO_2 particles, which provides sufficient dye/semiconductor interface [He, et al., 2012]. To capture most of the incident light, use of a dye monolayer with high molecular extinction as well as photo-electrodes with high surface roughness has been demonstrated [Duonghong, et al., 1984]. The use of volatile solvents in electrolytes has been found to repress outdoor use of DSSC solar panels [Papageorgiou, et. al., 1996]. These findings have led to the fabrication of DSSCs that do not degrade adversely under outdoor weather conditions - remaining stable for long periods of time [Helena, et al., 2003; Kato, et al., 2009; Kuang, et. al., 2011]. Studies on the effects of light soaking and heat stress have shown DSSCs' resilience [Jun-Ho, et al., 2010]. Studies to improve DSSCs' efficiencies have been on-going [Kroon, et al., 2007; Nelson, 2010; Han, et al., 2012]. The efficiency development roadmap for solar cells for different technologies from 1975 to 2010 is presented in figure 2.7.
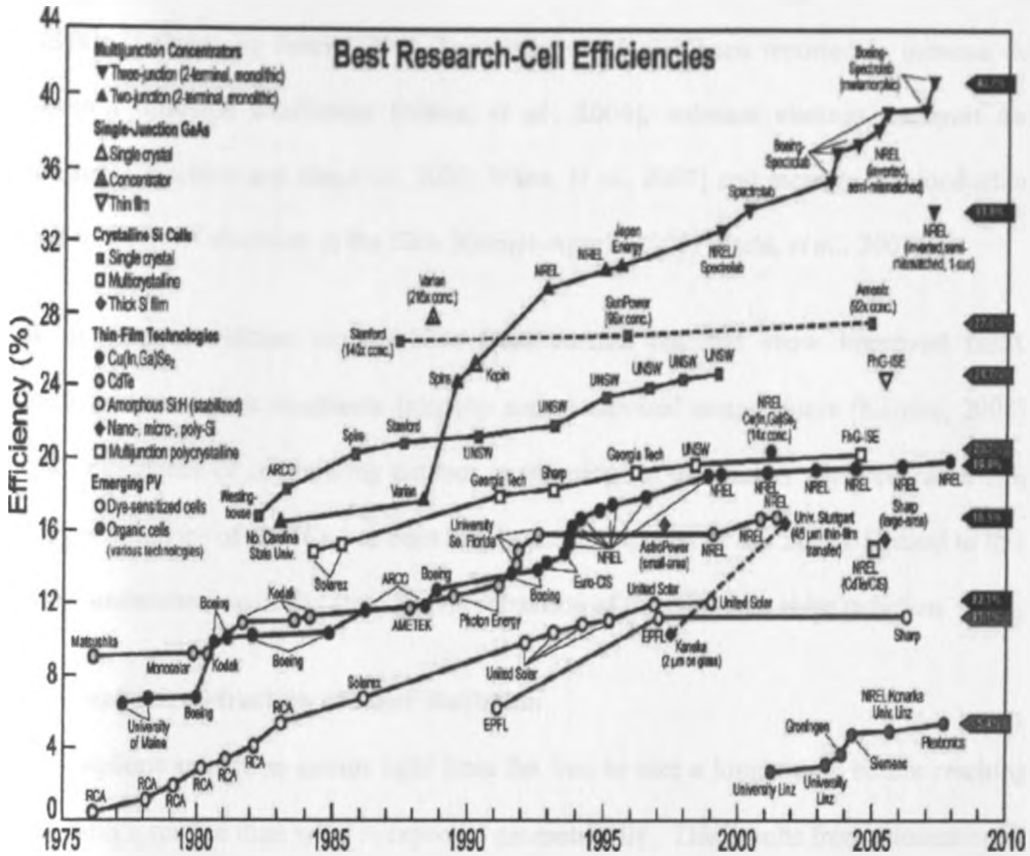
Figure 2.7: Solar cell development and efficiency roadmap: 1975 to 2010 [Nelson, 2010].

The latest validated efficiency for a DSSC is 12.3%, which has been achieved by employing a zinc porphyrin dye and a $Co^{(II/III)}$tris(bipyridyl)-based redox electrolyte [Yu, et al., 2012].

Other DSSC in-laboratory studies have been carried out and illustrated the strong dependence of V_{oc} on light intensity, temperature and device thickness [Snaith, et al., 2006]. Other studies have also been carried out and illustrate how increase in temperature, irradiance and iodine concentration in the electrolyte favourably influence the performance of DSSCs filled with ionic liquid electrolytes [Bergine, et al., 2008]. Temperature has been found to cause the electron quasi-Fermi level to shift towards the

conduction band edge of the TiO_2 semiconductor hence improving the performance of DSSCs [Lobato and Peter, 2006]. Temperature has also been reported to increase the electron diffusion coefficient [Nikos, *et al.*, 2006], enhance electron transport and lifetime [Boschloo and Hagfeldt, 2005; Waita, *et al.*, 2007] and increase the conduction and mobility of electrons in the TiO_2 [Greijer-Agrell, 2003; Waita, *et al.*, 2007].

A number of outdoor studies have been carried out and show improved DSSC performance at high irradiance intensity and at elevated temperatures [Katrine, 2008]. The importance of considering outdoor meteorological parameters when characterizing the performance of DSSCs has been emphasized [Cornaro, *et al.*, 2008]. Critical to this, is the understanding of the atmospheric refraction of the incoming solar radiation.

2.6 Atmospheric Refraction of Solar Radiation

Atmospheric refraction causes light from the Sun to take a longer path before reaching the earth's surface than what is expected geometrically. This results from attenuation of the light because of scattering and absorption by aerosols and atmospheric gaseous absorbers like the Ozone (O_3), Oxygen (O_2), precipitable water vapour (H_2O), Nitrogen (N_2) and Carbon dioxide (CO_2). The attenuation varies with the mass of the atmospheric gases and aerosols, which the light encounters on its path from the Sun to the earth's surface. These combined effects of scattering and absorption comprise what is known as atmospheric extinction. The contribution of atmospheric gases and aerosols to atmospheric extinction of solar radiation is articulated through AM studies.

AM is the path length traversed by the direct solar radiation as a ratio of the path traversed to a point at sea level when the sun is directly overhead. It plays a critical role in determining atmospheric refraction of solar radiation [Young, 1994]. Studying how solar radiation is attenuated by the atmosphere in terms of AM, optical thickness and

water vapour is important in understanding how solar devices would perform under various atmospheric conditions. Measurement of solar radiation in the form of global radiation is carried out at a horizontal surface at the concerned latitude.

To maximize the collected solar energy, solar collectors are usually tilted to capture maximum radiation. Optimum tilt angle, and hence J_{ph} are influenced by AM at the particular place [Heinemann, 2000]. A number of formulae have been developed for computing AM. In this work, the method of erecting a vertical post at a place where the shadow of the post is cast on a flat surface has been used. Dividing the length of the hypotenuse of the triangle created of the height of the post (h), its shadow length (s) and the resultant hypotenuse by the height of the post yields AM [Chambers, 1999; Wenham, et. al., 2007]:

$$AM = \left[1 + \left(\frac{s}{h}\right)^2\right]^{1/2}$$

(2.36)

where AM, h are s represent the air mass, height of a post and length of the shadow cast by the post respectively.

When the zenith angle is small, AM is determined using [Wenham, et. al., 2007]:

$$AM = \frac{1}{Cos\,\theta}$$

(2.37)

where AM and θ represent the air mass and the angle from the vertical (zenith) respectively.

Equation (2.37) assumes a homogenous atmosphere and ignores the earth's curvature. The earth is however not flat and equation (2.37) leads to an infinite AM at the horizons. The equation that is used to accurately compute AM, as it takes into account the earth's curvature is [Kasten and Young, 1989]:

- 36 -

$$AM = [Cos\theta + 0.50572\,(96.07995 - \theta)^{-16364}]^{-1}$$

(2.38)

where AM and θ represent the air mass and the solar zenith angle respectively.

2.7 Outdoor Studies on DSSC Devices

Studies on the effect of light levels on DSSC efficiencies have reported improved efficiencies at low light levels [Toyoda, *et al.*, 2004; Hinsch, 2007; Gavin, 2011]. Other studies currently underway include the use of DSSCs in energy-efficient glazing and Building Integrated Photovoltaics (BIPV) [Binions and Dunn, 2012] and testing of various DSSC products for field application [Dyesol, 2012a; Dyesol, 2012b; Greenoptimistic, 2012].

Outdoor studies on DSSCs have not been carried out in Kenya. Fabrication of DSSCs in Kenya has hence been based mainly on theoretical considerations and not on felt concerns arising from field performance characterization of the available DSSC products. This can be linked to the absence of DSSMs on the Kenyan PV market in spite of their reported advantages that can be tapped by the Kenyan solar PV consumers. Outdoor performance characterization of a DSSM at the Department of Physics, University of Nairobi as reported in this work bridges this gap.

CHAPTER THREE
MATERIALS AND METHODS

3.1 Introduction

In this chapter the method used to determine the geographic location of the study site is described, the materials and apparatus used in this work presented, and the relevant experimental set-ups described. The processes used in the calibration of relevant equipment, and in data acquisition have also been explained.

3.2 Materials

One functional dye-sensitized solar module (DSSM) was used in this study. The module; *Omny 11200 outdoor module* - model number HS Code 85414090 was used as supplied by G24 Innovations Limited (UK). It was made up of 11 cells, rated 0.5 W peak and 8 Volts. The overall module thickness (including the encapsulation) was 0.59 cm. The active area of each cell was 15.92 cm^2; bringing the total active area of the module to 175.12 cm^2.

3.3 Equipment and Apparatus

3.3.1 List of equipment and their respective suppliers

The equipment and apparatus used in the study were: a protractor and a metre rule supplied by Textbook Centre Limited (TBC), Kenya, a tilt-able metal rack supplied by Solargent Limited, Kenya, a 6 cm immersion thermometer supplied by Griffin & George Limited, UK, a GTH 1160 NiCr-Ni digital thermocouple sensor supplied by TC limited, UK, a Raytek$^®$ *Plus* laser beam thermometer supplied by Raytek, USA, a CM3-pyranometer supplied by Kipp & Zonen, Delft/Holland, a Haenni solar 130 radiation meter supplied by Jenensfort, Switzerland, a DT9205A* digital multimeter supplied by Taurus Electronics Limited, Kenya, a Tektronix TDS

3032 digital phosphor oscilloscope supplied by Tektronix inc., USA, a Keithley 2400 digital source meter supplied by Keithley inc., USA, a Laboratory Virtual Engineering Workbench (LabVIEW^{TM}) application software supplied by National Instruments inc., USA, a desktop computer supplied by Hewlett-Packard (HP), Kenya and an IEEE-488 GPIB cable supplied by National Instruments inc., USA.

3.3.2 Equipment preparation

All materials and apparatus required for the effective execution of the study were procured, checked and serviced, as was relevant for each, and their performances tested before deployment [Hishikawa, 2008]. The DSSM was purchased, its terminals tested for polarity using the DT9205A' digital multimeter and then appropriately labelled. The active area of the DSSM was computed from its actual dimensions obtained using a meter rule. Information on the DSSM was sought from G24i in line with learnings from previously done work [Hishikawa, *et al.,* 2000; Hishikawa, 2006]. This information included the power output, the operating voltage, the typical V_{oc}, the typical I_{sc}, and the type of semiconductor, dye, electrolyte and electrodes used in the DSSM's fabrication.

3.4 Methods

3.4.1 Determination of the geographic location of the study site

The geographic location (longitude and latitude) of the site for this study (Department of Physics, School of Physical Sciences, University of Nairobi) was determined by zooming in and locating it on the Google maps. The browser bar then gave the site longitude and latitude [Gorissen, 2012]. Latitude is measured from the equator, with positive values going north and negative values going south. Longitude on the other hand is measured from the Prime Meridian (which is the longitude that runs through Greenwich, England), with positive values going east and negative values going west [Ozone Processing Team – NASA/GSFC Code 613.3, 2012].

3.4.2 Calibration of the CM3-pyranometer

The CM3-pyranometer was calibrated using a previously calibrated Haenni solar 130 radiometer. The pyranometer was connected to the DT9205A⁺ digital multimeter and placed on a flat surface close to, and in plane of array with the Haenni Solar 130 Radiometer. Voltage readings by the DT9205A⁺ digital multimeter were validated using a Tektronix TDS 3032 digital phosphor oscilloscope connected in parallel to it. Figure 3.1 presents the block diagram of the calibration set-up.
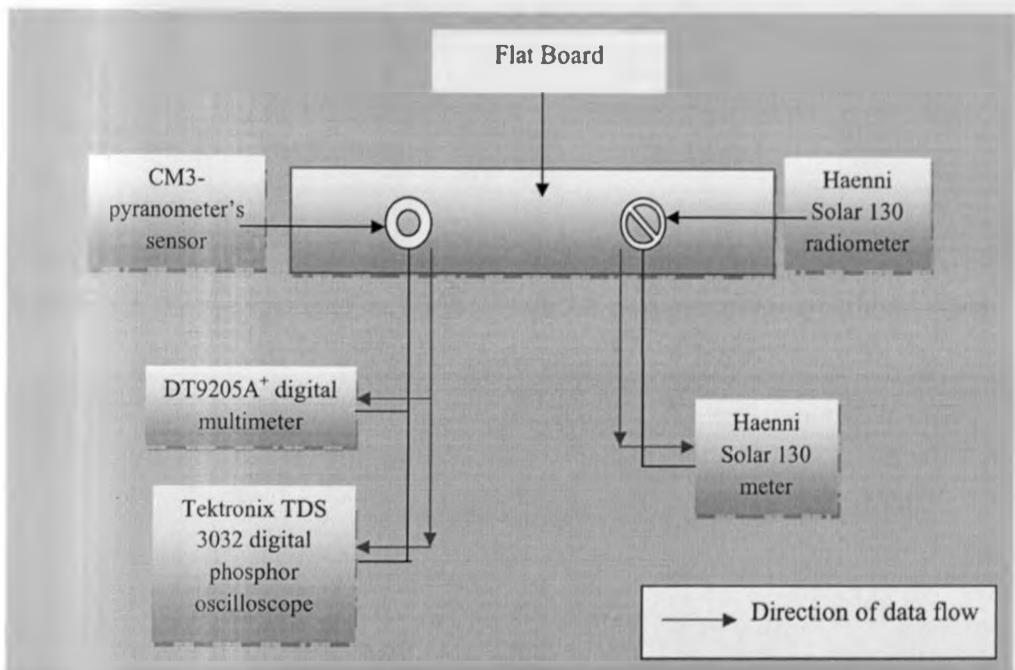
Figure 3.1: Block diagram of the CM3-pyranometer calibration set-up.

Voltage readings from the DT9205A⁺ digital multimeter and the corresponding radiation intensity values as read from the Haenni Solar 130 Radiometer were recorded. These results were confirmed from data obtained through calculations based on the CM3-pyranometer sensitivity of 22.36×10^{-6} $VW^{-1}m^{-2}$ as recorded on the device. The data was used to plot a curve that was used to estimate the radiation intensities relating to the different real-time voltage readings by the DT9205A⁺ digital multimeter.

3.4.3 Dark J-V characterization

Figures 3.2 and 3.3 are the block diagram of the DSSM's dark *J-V* characterization experiment set-up and a photograph of the actual experiment set-up, respectively.
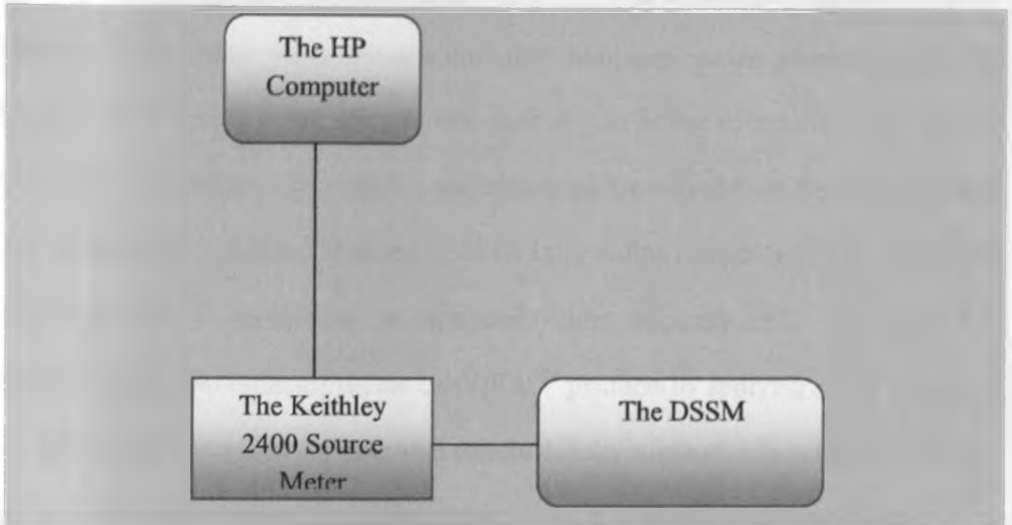
Figure 3.2: Block diagram of the DSSM's dark *J-V* characterization experiment set-up.

Figure 3.3: Photograph of the DSSM's dark *J-V* characterization experiment set-up [The DSSM was not covered when taking this photograph for purposes of visibility. It was however covered during the actual dark *J-V* characterization].

To investigate J_{dark}, the DSSM was connected to the Keithley 2400 source meter using alligator clips. The Keithely 2400 digital source meter was connected via the IEEE-488 GPIB interface to the HP desktop computer. The computer had LabVIEW™ application software previously installed on it. The LabVIEW™ application communicated with the Keithley 2400 source meter through the GBIP hardware via an interface card. The Keithley 2400 source meter drivers were used as part of the communication with the LabVIEW™ application in acquiring and measuring the output from the DSSM, which was stored in the American Standard Code for Information Interchange (ASCII) format. The LabVIEW™ application is described under appendix A2. The dark J-V measurements were obtained via the LabVIEW™ platform by applying a bias voltage to the DSSM and measuring the generated current density automatically using the Keithley 2400 digital source meter. The DSSM's dark J-V data is presented in appendix A3.

3.4.4 Determination of optical air mass and the calibration of the tilt-able metal rack

AM of Chiromo was determined using an upright post. The post was erected at a suitable flat location on the rooftop of the Department of Physics, College of Physical and Biological Sciences (Chiromo Campus), University of Nairobi as illustrated by figure 3.4. The post's height from the surface of the flat location was obtained using a meter rule. The length of the shadow cast by the vertically erected post was measured every hour from 8:00 am to 5:00 pm on three non-consecutive sunny days.

From the data, and using equation (2.36), *AM* values at different times of the day were computed. The computed values for *AM* from equation (2.36) were equated to equation (2.37) to obtain the zenith angle values at the different times. Data on *AM* is presented in appendix A4.
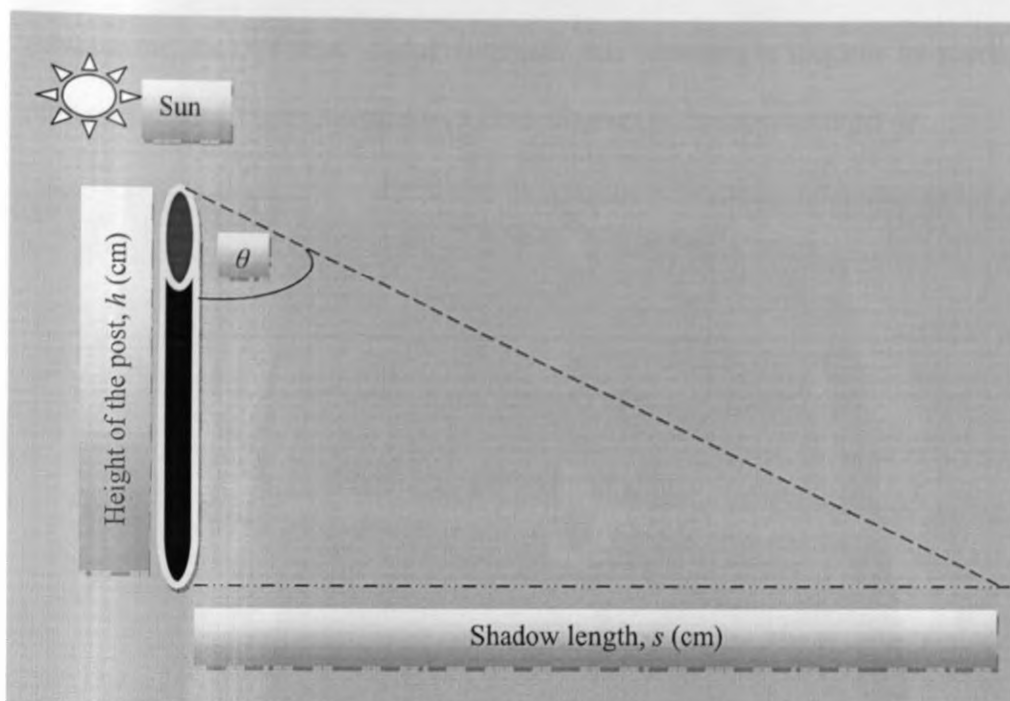
Figure 3.4: Diagram illustration of how *AM* was determined using the shadow of a vertical pole.

3.4.5 J-V characterization of the DSSM under illumination

The DSSM was fixed on the tilt-able metal rack and the CM3-pyranometer positioned in plane of array with the DSSM as illustrated in figure 4.5. The set-up was positioned on the roof-top of the Department of Physics, College of Physical and Biological Sciences (Chiromo Campus), University of Nairobi, at a suitable location where shadows could not be cast on either the DSSM or the CM3-pyranometer, when the experiment was in progress. The DSSM was connected to the Keithley 2400 digital source meter using alligator clips. The Keithley 2400 digital source meter was connected to the HP desktop computer via an IEEE-488 GPIB interface. The computer was pre-installed with LabVIEW™ application software. The *J-V* characteristics for the DSSM under illumination were obtained via the LabVIEW™ Platform. To CM3-the

pyranometer, the DT9205A' digital multimeter was connected to facilitate monitoring of irradiance data. Figure 3.6 presents a block diagram of the experiment set-up.
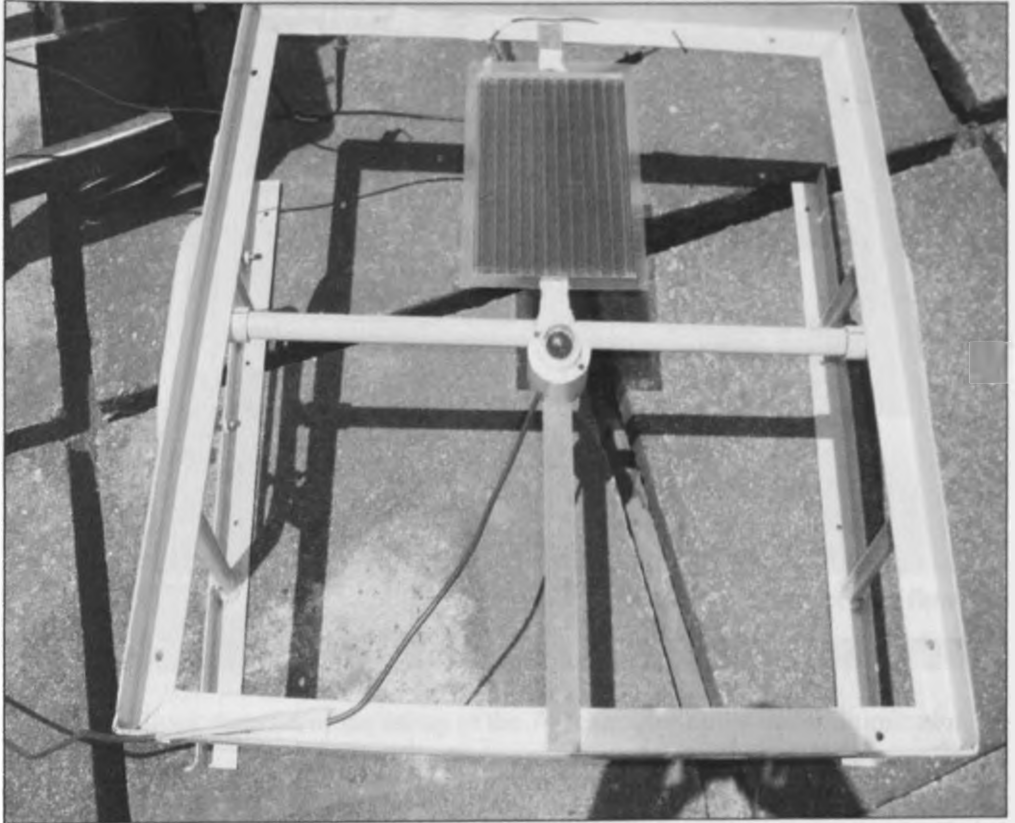
Figure 3.5: Photograph of the DSSM and the CM3-pyranometer set-up on the roof-top.
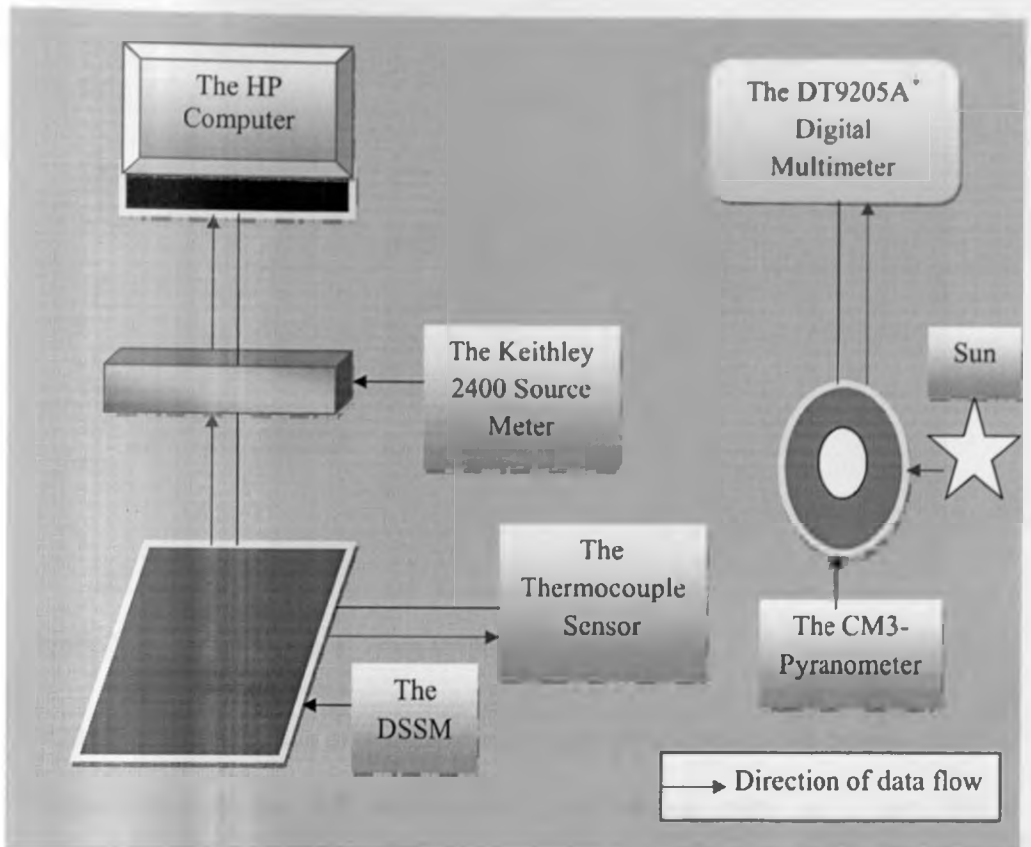
Figure 3.6: Block diagram of the set-up of the *J-V* characterization under illumination.

J-V characteristics were acquired at normal incidence of the incoming solar beam radiation by varying the tilt to coincide with the optimum tilt angle at the period. Optimum tilt angle at the various times of the day were obtained from the *AM versus* optimum tilt angle curve presented in figure 3.7. The curve is based on the *AM* data and the corresponding zenith angles presented in appendix A4. Data on the effect of irradiance intensities on the performance of the DSSM is presented in appendix A5.
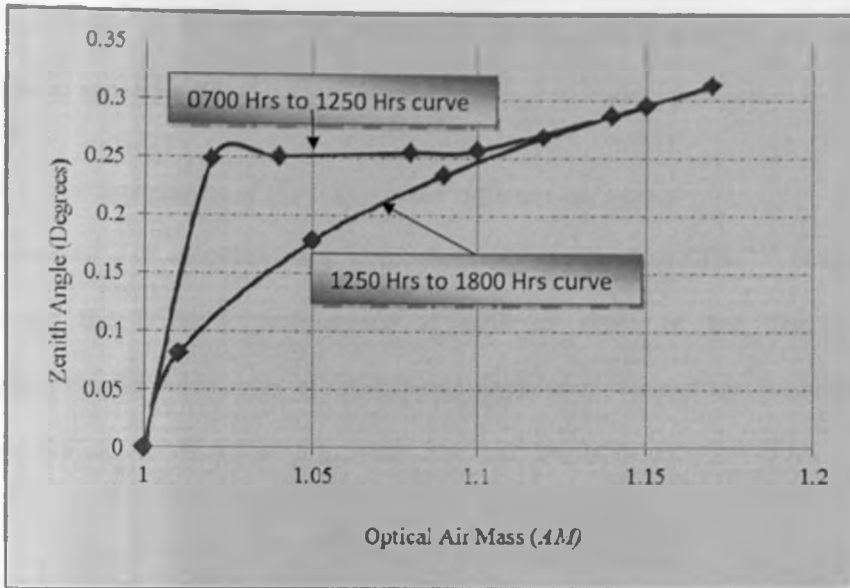
Figure 3.7: Optical air mass *versus* optimum tilt angle curve.

3.4.6 J-V characterisation of the DSSM under different module surface temperatures

Temperature-dependent *J-V* characteristics were obtained with *AM* 1 and 700 to 800 Wm^{-2} irradiance intensity as the reference point. Both the ambient and the DSSM surface temperatures were recorded at the time of the *J-V* data acquisition. Ambient temperatures were measured using the 6 cm immersion thermometer – measurements that were confirmed with those from the Kenya Meteorological Department (KMD).

The DSSM's surface temperatures were obtained by attaching the GTH 1160 NiCr-Ni digital thermocouple sensor to the back side of the DSSM and recording the readings. Readings from the thermocouple sensor were checked by simultaneously pointing a laser beam from the Raytek® *Plus* laser beam thermometer, positioned at a distance of about one meter from the DSSM and perpendicular to the top surface of the DSSM. In this work, the *J-V* measurements were obtained via the LabVIEW™ platform at different DSSM surface temperatures, but at about *AM*1 and 700 – 800 Wm^{-2} irradiance

intensities. Data on the effect of temperature on the performance of the DSSM is presented in appendix A6.

3.4.7 J-V characterisation of the DSSM under different AM values

AM-dependent J-V characteristics were obtained via the LabVIEW™ platform by monitoring the DSSM's performance at different times of the day, and the corresponding AM values. AM at the different times was obtained as illustrated under section 3.4.4.

CHAPTER FOUR

RESULTS AND DISCUSSION

4.1 Introduction

In this chapter, the geographical location of the study site, and the results of the calibration of the CM3-pyranometer are presented. Analyses of the DSSM's characteristics in the dark and under illumination at different *AM* values, irradiance intensities and module surface temperatures are also presented and discussed. A comparison of the DSSM's performance with what is reported of a-Si modules operating under similar weather conditions is also presented.

4.2 The Geographical Location of the Study Site

The global positioning of The Department of Physics, School of Physical Sciences, College of Physical and Biological Sciences, University of Nairobi was found to be 36.81° East and 1.28° South.

4.3 Calibration of the CM3-Pyranometer

The voltage response of the CM3-pyranometer was related to the radiation intensity readings from the Haenni Solar 130 radiometer as illustrated in figure 4.1. The graph for the CM3-pyranometer's response, which is based on the CM3-pyranometer's sensitivity of 22.36×10^{-6} VW^{-1} m-2, also forms part of figure 4.1. The graph based on the CM3-pyranometer's sensitivity was referred to in confirming the experimental results.
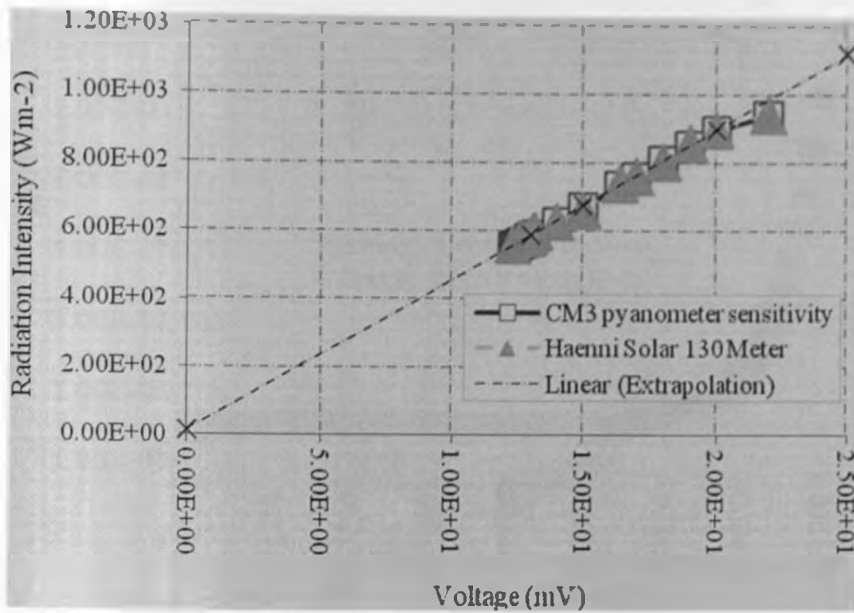
Figure 4.1: Calibration curve for the CM3-pyranometer.

The two graphs, i.e., the one based on the calibrated Haenni Solar 130 radiometer and that which is based on the CM3-pyranometer sensitivity were observed to map onto each other. This affirms the experimental results. Extrapolating the linear section of the curves as illustrated in figure 4.1 resulted in a linear correlation between the voltage readings recorded by the multimeter and the irradiance intensity registered by the calibrated Haenni Solar 130 Meter. The extrapolated curve was therefore used to estimate the irradiance intensity at the various recorded voltages as most of the data was collected at irradiance intensities below one sun.

4.4 The Dark *J-V* Characteristics of the DSSM

Figures 5.2 to 5.5 present the dark *J-V* characteristics for the DSSM. The characteristics were obtained by applying voltage from V = 0 to V = 8 and from V = 8 to V = 0 sweep directions, at 2.5 to 25 seconds sweep times. The dark *J-V* characteristics show that at lower biases, the non-ohmic shunt current-density (J_{sh}) dominates while at higher biases, the exponential; diode current-density (J_D) takes over, such that, $J_{dark} = J_{sh} + J_D$.
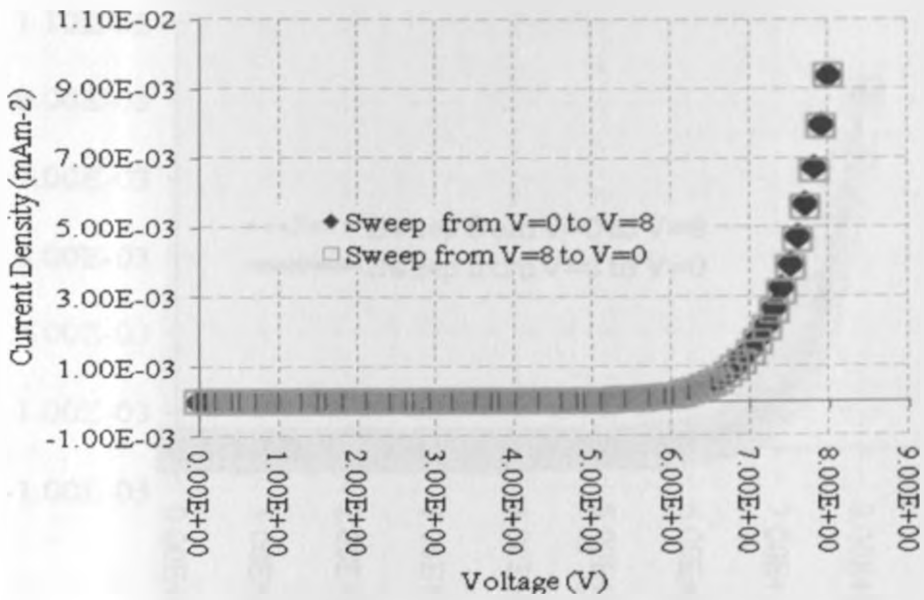
Figure 4.2: The dark J-V characteristics of the DSSM for sweeps from $V = 0$ to $V = 8$ and from $V = 8$ to $V = 0$ at 2.5 seconds.
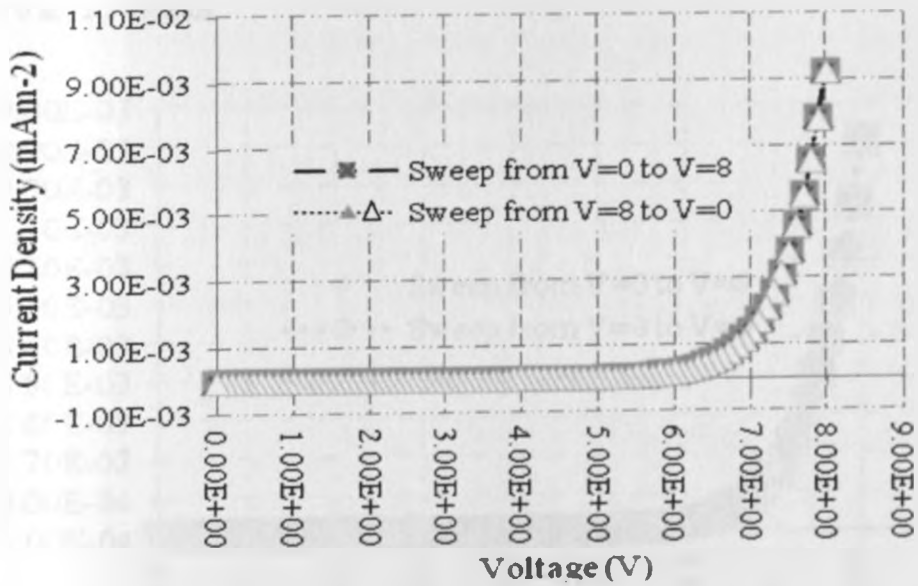
Figure 4.3: The dark J-V characteristics for the DSSM for sweeps from $V = 0$ to $V = 8$ and from $V = 8$ to $V = 0$ at 5 seconds.
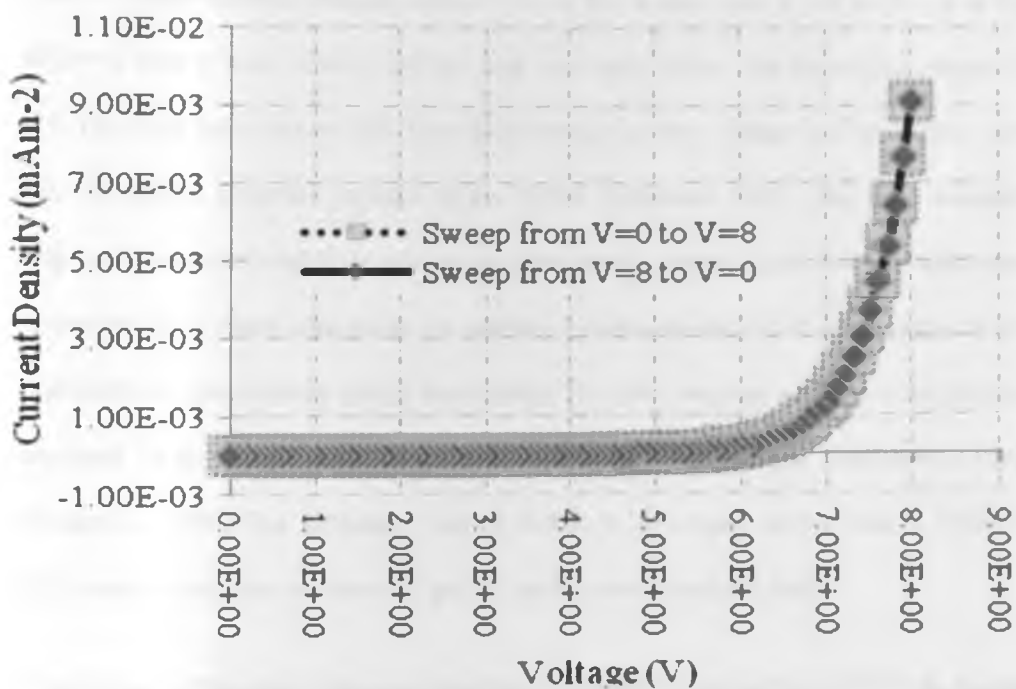
Figure 4.4: Dark *J-V* characteristics for sweeps from V = 0 to V = 8 and from V = 8 to V = 0 at 12.5 seconds.
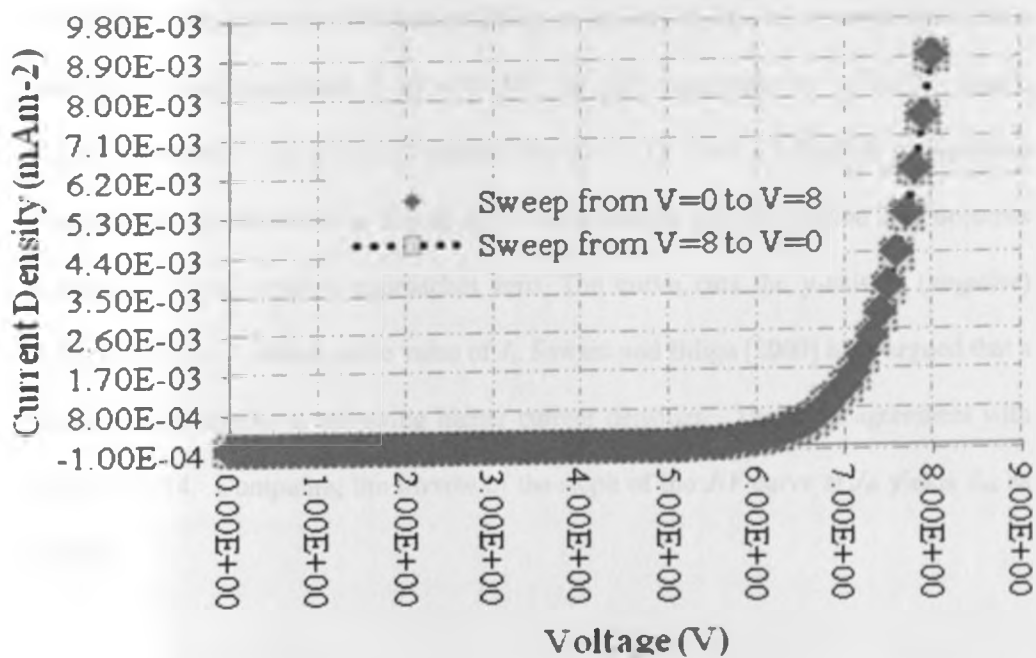
Figure 4.5: Dark *J-V* curves for sweeps from V = 0 to V = 8 and from V = 8 to V = 0 at 25 seconds.

The J-V characteristics obtained from V = 0 to V = 8 and from V = 8 to V = 0 at the different sweep times show a perfect map onto each other. The behaviour points to: (1). The reproducibility of data from high voltage to low voltage and vice versa, and (2). The quick temporal response of the DSSM [Hishikawa, 2006]. The quick temporal response can be attributed to the thin nature of the module, which implies few trap states were present in the semiconductor, hence the electrons injected into the CB do not get trapped, but contribute to current-density output immediately. The quick response contradicts the findings obtained using DSSC samples prepared by Pioneer Corporation [Hishikawa, 2006; Hishikawa, 2008]. The difference can be linked to the rapid innovations in DSSCs' fabrication techniques and product quality that this work benefitted from.

Data for any of the sweep times could therefore be used in determining the DSSM's R_s, R_{sh} and J_s, which dictate its electrical performance. To extract J_s, R_s and R_{sh} data relating to the 2.5 seconds sweep time was used. This is because improved sensitivity for R_s is determined at higher values of current [King, et al., 1997]. The 2.5 seconds sweep time had the highest measured J of 9.42×10^{-3} mAcm^{-2} compared to 9.27×10^{-3} Acm^{-2}, 9.13×10^{-3} mAcm^{-2} and 8.95×10^{-3} mAcm^{-2} for the 5, 12.5 and 25 seconds sweep times respectively. As illustrated by figure 4.6, the exponential part of equation 2.13 becomes a straight line as voltage approaches zero. The curve cuts the y-axis at (negative) 7.53×10^{-7} mAcm^{-2}, which is the value of J_s. Sawant and Biliga [2000] have argued that a lower J_s is desirable in achieving higher current densities. This is in agreement with equation 2.14. Computing the inverse of the slope of the J-V curve at J_{sc} yields R_{sh} as infinity.
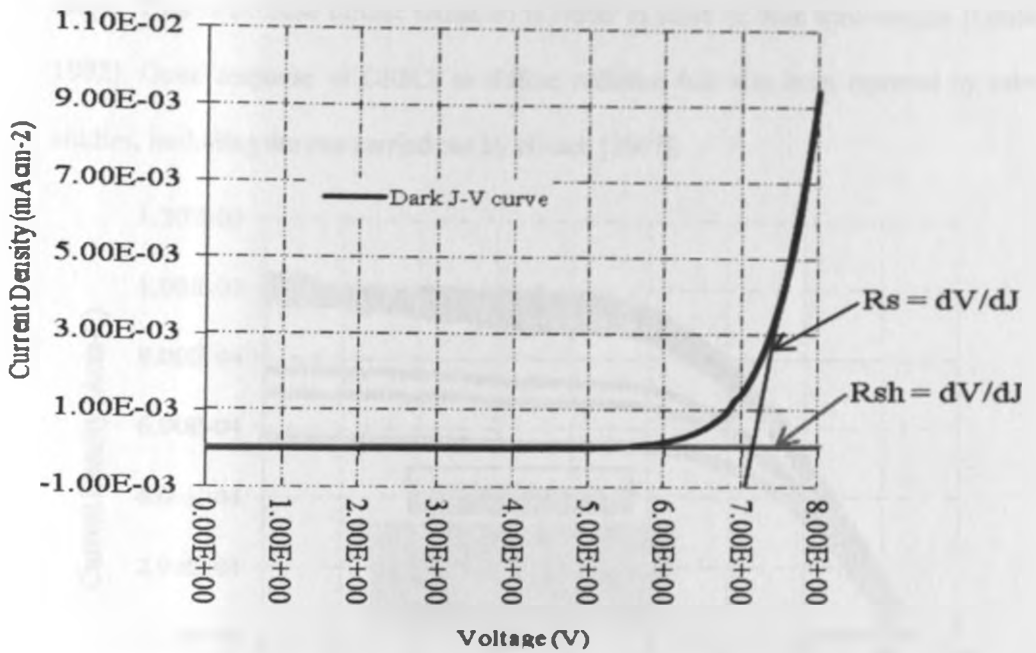
Figure 4.6: The dark *J-V* characteristics of the DSSM with illustration on how J_s, R_s and R_{sh} for the DSSM were obtained.

The high R_{sh} obtained of the DSSM is good when compared to a-Si PV devices that are known to have low R_{sh} of as little as $10.5 - 11.5\Omega$ [Ghoneim, *et al.*, 2011]. R_s was obtained by computing the inverse of the slope of the *J-V* curve at V_{oc} and found to be $0.1\ \Omega$.

4.5 *AM*-dependence of the DSSM's *J-V* Characteristics

Figure 5.7 presents the *J-V* characteristics of the DSSM obtained between *AM* 1 and *AM* 1.09. J_{sc} measured between *AM* 1 and 1.09 ranged from 1.04×10^{-3} Acm^{-2} to 7.69×10^{-4} Acm^{-2}. The maximum power point (P_{mpp}) reduced as values of *AM* increased. This can be linked to the increase in irradiance intensity at lower *AM* values, which affected the voltage-controlled portion of the *J-V* curve by reducing R_s. This shows that increase in *AM* favourably affected the DSSM, since smaller R_s values for solar PV devices are usually good [National Instruments, 2009]. It further shows that the DSSM responded well to short wavelength radiation or diffuse radiation in the 200 – 300 nm

range. This is because diffuse radiation is richer in short or blue wavelengths [Green, 1992]. Good response of DSSCs to diffuse radiation has also been reported by other studies, including the one carried out by Hinsch [2007].
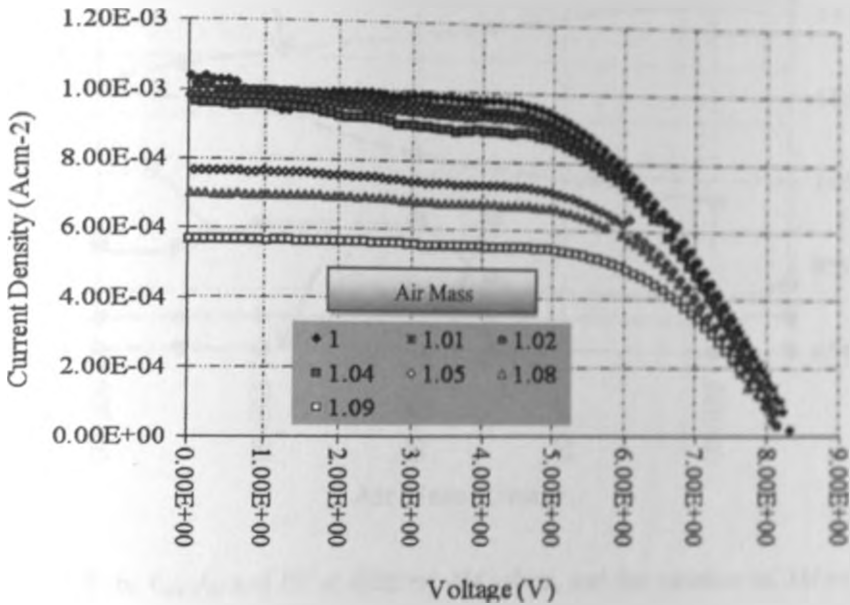
Figure 4.7: *J-V* characteristics for the DSSM at different values of air mass (*AM*).

Table 4.1 shows how V_{oc}, J_{sc}, *FF* and η varied with *AM*. The table supports the analyses by figure 4.8.

Table 4.1: Variation in the DSSM's V_{oc}, J_{sc}, *FF* and η at different times and *AM*.

AM	1	1.01	1.02	1.04	1.05	1.08	1.09
Time (Hrs)	1245	1300	1200	1100	1400	1000	1500
V_{oc} (V)	8.31	8.24	8.09	8.07	8.32	8.07	8.14
J_{sc} (Acm^{-2}) x10^{-3}	1.04	1.01	9.84	9.66	7.84	7.69	5.68
FF	0.51	0.52	0.57	0.56	0.56	0.47	0.63
η (%)	1.77	1.75	1.88	2.26	1.27	1.06	1.19
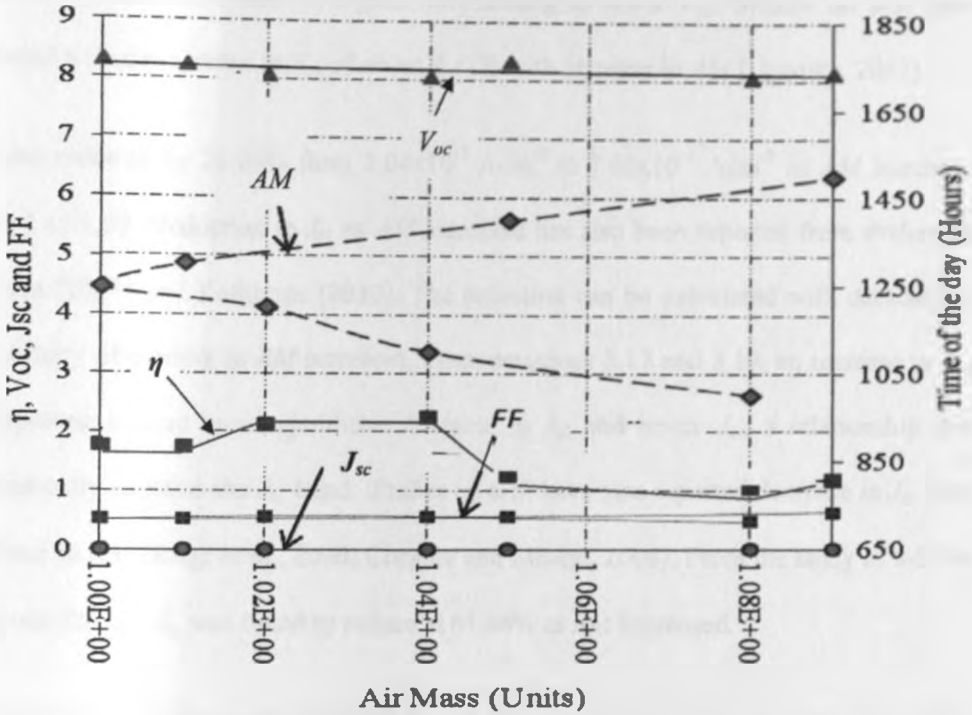
Figure 4.8: η, V_{oc}, J_{sc} and FF at different AM values, and the variation of AM values at different times of the day.

As can be observed from figure 5.8, V_{oc} reduced linearly by 2.05% from 8.31 V at AM 1 to 8.14 V at AM 1.09. Studies by Rijnberg [1998] have also reported decay of V_{oc} at higher AM values. This can be attributed to reduction in photo-generation at higher AM resulting mainly from attenuation of the effective component of the radiation, which is necessary for PV effect. This inference is based on studies that have reported reduced irradiance intensities at higher AM [Meinel and Meinel, 1976].

Apart from atmospheric attenuation due to Rayleigh scattering, scattering by aerosols and atmospheric absorption through constituent gases (oxygen, ozone, water vapour and carbon dioxide), the power of incident light (P_{in}) reduces also due to the longer optical path that it travels through the atmosphere to reach the earth's surface at higher AM [Antón, et al., 2009]. The density of electrons that get photo-ejected to conduct

electricity, therefore reduce at higher AM, leading to lower V_{oc}. Studies on a-Si have reported a linear increase in V_{oc} of about 2.12% with increase in AM [Ugwoke, 2012].

J_{sc} also reduced by 26.06% from $1.04\text{x}10^{-3}$ Acm^{-2} to $7.69\text{x}10^{-4}$ Acm^{-2} as AM increased from 1 to 1.09. Reduction in J_{sc} as AM increased has also been reported from studies by Katrine [2008] and Katherine [2010]. The reduction can be associated with decrease in the density of carriers as AM increases. From equations 3.17 and 3.19, an increase in V_{oc} is expected to lead to a logarithmic decrease in J_{ph} and hence J_{sc}; a relationship that theoretically explains the J_{sc} trend. Studies on a-Si have also reported decrease in J_{sc} with increase in AM [King, et al., 2000; Chagaar and Mialhe, 2008]. From the study of a-Si by Ugwoke [2012], J_{sc} was found to reduce at 61.84% as AM Increased.

The DSSM's FF increased by 19.05% from 0.51 at AM 1 to 0.63 at AM 1.09. This points to the DSSM's favourably response to shorter wavelength radiation. Short wavelength radiation, ranging between 200 – 300 µm is prevalent at higher AM. The reduction in V_{oc} and J_{sc} led to this increase as is confirmed by equation 3.21. Studies on a-Si by Ugwoke [2012] have shown a reduction of 41.94% in FF with increase in AM.

Closely associated with FF, V_{oc} and J_{sc} by equation 3.25 η. η increased by 27.68% from 1.77% to 2.26% as AM increased from 1 to 1.04, and then reduced to 1.27%, 1.06% and 1.19% at AM values of 1.05, 1.08 and 1.09 respectively. This agrees with studies by Hinsch [2007]. The behaviour can be attributed to the good response of the DSSM to low wavelength radiation as well the increase in FF. On their part, a-Si PV modules are reported to have a narrow spectral response and do not perform well in the red rich part of the spectrum [Chianese, et al., 2011]. Other studies on a-Si have reported decrease in η as AM increases [Chagaar and Mialhe, 2008; Ugwoke, 2012] with Ugwoke [2012] reporting a decrease of 29.17% as AM increased.

In figure 4.9 performance of the DSSM in the morning hours (0650 – 1200 hours) as compared to the afternoon hours (1201 to 1850 hours) is illustrated.
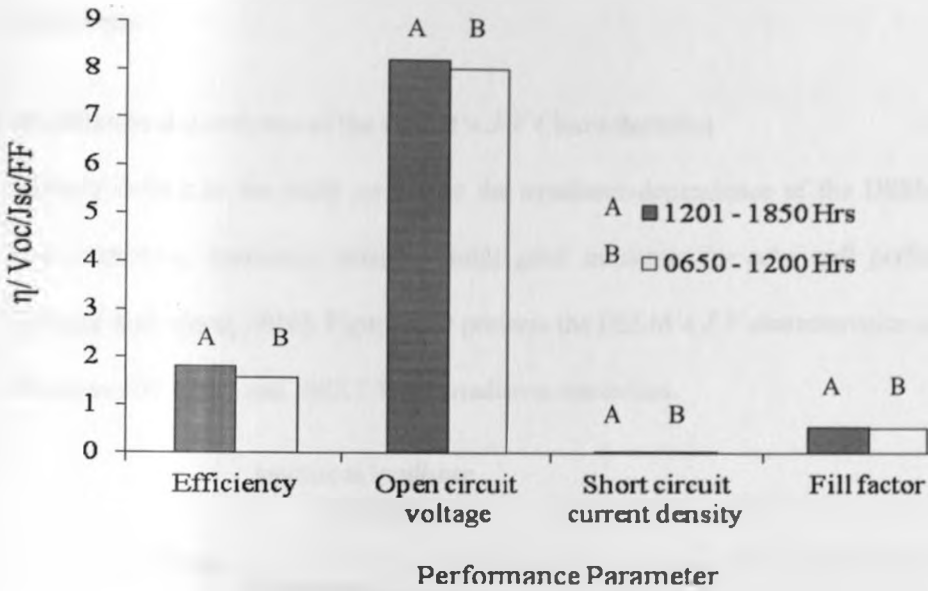
Figure 4.9: Comparative performance of the DSSM in the morning (0650 – 1200 hours) and in the afternoon (1201 – 1850 hours).

Better performance was observed during the afternoon than morning hours. This can be attributed to presence of more atmospheric gaseous absorbers like H_2O, O_2, O_3 and CO_2 during the morning than afternoon hours [Louche, *et al.*, 2000]. These lead to increased atmospheric turbidity and Rayleigh scattering in the morning than in the afternoon hours, resulting in the extinction of solar beams [Kasten and Young, 1989; Hahn, 2009].This affects *AM* values by varying the intensity of the direct component of sunlight [Thavasi, *et al.*, 2009].

a-Si PV modules have a stronger dependence on irradiance than the DSSM. They peak their performance closer to *AM* 1, when irradiance is highest [Jensen, 2008]. As *AM* influences both the intensity and spectral distribution of the solar beam reaching the earth's surface [Nayaab, *et al.*, 1983], an understanding of irradiance-dependence of the

DSSM as compared to an a-Si module as presented in the next section will be helpful in further analysis of the two technologies in respect of the Kenyan outdoor weather conditions.

4.6 Irradiance-dependence of the DSSM's *J-V* Characteristics

Closely linked to the study on *AM* is the irradiance-dependence of the DSSM's *J-V* characteristics. Irradiance intensity holds great influence for solar cell performance [Dinçer and Meral, 2010]. Figure 5.10 presents the DSSM's *J-V* characteristics acquired between 653 Wm^{-2} and 1095.7 Wm^{-2} irradiance intensities.
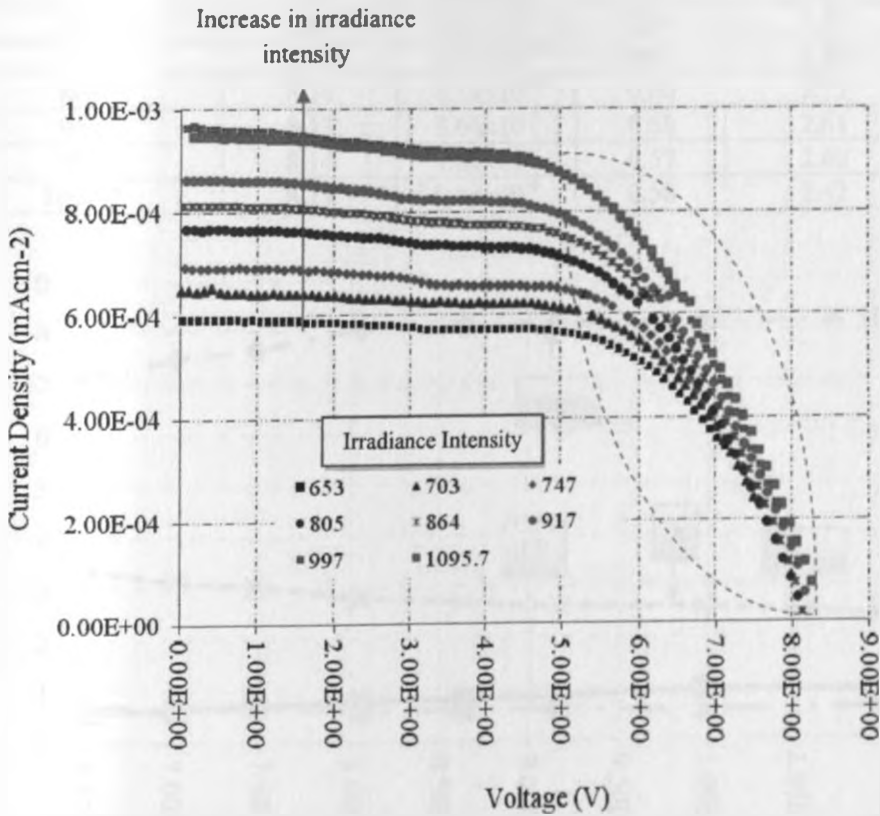
Figure 4.10: *J-V* characteristics of the DSSM at different irradiance intensities.

As observed from figure 4.10, the voltage-controlled sections of the *J-V* characteristics, (the section in a dashed green oval shape) shift away from the origin and become steeper in slope as irradiance intensity increases. This signifies a reduction in R_s as

- 58 -

irradiance intensity increases, which is good for a PV device as it signifies reduction in the bulk resistance of the semiconductor used in the fabrication of the device and of the contacts of the device [Mwabora, 1999]. The J-V characteristics also show how J_{sc} significantly dependents on irradiance intensity. Table 4.2 and figure 4.11 present analyses of how the DSSM's V_{oc}, J_{sc}, FF and η varied with irradiance intensity.

Table 4.2: Variation of the DSSM's V_{oc}, J_{sc}, FF and η at different irradiance intensities.

Irradiance Intensity (Wm^2)	V_{oc} (V)	J_{sc} (Acm^{-2})	FF	η $(\%)$
653	7.12	5.92×10^{-4}	0.73	3.39
703	7.50	6.50×10^{-4}	0.67	3.14
747	7.65	6.93×10^{-4}	0.66	3.07
805	8.07	7.69×10^{-4}	0.60	2.80
864	8.14	8.14×10^{-4}	0.60	2.73
917	8.17	8.66×10^{-4}	0.58	2.61
997	8.14	9.66×10^{-4}	0.57	2.60
1095.7	8.19	9.48×10^{-4}	0.58	2.42
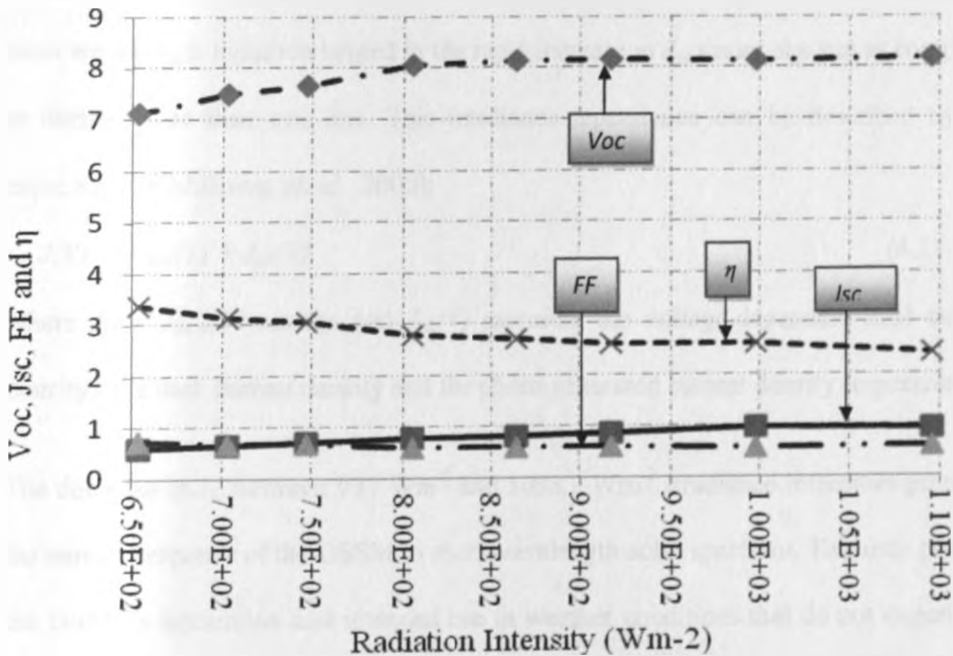
Figure 4.11: Illustration of how V_{oc}, J_{sc}, FF and η vary with irradiance.

From table 4.2 and figure 4.11, V_{oc} for the DSSM increased linearly by 11.94% between 7.12 V and 8.07 V from 653 Wm^{-2} to 805 Wm^{-2}. Between 805 Wm^{-2} and 1095.7 Wm^{-2} irradiance intensities, increase in V_{oc} slowed by 1.49% to 8.19 V. This affirms the discussion under the DSSM's *AM* response, that the DSSM favoured low irradiance intensities. Reports from studies on a-Si modules at varying irradiance intensities show that V_{oc} decreases by about 2.07% with increase in irradiance intensity [Ugwoke, 2012].

The DSSM's J_{sc} increased linearly by 64.41% between 5.92x10^{-4} Acm^{-2} and 9.66x10^{-4} Acm^{-2} from 653 Wm^{-2} to 997 Wm^{-2} irradiance intensities. From 997 Wm^{-2} to 1095.7 Wm^{-2} irradiance intensities, J_{sc} decreased linearly by 2.06% between 9.66x10^{-4} Acm^{-2} and 9.48x10^{-4} Acm^{-2} as can be observed from table 4.2 (since the decrease was minimal, it can insignificantly be observed from figure 4.11). The increase in J_{sc} between 653 Wm^{-2} and 997 Wm^{-2} can be attributed to increased photo-generation with increase in irradiance intensity. It is also believed that the good spectral response of the DSSM to short wavelength radiation helped in the rapid increase in J_{sc} under one sun as compared to during more than one sun. This irradiance-dependence can be described by the expression [Hishikawa, *et. al.*, 2000]:

$$J(V) = J_{dark}(V) + J_{ph}(V) \qquad\qquad (4.1)$$

where $J(V)$, $J_{dark}(V)$ are the and $J_{ph}(V)$ represent the voltage-dependent total current density, the dark current density and the photo-generated current density respectively.

The decrease in J_{sc} between 997 Wm^{-2} and 1095.7 Wm^{-2} irradiance intensities points to the narrow response of the DSSM to short wavelength solar spectrum. This may point to the DSSM's fabrication and intended use in weather conditions that do not experience more than one sun. Recent studies on a-Si have reported a 162.07% increase in J_{sc} at irradiance intensities of between 300 Wm^{-2} and 1000 Wm^{-2} [Ugweko, 2012].

FF of the DSSM showed a 20.55% linear improvement of between 0.58 and 0.73 as irradiance intensity reduced from 1095.7 Wm to ^{2}653 Wm^{-2}. The increase in *FF* as irradiance intensity reduced can be linked to the reduction in charge leakages under low irradiance intensities, mainly due to low incidences of recombinations, and resistance in charge transfer. In a-Si PV modules, *FF* has been reported to increase by 125.70% between 300 Wm^{-2} and 600 Wm^{-2} irradiance intensities and to reduce by 23.69% between 600 Wm^{-2} to one sun [Ugwoke, 2012].

The DSSM's η increased linearly by 5.74% from 4.70% to 4.97% as irradiance intensity increased from 653 Wm^{-2} to 747 Wm^{-2}, after which it reduced linearly by 8.65% to 4.54% as irradiance intensity increased from 747 Wm^{-2} to 1095.7 Wm^{-2}. The initial increase can be linked to the influence of increase in V_{oc}, J_{sc} and *FF* as irradiance intensity increased to 747 Wm^{-2} as shown by equation 2.25. Similar results have been reported by a number of studies [Jensen, 2008; Dinçer and Meral, 2010]. The decrease observed after the 747 Wm^{-2} irradiance intensity can be linked to, as illustrated by equation 2.25, the decrease in V_{oc}, J_{sc} and *FF* at high radiation intensities.

Studies on a-Si modules have reported η to increase as irradiance intensity increases. This is because of the strong irradiance-dependence of V_{oc} and J_{sc} [Ghonein, *et al.* 2011; Katrine, 2008; Jensen, 2008]. Reports from studies on a-Si by Ugwoke [2012] show the increase in η observed between 300 Wm^{-2} and 600 Wm^{-2} irradiance intensities to be 80.95%, and a reduction of 26.72% observed between 600 Wm^{-2} irradiance intensity and one sun.

4.7 Temperature-dependence of the DSSM's *J-V* Characteristics

The surface temperature of a solar cell affects the speed of reactions within the cell [Dinçer and Meral, 2010]. Figure 4.12 presents the *J-V* characteristics for the DSSM

obtained between 31.6°C and 43.8°C module surface temperatures. From the figure, V_{oc} is observed to be strongly influenced by temperature unlike J_{sc}. As the DSSM voltage increased from short circuit condition, the J-V characteristics became steeper at J_{sc} as temperature increased. Steeper slopes signify reduced R_{sh}. Table 5.3 and figure 5.13 present analyses on the module surface temperature effect on the DSSM's V_{oc}, J_{sc}, FF and η.
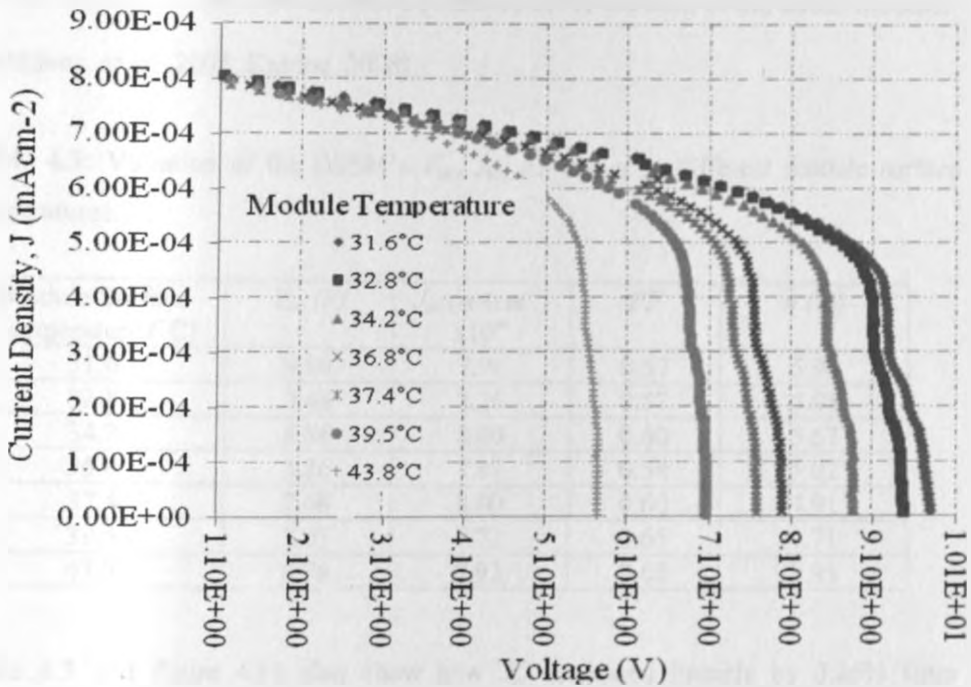
Figure 4.12: J-V characteristics of the DSSM at different module surface temperatures.

As can be observed from table 4.3 and figure 4.13, V_{oc} decreased linearly by 41.22% from 9.80 V to 5.76 V as the DSSM surface temperature increased from 31.6°C to 43.8°C. A change of -0.33 V/°C was observed. The decrease in V_{oc} with increase in temperature can be attributed to changes in charge carrier trapping and recombination centres that cause changes in charge distribution, coupled with the entropy that results from more atoms getting into excited states as temperature increases [Clement and Quinnel, 1952]. An increase in resistivity to charge transport through the semiconductor

nanoparticle network causes some of the electrons already injected into the CB of the semiconductor to migrate back to the HOMO level of the dye molecules or to the electrolyte as illustrated by steps (b) and (c) in figure 2.5 on page 28, due to electron trapping effects. This results in recombinations described by equations 2.34 and 2.35 and respectively. The decrease could also be as a result of radiative external quantum efficiency (REQE) [Martin, 2003]. Studies on a-Si have reported a decrease in V_{oc} as module surface temperature increased [Carlson, 1977; Carlson, *et al.*, 2000; Meneses-Rodríguez, *et al.*, 2005; Katrine, 2008].

Table 4.3: Variation of the DSSM's V_{oc}, J_{sc}, *FF* and η at different module surface temperatures.

Module Surface Temperature (˚C)	V_{oc} (V)	J_{sc} (mAcm^{-2}) x10^{-4}	FF	η (%)
31.6	9.80	7.98	0.57	5.94
32.8	9.48	8.26	0.57	5.95
34.2	8.86	8.00	0.60	5.67
36.8	8.86	7.87	0.54	5.02
37.4	7.68	8.00	0.60	4.91
39.5	7.05	7.72	0.65	4.71
43.8	5.76	7.92	0.65	3.95

Table 4.3 and figure 4.13 also show how J_{sc} decreased linearly by 3.26% from 7.98x10^{-4} Acm^{-2} to 7.72x10^{-4} Acm^{-2} as the DSSM surface temperature increased from 31.6˚C to 43.8˚C. The change was at the rate of -2.13x10^{-6} Acm^{-2}˚C^{-1}. This can be attributed to the kinetics of the catalytic reactions at the CE [Thavasi, *et al.*, 2009]. It was not clear whether the DSSM's CE had been coated with a layer of platinum to improve J_{sc} (as G24i was not willing to disclose the materials used in fabricating the DSSM). Studies on the temperature-dependence of J_{sc} in a-Si PV modules operated outdoors have shown negligible or no variation as temperature changed [Katrine, 2008]. Theoretically, however, J_{sc} for a-Si PV modules is expected to increase with increase in

temperature due to the decrease in the band gap and the corresponding band-to-band absorption coefficient across the solar spectrum [Martin, 2003].
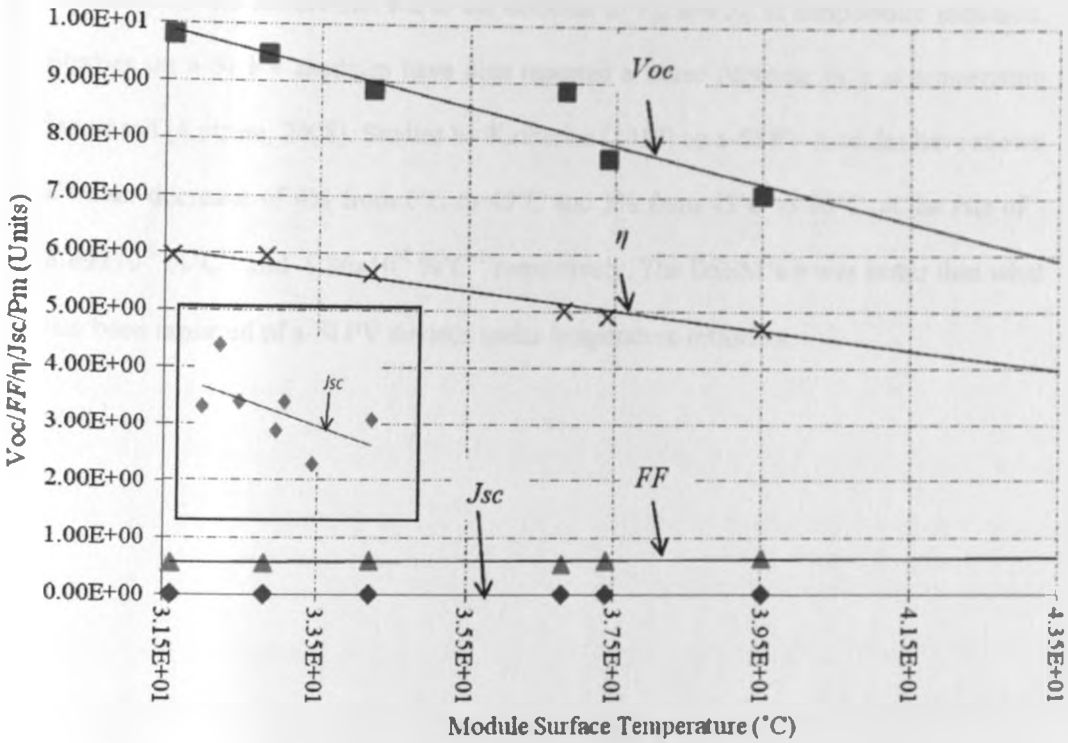
Figure 4.13: Relationship of *FF*, V_{oc}, η, J_{sc}, and P_m as functions of the DSSM surface temperature. [Inset is the relationship for J_{sc}, as a function of the DSSM surface temperature as the change was too small to be observed at the scale of the main figure].

The DSSM's *FF* increased by 14.04% from 0.57 to 0.65 as the DSSM surface temperature increased from 31.6°C to 43.8°C. The rate of change was 6.56×10^{-3} °C^{-1}. The increase can be attributed to an increase in E_F of the semiconductor as the DSSM surface temperature increased. This detrapped electrons from the trap states below the semiconductor's CB edge. *FF* from studies on a-Si PV devices have indicated a negative temperature dependence [Katrine, 2008], with studies by Katherine [2010] reporting a decrease of 14.29% from 0.64 to 0.56 as the module surface temperature increased from 45°C to 122°C. This puts the change to -1.04×10^{-3} °C^{-1}. The DSSM's *FF* temperature-dependence was better than what has been reported of a-Si PV devices.

- 64 -

η decreased linearly by 33.50% from 5.95% to 3.95% as the DSSM surface temperature increased from 31.6°C to 43.8°C. The rate of change was -1.63×10^{-1} %°C^{-1}. This can be attributed to the factors that led to the decrease in V_{oc} and J_{sc} as temperature increased. Studies on a-Si PV modules have also reported a linear decrease in η as temperature increased [Katrine, 2008]. Studies by Katherine [2010] on a-Si PV modules have shown a linear decrease of 4% from 0°C to 45°C and 3% from 45°C to 80°C, at the rate of -8.89×10^{-2} %°C^{-1} and -8.86×10^{-2} %°C^{-1} respectively. The DSSM's η was better than what has been reported of a-Si PV devices under temperature influence.

CHAPTER FIVE

CONCLUSION AND RECOMMENDATIONS

5.1 Conclusion

This thesis has presented detailed experimental results showing how an Omny 11200 outdoor DSSM's V_{oc}, J_{sc}, FF and η were affected by AM, irradiance intensity as well as module surface temperatures. A comparison of the DSSM's performance with what is reported of a-Si modules is also presented.

The results showed that the DSSM's V_{oc} reduced linearly by 2.05% from 8.31 V to 8.14 V as AM increased from 1 to 1.09. Studies on a-Si have reported an increase in V_{oc} of about 2.12% with increase in AM. The DSSM's J_{sc} reduced linearly by 26.06% from 1.04×10^{-3} Acm^{-2} to 7.69×10^{-4} Acm^{-2} as AM increased from 1 to 1.09. Studies on a-Si have reported a linear reduction in J_{sc} of 61.84% with increase in AM. The DSSM's FF increased linearly by 19.05% from 0.51 to 0.63 as AM increased from 1 to 1.09. Studies on a-Si have reported a reduction of 41.94% in FF with increase in AM. The DSSM's η increased by 27.68% from 1.77% to 2.26% as AM increased from 1 to 1.04, and then reduced to 1.27%, 1.06% and 1.19% at AM values of 1.05, 1.08 and 1.09 respectively. Studies on a-Si have reported a 29.17% decrease in η with increase in AM. The DSSM performed better under AM considerations as compared to what is reported of a-Si PV devices.

With respect to irradiance intensity, the DSSM's V_{oc} increased linearly by 11.94% from 7.12 V to 8.07 V as irradiance intensity increased from 653 Wm^{-2} to 805 Wm^{-2}. V_{oc} then reduced linearly by 1.49% from 8.07 V to 8.19 V as irradiance intensity increased from 805 Wm^{-2} to 1095.7 Wm^{-2}. Studies on a-Si have reported a 2.07% decrease in V_{oc} with increase in irradiance intensity. The DSSM's J_{sc} increased linearly by 64.41% from

5.92 x 10^{-4} Acm^{-2} to 9.66x10^{-4} Acm^{-2} as irradiance intensity increased from 653 Wm^{-2} to 997 Wm^{-2}. J_{sc} then reduced linearly by 2.06% from 9.66x10^{-4} Acm^{-2} to 9.48x10^{-4} Acm^{-2} as irradiance intensity increased from 997 Wm^{-2} to 1095.7 Wm^{-2}. Studies on a-Si have reported a 162.07% increase in J_{sc} with increase in irradiance intensity. The DSSM's FF reduced linearly by 20.55% from 0.73 to 0.58 as irradiance intensity increased from 653 Wm^{-2} to 1095.7 Wm^{-2}. In a-Si PV modules, FF is reported to reduce by 23.69% between 600 Wm^{-2} and One Sun. The DSSM's η increased by 5.74% from 4.70% to 4.9% as irradiance intensity increased from 653 Wm^{-2} to 747 Wm^{-2}. It then reduced linearly by 8.65% from 4.9% to 4.54% as irradiance intensity increased from 747 Wm^{-2} to 1096.7 Wm^{-2}. In a-Si PV modules, η has been reported to reduce by 26.72% between 600 Wm^{-2} irradiance intensity to one Sun. The DSSM performed better under varying irradiance intensities as compared to what is reported of a-Si PV devices.

The DSSM's V_{oc} showed a temperature dependence of -0.33 V˚C^{-1} with linear decrease in V_{oc} of 41.22% observed from 9.80 V to 5.76 V as the module surface temperature increased from 31.6˚C to 43.8˚C. Studies on a-Si have reported a V_{oc} temperature dependence of -0.059 V˚C^{-1}. The DSSM's J_{sc} linearly decreased by 3.26% from 7.98x10^{-4} Acm^{-2} to 7.92x10^{-4} Acm^{-2} as the DSSM's surface temperature increased from 31.6˚C to 43.8˚C. A temperature dependence of -4.92x10^{-7} Acm^{-2}˚C^{-1} was observed. Studies on a-Si PV modules have reported no temperature dependence of J_{sc}. FF for the DSSM increased linearly by 14.04% from 0.57 to 0.65 as the DSSM's surface temperature increased from 31.6˚C to 43.8˚C. A temperature dependence of 6.56x10^{-3}˚C^{-1} was observed. Studies on a-Si modules have reported a linear reduction in FF by 14.29% observed from 0.56 to 0.64 between 45˚C to 122˚C. A FF temperature dependence of -1.04x10^{-3}˚C^{-1} was also observed of the DSSM. The DSSM's η

decreased linearly by 33.50 % from 5.95 % to 3.95 % as its surface temperature increased from 31.6°C to 43.8°C. A temperature dependence of -1.63×10^{-1} %°C^{-1} was observed. Studies on a-Si PV modules have also reported a linear decrease in η and a temperature dependence of -8.89×10^{-2}%°C^{-1}. The DSSM performed better under different module surface temperatures as compared to what is reported of a-Si PV devices.

The DSSM therefore performed better than what is reported of a-Si PV modules. The DSSM's good performance under low irradiance intensity as well as its improved performance under a combination of high irradiance intensity and temperatures makes it a promising technology for widespread application in Kenya. The low-cost consideration further enhances the favourable prospects for the DSSC technology.

5.2 Recommendations

5.2.1 Up scaling the use of DSSCs in Kenya

This research has established the potential inherent in DSSCs towards unlocking the energy challenge, especially for the majority of Kenyans that cannot access energy because of its high cost. The following is recommended to spur scale up in DSSC work and uptake of the technology in Kenya:

- At policy level, including the Ministry of Energy, learning institutions and other macro and meso-level actors in the area of energy: To provide leadership by establishing clear bench-marks towards renewable energy use, e.g., by 2030, every department of government, learning institution or organization to have, at least 30% of its power consumption from renewable sources. Lobbying and advocacy for this can be done with the International Organization of Standardization (ISO) to include use of renewable energy as part of its evaluation bench-marks. To implement this, 'smart meters' that can show how much of the conventional power is consumed in a

building as compared to the power from renewable energy sources should be introduced.

- Based on the above, households are expected to pick cue from the leadership of government, learning institutions and other macro and meso-level actors. As pioneers to the DSSC work, which will gain prominence due to its low-cost and easy fabrication techniques; it is recommended that the School of Physical Sciences, University of Nairobi provides leadership in establishing a multi-department project aimed at moving the DSSC work from the laboratory to production. Further research in the area should henceforth be informed by the real issues that consumers of the DSSC products report. To this end, therefore, it is strongly observed that domesticating DSSC research in one department, yet the work spans across all the four departments of the School of Physical Sciences, University of Nairobi is synonymous to performing below average. The synergy that a project that draws together expertise from all the school's departments, and indeed the School of Architecture and Design (due to the Building Integrated Photovoltaics articulated in this thesis) can be revolutionizing – it will, to say the least, attract more resources to the benefit of not only the school, but also the entire University and the country as well.

- During review of literature relating to what has been done by the Department of Physics, School of Physical Sciences, University of Nairobi in the area of solar PV; including DSSCs, a deliberate consultative forum of the researchers to share what each is doing on the area is recommended to be critical. Lack of such an initiative could be observed as one of the reasons that we don't have DSSMs in the Kenyan PV market today.

- The interest in the work that this thesis reports on, as evidenced from the remarks and publications done shows how novel it is. Work in DSSCs, and indeed renewable

energy in general is an area that has huge potential and interest as the world grapples with climate change and its impacts. Its is recommended that the School of Physical Sciences, University of Nairobi moves towards establishing a scientific journal in this area besides setting up of a programme in the area, as alluded to above. The journal will spur increased activity in work relating to DSSCs and renewable energy.

- Working with the glass industry to move towards production of smart glasses and well as glasses that not only let in adequate light but also generate power is recommended. This has already begun to be rolled out in Korea and Japan as illustrated by the pictures in figures 5.1 and 5.2.

Figure 5.1: Picture of DSSCs used to make an energy-generating door in Korea.

Figure 5.2: Picture of DSSCs used to make energy-generating windows in Korea.

5.2.2 Further Research Work

Research on the field application of the DSSC technology still has many areas that need to be explored. However with regard to the work that was carried out in this thesis, the following areas need further studies:

- *Carrying out after-exposure degradation studies on the DSSMs that have the potential of being used in Kenya.* Studies on the degradation of the DSSMs available on the PV market, and which show potential for use in Kenya need to be done after certain periods of the DSSMs' exposure. This information will provide useful areas for further fundamental research aimed at enhancing uptake of the DSSC technology in Kenya

- *Investigate the spectral response of the available DSSMs under Kenya's field weather conditions.* In this work, studies on the performance of the DSSM under high values of *AM* and under diffuse radiation have shown improved response to shorter wavelength radiation. Further work needs to be done to establish the response to the whole solar radiation spectrum. In this recommended work, the fraction of recombination represented by the re-emission of photons of energy higher than E_g for various DSSMs should be investigated.

References

Abrams, Z., Gharghi, M., Niv, A., Gladden, C. and Zhang, X., (2012), Theoretical Efficiency of 3rd Generation Solar Cells: Comparison between Carrier Multiplication and Down-Conversion, *Solar Energy Materials and Solar Cells,* DOI:10:1016/j.solmat.2011.12.019.

Ajuoga, P., (2009), Effects of Concentration on Dopant States in Photo activity in Niobium doped TiO_2, *M.Sc. proposal for the Department of Physics, University of Nairobi,* 1 - 20.

Aleklett, K., (2007), Reserve driven Forecasts for Oil, Gas and Coal and Limits in CO_2, *In discussion paper number 2007-18, Joint Transport Research Centre,* 1 – 20.

Aliyu, M., Islam, M., Hamzah, N., Karim, M., Matin, M., Sopian, K. and Amin, N., (2012), Recent Developments in Flexible CdTe Solar Cells on Metallic Substrates: Issues and Prospects, *International Journal of Photo-energy,* 1 – 10.

Antoniadis, H., (2011), High Efficiency, Low Cost Solar Cell Manufactured using 'Silicon Ink' on Thin Crystalline Silicon Wafers, *In National Resource Ecology Laboratory (NREL)/SR-5200 – 50824, Innovalight, Incorporated,* 1 – 44.

Antón, M., Serrano, A., Cancillo, M. and Garcia, J., (2009), Influence of the Relative Optical Air Mass on Ultraviolet Erythermal Irradiance, *Journal of Atmospheric and Solar Terrestrial Physics,* 71 (17-18), 2027 – 2030.

ASME, (2010), Energy Choices – A Guide to Facts and Perspectives, *American Society of Mechanical Engineers (ASME),* 1 – 54.

Bailis, R., Kirubi, C., Jacobsen, A., (2006), Searching for Sustainability: Kenya's Energy Past and Future. *African Centre for Technology Studies (ACTS), Nairobi, Kenya,* 1 - 5.

Bakas, I., (2011), Solar Energy/Photovoltaics, *In solar energy and housing – Corpus. Copenhagen Resource Institute (CRI),* 1 – 6.

Bárd, H. (2012), Buy Coal! A Case for Supply-Side Environmental Policy, *Journal of Political Economy,* 120 (1): 77 DOI: 10.1086/665405.

Barnes, D. and Toman, M., (2006), Energy, Equity and Economic Development, *In Economic Development and Environmental Sustainability, Oxford University Press,* 1 – 52.

References

Abrams, Z., Gharghi, M., Niv, A., Gladden, C. and Zhang, X., (2012), Theoretical Efficiency of 3rd Generation Solar Cells: Comparison between Carrier Multiplication and Down-Conversion, *Solar Energy Materials and Solar Cells,* DOI:10:1016/j.solmat.2011.12.019.

Ajuoga, P., (2009), Effects of Concentration on Dopant States in Photo activity in Niobium doped TiO_2, *M.Sc. proposal for the Department of Physics, University of Nairobi,* 1 - 20.

Aleklett, K., (2007), Reserve driven Forecasts for Oil, Gas and Coal and Limits in CO_2, *In discussion paper number 2007-18, Joint Transport Research Centre,* 1 – 20.

Aliyu, M., Islam, M., Hamzah, N., Karim, M., Matin, M., Sopian, K. and Amin, N., (2012), Recent Developments in Flexible CdTe Solar Cells on Metallic Substrates: Issues and Prospects, *International Journal of Photo-energy,* 1 – 10.

Antoniadis, H., (2011), High Efficiency, Low Cost Solar Cell Manufactured using 'Silicon Ink' on Thin Crystalline Silicon Wafers, *In National Resource Ecology Laboratory (NREL)/SR-5200 – 50824, Innovalight, Incorporated,* 1 – 44.

Antón, M., Serrano, A., Cancillo, M. and Garcia, J., (2009), Influence of the Relative Optical Air Mass on Ultraviolet Erythermal Irradiance, *Journal of Atmospheric and Solar Terrestrial Physics,* 71 (17-18), 2027 – 2030.

ASME, (2010), Energy Choices – A Guide to Facts and Perspectives, *American Society of Mechanical Engineers (ASME),* 1 – 54.

Bailis, R., Kirubi, C., Jacobsen, A., (2006), Searching for Sustainability: Kenya's Energy Past and Future. *African Centre for Technology Studies (ACTS), Nairobi, Kenya,* 1 - 5.

Bakas, I., (2011), Solar Energy/Photovoltaics, *In solar energy and housing – Corpus. Copenhagen Resource Institute (CRI),* 1 – 6.

Bård, H. (2012), Buy Coal! A Case for Supply-Side Environmental Policy, *Journal of Political Economy,* 120 (1): 77 DOI: 10.1086/665405.

Barnes, D. and Toman, M., (2006), Energy, Equity and Economic Development, *In Economic Development and Environmental Sustainability, Oxford University Press,* 1 – 52.

Becquerel, E., (1848), On the Coloured Photographic Image of the Solar Spectrum, *Journal of the Franklin Institute*, 238.

Benanti, T. and Venkataraman, D., (2006), Organic Solar Cells: An Overview Focusing on Active Layer Morphology, *Photosynthesis Research*, 87 (1), 73.

Bergine, M., Krašovec, U., Hočevar, M. and Topič, M., (2008), Performance of DSSCs Based on Ionic Liquids: Effect of Temperature and Iodine Concentration, *Thin Solid Films*, 516, 7155 – 7159.

Berkeley, (2003), The Diode, *icbook*, p. 1 – 22 [Retrieved on 29th March 2012 from bwrc.eecs.berkeley.edu/icbook/Additional Material/diode.pdf].

Binions, R. and Dunn, S., (2012), School of Engineering and Materials Science Research Studentship, *Queen Mary University of London* [Accessed on 27th March 2012 at http://www.semsqmul.ac.uk/research/studentship].

Birkmire, R. and Eser, E., (1997), Polycrystalline Thin-Film Solar Cells: Present Status and Future Potential, *Annual Review of Materials Science*, 27, 625.

Boucher, C., (2008), Solar Cell Industry – Trends and Opportunities, *Boucher-Lensch Associates LLC.*, 1 – 39.

Boschloo, G. and Hagfeldt, A., (2005), Activation Energy Electron Transport in Dye-Sensitized TiO_2 Solar Cells, *Journal of Physical Chemistry*, B, 109 (24), 12093 – 12098.

Carlo, A., (2008), DSSCs: Towards Low Cost, Industrial Viable Photovoltaics – Workshop on Nanoscience for Solar Energy Conversion, 21-29 October, 2008, *International Centre for Theoretical Physics (ICTP), 1938-7*, 1 - 42.

Carlson, D., (1977), The Effects of Impurities and Temperature on Amorphous Silicon Solar Cells, *Institute of Electrical and Electronics Engineers (IEEE)*, 214 – 217.

Carlson, D., Lin, G. and Grungnly, (2000), Temperature Dependence of Amorphous Silicon Solar Cell Photovoltaic Parameters, *Institute of Electrical and Electronics Engineers (IEEE)*, 707 – 712.

Chagaar, M. and Mialhe, P., (2008), Effects of Atmospheric Parameters on the Silicon Solar Cells Performance, *Journal of Electron Devices*, 6, 173 – 176.

Chambers, P., (1999), Teaching Pythagoras Theorem, *In Mathematics in School, The Mathematical Association, Leicester,* 28 (4), 22 – 24.

Chapin, D., Fuller, C. and Pearson, G., (1954), A New *p-n* Silicon Junction Photocell for Converting Solar Radiation into Electrical Power, *Journal of Applied Physics,* 25, 676 - 677.

Charron, R. and Athienitis, A., (2006), Design and Optimization of Net Zero Energy (NZE) Solar Homes, *In American Society of Heating, Refrigeration and Air Conditioning Engineers (ASHRAE) transactions, ASHRAE Incorporated,* 112 (2), 1 – 12.

Chen, Z., Tang, Y., Yang, H., Xia, Y., Li, F., Yi, T. and Huang, C., (2007), Nanocrystalline TiO_2 Film with Textural Channels: Exhibiting Enhanced Performance in Quasi-Solid/Solid-State DSSCs, *Journal of Power Sources,* 171, 990 - 998.

Chianese, D., Skoczek, A., Virtuari, A. and Ceberauer, T., (2011), Energy Yield Prediction of a-Si Photovoltaic Modules Using Full Data Series of Irradiance and Temperature for Different Geographical Locations, *26th European Photovoltaics Solar Energy Conference, September 2011, Hamburg, Germany,* 1 – 7.

Chloride Exide, (2010), *Interview by Ondraczek, 2011 with Guy Jack of Chloride Exide Kenya Ltd., Nairobi, Kenya.*

Chun, A., (2012), TiO_2 Nanoparticles – A Prevalent Additive, *Nature Nanotechnology,* DOI: 10.1038/nnano.2012.31.

Clement, J. and Quinnel, E., (1952), The Low Temperature Characteristics of Carbon Composition Thermometers, *Review of Scientific Instruments,* 23 (5), 213 – 216.

Conibeer, G., (2007), Third Generation Photovoltaics, *ARC Photovoltaics Centre of Excellence, School of Photovoltaic and Renewable Energy Engineering, University of New South Wales, Sidney, Australia,* 42 – 50.

Cornaro, C., Spena, A., Brown, T., Carlo, A. and Reale, A., (2008), The Impact of Outdoor Meteorological Parameters on the Performance of DSSCs, *Institute of Electrical and Electronics Engineers (IEEE) Xplore,* 1 – 4.

Crain, D., Garland, J., Rock, S. and Roy, D., (2012), Quantitative Characterization of Silicon Solar Cells in the Electro-Analytical Approach: Combined Measurements of Temperature and Voltage Dependent Parameters, *Analytical Methods,* 4, 106 – 117.

Cusano, D., (1963), CdTe Solar Cells and Photovoltaic Heterojunctions in II – VI Compounds, *Solid State Electronics,* 6 (3), 217.

Daguerre, L., (1839), Practical Definition of Daguerreotype, *Journal of the Franklin Institute,* 33, 3.

Dincar, I., (2003), The Role of Energy in Energy Policy Making, *Energy Policy,* 30, 137 – 149.

Dinçer, F. and Meral, M., (2010), Critical Factors Affecting Efficiency of Solar Cells, *Smart Grid and Renewable Energy,* 1, 47 – 50.

Duke, D., Jacpbsen, A. and Kammen, D., (2002), Photovoltaic Module Quality in the Kenyan Solar Home Systems Market, *Energy Policy,* 30, 477 – 499.

Duonghong, D., Serpone, N. and Grätzel, M., (1984), Integrated Systems for Water Cleavage by Visible Light; Sensitization of Titanium Dioxide Particles by Surface Derivatization with Ruthenium Complexex, *Helvetica Chemica Acta,* 6 (4), 1012.

Dyesol, (2012a), Dyesol Technology Drives Large Panel Development. *Dyesol Market Release,* [Communication to Raphael Otakwa from Dyesonnews@dyesol.com received on 20th March, 2012].

Dyesol, (2012b), A Beautiful Future Emerges in Korea. *Dyesol Market Release,* [Communication to Raphael Otakwa from Dyesolnews@dyesol.com received on 20th March, 2012].

Ferber, J. Stangl, R. and Luther, G., (1998), An Electrical Model of the Dye-Sensitized Solar Cell, *Solar Energy Materials and Solar Cells,* 53, 29.

Fujishima, A. and Honda, K., (1971), Electrochemical Evidence for Mechanisms of the Primary Stage of Photosynthesis, *Bulletin of the Chemical Society of Japan,* 44, 1148.

Gao, F., Wang, Y., Shi, D., Zhang, J., Wang, M., Jing, X., Humphry-Baker, R., Wang, P., Zakeeruddin, S. and Grätzel, M., (2008), Enhance the Optical Absorptivity of

Nanocrystalline TiO$_2$ Film with High Molar Extinction Coefficient Ruthenium Sensitizers for High Performance Dye-Sensitized Solar Cells, *Journal of American Chemical Society*, 130, 10720 – 10728.

Gavin, T., (2011), Solar Power as an Integral Part of Society – not as an Annex to Grid Power, *Presentation at Dyesol group of companies' Global Leaders in Dye Solar Cell Technology*, 10 - 50.

Ghoneim, A., Kandil, K., Al-Hasan, A., Altouq, M., Al-asaad, A., Alshamari, L. and Shamsaldein, A., (2011), Analysis of Performance Parameters of Amorphous Silicon Modules under Different Environmental Conditions, *Energy Science and Technology*, 2 (1), 43 – 50.

Gorissen, (2012), http://www.gorissen.info/Pierre/maps/gooleMapLocation.php?lat=-1.2774030&lon=36.807563&setLatLon=Set [Accessed on 20th December, 2011].

Grätzel, M., (2009), Recent Advances in Sensitized Mesoscopic Solar Cells, *Accounts of Chemical Research*, 42, 1788 – 1798.

Grätzel, M., (2003), Dye-Sensitized Solar cells, *Journal of Photochemistry and Photobiology C: Photochemistry Reviews*, 4, 145 – 153.

Grätzel, M. and Durrant, J., (2008), Dye-Sensitized Mesoscopic Solar Cells, *In Mary D. Archer and Arthur, J. (eds.) Series on Photoconversion of Solar Energy Vol. 3: Nanostructured and Photoelectrochemical Systems for Solar Photon Conversion, Imperial College Press, Norzik*, 503 – 536.

Green, M., (2003), Crystalline and Thin-Film Silicon Solar Cells: State of the Art and Future Potential, *Solar Energy*, 74 (3), 181.

Green, M., (2001), Solar Cell Efficiency Tables (version 18), *Progressive Photovoltaics Research and Application*, 9, 287 – 293.

Green, M., (1992), Solar Cells: Operating Principles, Technology and System Applications, *Bridge Printery Pty Limited, Roseberg*, 5 – 8.

Greenoptimistic, (2012), G24 Innovations Cells – Gratzel's Cells Dye-Sensitized Solar Cell for the First Time (2009), *http://www.greenoptimistic.com*. [Accessed on 23 March, 2012].

Greijer-Agrell, H., (2003), Interactions in DSSCs, *Acta Universitatis Upsaliensis Comprehensive Summaries of Uppsala Dissertations for the Faculty of Science and Technology,* 901 (59), 2 – 68.

GTZ, (2009a), *Potential for investment in solar energy in East Africa: Business Opportunities for German Companies,* Presentation by Mark Hankins on behalf of GTZ, November, 17, 2009, Berlin, Germany, 2 - 12.

GTZ, (2009b), *Market Potentials for German Solar Energy Companies in East Africa, Presentation held by Mark Hankins on behalf of GTZ.* Hannover Messe, April 22, 2009, Hannover, Germany, 1 - 15.

GTZ, (2009c), *Target Market Analysis: The Solar Energy Market in Kenya,* Deutsche Gesellschaft für Technische Zusammenarbeit (GTZ), October, 30, Berlin, Germany, 1 - 10.

Gunerhan, H., Hepbasli, A. and Giresunlu, U., (2009), Environmental Impacts from Solar Energy Systems, *Energy Sources, A,* **31,** 131 – 138.

Hadipour, A., Cheyns, D., Heremans, P. and Rand, B., (2011), Electrode Considerations for the Optical Enhancement of Organic Bulk Heterojunction Solar Cells, *Advanced Energy Materials,* 1 (5), 930 – 935.

Hahn, D., (2009), Light Scattering Theory, *In lecture notes, Department of Mechanical and Aerospace Engineering, University of Florida,* 1 – 13.

Hahn, R., Litan, R. and Singer, H., (2007), The Economics of 'Wireless Net Neutrality', *American Enterprise Institute (AEI) – Brookings Joint Centre for Regulatory Studies,* 1 – 54.

Halliday, D., Resnick, R. and Krane, K., (2009), Physics Fifth Edition, *Wiley,* **2,** 1114.

Halme, J., (2002), Dye-Sensitized Nanostructured and Organic Cells: Technical Review and Preliminary Tests, *M.Sc. (Technology) Thesis of the Helsinki University of Technology,* 1 – 115.

Han, L., Islam, A., Chen, H., Malapaka, C., Chiranjeevi, B., Zhang, S., Yang, X. and Yanagida, M., (2012), High Efficiency Dye-Sensitized Solar Cell with a Novel Co-adsorbent, *Energy and Environmental Science,* 2, 149.

Haneman, D., (2006), Properties and Applications of Copper Indium Diselenide, *Critical Reviews in Solid State and Materials Sciences*, 14 (4), 377 – 413.

He, L., Jiang, C., Wang, H., Lai, D., Tan, Y., Tan, C. and Rusli, (2012), Effects of Nanowire Texturing on the Performance of Si/Organic Hybrid Solar Cells Fabricated with 2.2 μm Thin Film Si Absorber, *American Institute of Physics*, doi.org/10.1063/1.3692590.

Hedegus, S. and Shafarman, N., (2004), Thin Film Solar Cells: Device Measurement and Analysis, *Progress in Photovoltaic Research and Application*, 12, 155-176.

Heinemann, D., (2000), Energy Meteorology, *In Lecture Notes for Postgraduate Programme 'Renewable Energy'*, *Carl Von Ossietzky Universität*, 1 – 102.

Helena, G., Lindgren, J. and Hagfeldt, A., (2003), Degradation mechanisms in a DSSC studied by UV-VIS and IR spectroscopy, *Solar Energy*, 169 - 180.

Heymann, E. (2011), Carbon Capture and Storage for Climate Protection – Important, Tedious and Costly, *Deutsche Bank*, 1 – 5.

Hinsch, A., (2007), DSSCs for Façade Applications: Recent Results from Project ColorSol 17th *International Photovoltaic Science Engineering Conference*, 3 – 7 December, 2007, Fukuoka, Japan.

Hishikawa, Y., (2008), Performance Measurement of DSSCs and Organic Polymer Solar Cells, *Natural Institute of Advanced Industrial Science and Technology (AIST), Research Centre for PVs (RCPV)*, 1 – 8.

Hishikawa, Y., (2006), Characterization of the Performance of DSSCs, *Proceedings of the Renewable Energy, Makuhari, Japan*, 184 – 188.

Hishikawa, Y., Imuna, Y. and Oshiro, T., (2000), Irradiance-Dependence and Transition of the I-V Characteristics of Crystalline Silicon Solar Cells, *Proceedings of the 28th Institute of Electrical and Electronics Engineers (IEEE) Photovoltaic Specialists Conference, Anchorage*, 1464 – 1467.

Hishikawa, Y. and Okamoto, S., (1994), Dependence of the I-V characteristics of a-Si Solar Cells on Illumination Intensity and Temperature, *Solar Energy Materials and Solar Cells*, 33-2, 157 – 168.

http://www.konzacity.co.ke, (2012), *Accessed on 20th March, 2012.*

Hu, L., Dai, S., Weng, J., Xiao, S., Sui, Y., Huang, Y., Chen, S., Kong, F., Pan, X., Liang, L. and Wang, K., (2007), Microstructure Design of Nanoporous TiO_2 Photoelectrodes for DSSCs, *Journal of Physical Chemistry*, B, 111, 358 - 362.

IEA, (2007), Key World Energy Statistics 2007, International *Energy Agency (IEA), 2007.*

Iles, P., (2001), Evolution of Space Solar Cells, *Solar Energy Materials and Solar Cells*, 68, 1 – 13.

IPCC, (2007), Climate change 2007: The Physical Science Basis: Summary of Policy Makers, *Intergovernmental Panel on Climate Change (IPCC) Secretariat*, 2007.

Jacobsen, A., (2004), Connective Power: Solar Electrification and Social Change in Kenya. *PhD Dissertation, University of California, Berkeley, USA*, 120-180.

Jensen, K., (2008), Performance Comparison of a DSSC and a Silicon Solar Cell under Idealized and Outdoor Conditions, *M.Sc. Thesis for the Technical University of Denmark,* 1 – 131.

Jun-Ho, Y., Humphry-Baker, R., Shaik, M., Zakeeruddin, S., Mohammed, K., Nazeeruddin, M_d. and Grätzel, M., (2010), Effects of Heat and Light on the Performance of DSSCs Based on Organic Sensitizers and Nanostructured TiO_2, *Nano Today*, 5, 91 - 98.

Kahuthu, S., (2008), Theoretical Approach to the Transport Phenomenon of Photo Injected Electrons in Dye-Sensitized Solar Cells, *M.Sc. thesis for the University of Nairobi.*

Kalaignan, G. and Kang, Y., (2006), A Review on Mass Transport in DSSC's, *Journal of Photochemistry and Photobiology C: Photochemistry Reviews,* 7, 17 – 22.

Kalowekamo, J. and Baker, E., (2009), Estimating the Manufacturing Cost of Purely Organic Solar Cells, *Solar Energy*, 3, 42 – 51.

Kalyanasundaram, K. and Grätzel, M., (1998), Applications of Functionalized Transition Metal Complexes in Photonic and Optoelectronic Devices, *Co-ordination Chemistry Reviews*, 77, 347 – 414.

Karekezi, S. and Kithyoma, W., (2003), Renewable Energy Strategies for Rural Africa: Is a PV-Led Renewable Energy Strategy the Right Approach for Providing Modern Energy to the Rural Poor of Sub-Saharan Africa?' *Energy Policy*, 30, 11-12.

Kasten, F. and Young, A., (1989), Revised optical air mass tables and approximation formula, *Applied Optics*, 28 (22), 4735 – 4738.

Katherine, L., (2010), Photovoltaic Cell Efficiency at Elevated Temperatures, *B.Sc. Thesis for the Department of Mechanical Engineering, Massechusetts Institute of Technology*, 1 – 23.

Kato, N., Takeda, Y., Higuchi, K., Takeichi, A., Sudo, E., Tanaka, H., Motohiro, T., Sano, T. and Toyoda, T., (2009), Degradation Analysis of DSSM after Long-Term Stability Test under Outdoor Working Conditions, *Solar Energy Materials and Solar Cells*, 93 (6-7), 893 – 897.

Katrine, F., (2008), Performance Comparison of a DSSC and a Silicon Solar Cell under Idealized and Outdoor Conditions, *M.Sc. Thesis for the Technical University of Denmark*, 106 – 110.

Kao, Z., Naghavi, N., Erforth, F., Guillemoles, J., Gēvard, T., Etcheberry, A., Pelouard, J., Collin, S., Voorwinden, G. and Lincot, D., (2012), Towards Ultrathin Copper Indium GaSe$_2$ Solar Cells: Proof of Concept Study by Chemical Etching and Gold Back Contact Engineering, *Progress in Photovoltaics: Research and Applications*, DOI: 10.1002/pip.2162.

Kay, A. and Grätzel, M., (1999), Low-Cost PV Modules Based on Dye-Sensitized Nanocrystalline TiO_2 and Carbon Powder, *Solar Energy Materials and Solar Cells*, 44 (1), 99 – 117.

Kazmerski, L., White, F. and Morgan, G., (1976), Thin-Film CuInSe$_2$-CdS Heterojunction Solar Cells, *Applied Physics Letters*, 29 (4), 268.

Kenya Electricity Generating Company (KenGen), (2010), *Interview by Ondraczek, 2011 with Simon Ngure of Kenya Electricity Generation Company Ltd. (KenGen), Nairobi, Kenya.*

Kenya Institute of Public Policy Research (KIPPRA), (2010), *Interview by Ondraczek,2011 with Moses Ikiara and Nahasghon Mwongera of the Kenya Institute for Public Policy Research (KIPPRA), Nairobi, Kenya.*

Kenya. Ministry of Planning and National Development Kenya. National Economic and Social Council, (2007), Kenya: Vision 2030, *Government of the Republic of Kenya. Ministry of Planning and National Development and the National Economic and Social Council (NESC). Office of the President,* 1 – 136.

King, D., Hansen, B., Kratochvil, J. and Quintana, M., (1997), Dark *I-V* Measurements on PV Modules as a Diagnostic or Manufacturing Tool, *Institute of Electrical and Electronics Engineers (IEEE),* 1125 – 1128.

King, D., Kratochvil, A. and Boyson, W., (2000), Stabilization and Performance Characteristics of Commercial a-Si PV Modules, *Sandia National Laboratories, Albuquerque, NM,* 87185, 1 – 5.

Kittel, C., (1958), Elementary Statistical Physics, *Wiley,* 86 – 90.

Kroon, J., Bakker, N., Smit, H., Liska, P., Thampi, K., Wang, P., Zakeeruddin, S., Grätzel, M., Hinch, A., Hore, S., Würfel, U., Sastrawan, R., Durrant, J., Palomares, E., Pettersson, H., Gruszecki, T., Walter, J., Skupien, K. and Tulloh, G., (2007), Nanocrystalline DSSCs having Maximum Performance, *Progress in Photovoltaics: Research and Applications,* 15, 1 – 18.

Krugmann, P., (2011), That's Right: Solar Power is Now Cost-Effective, *The Seattle Times,* [retrieved on 23rd March, 2012 at http://seattletimes.nwsource.com/html/opinion].

Kuang, D., Comte, P., Zakeeruddin, S., Hagberg, D., Karlsson, K., Sun, L., Nazeeruddin, M_d. and Grätzel, M., (2011), Stable DSSCs Based on Organic Chromophores and Ionic Liquid Electrolyte, *Solar Energy,* 85, 1189 - 1194.

Kuhlbrodt, T., Griesel, A., Montoya, M., Levermann, A., Hofmann, M. and Rahmstorf, S., (2006), On the Driving Processes of Atlantic Meridional Overturning Circulation, *Potsdam Institute for Climate Research,* 1 – 69.

Lantratov, V., Kalyuzhnyi, N., Mintairov, S., Timoshina, N., Shvarts, M. and Andreev, V., (2007), High Efficiency Dual-Junction GaInP/GaAs Tandem Solar Cells obtained by the Method of MOCVD, *Semiconductors*, 41 (6), 727.

Leng, R., (2005), Implications of the Decline in World Oil Reserves for Future World Livestock Production, *School of Rural Science and Agriculture, University of New England*, 95 – 105.

Lewis, N. and Crabtree, G., (2007), Solar Energy Conversion, *Physics Today*, 60, 37 - 42.

Lillich, R., (1975), Economic Coercion and the International Legal Order, *Royal Institute of International Affairs*, 51 (3), 358 – 371.

Ling, M. and Bao, Z,, (2004), Thin Film Deposition, Pattering, and Printing in Organic Thin Film Transistors, *Chemistry of Materials*, 16 (23), 4824 – 4840.

Lobato, K., (2007), Charge Transport and Recombination in Dye-Sensitized Nanocrystalline Solar Cells, *Ph.D Thesis (Chemistry) for the University of Bath*, 1 – 151.

Lobato, K. and Peter, L., (2006), Direct Measurement of the Temperature Coefficient of the Electron Quasi-Fermi Level in Dye-Sensitized Nanocrystalline Solar Cells using a Titanium Sensor Electrode, *Journal of Physical Chemistry*, B, 110 (43), 21920 – 21923.

Louche, A., Maurel, M., Simonnot, G., Peri, G. and Iqbal, M., (2000), Determination of □ngstr□m's Turbidity Coefficient from Direct Total Solar Irradiance Measurements, *Laboratoire d'Hèlioènergètique*, 1622 – 1630.

Lundstorm, M., (1995), Heterostructure fundamentals, *School of Electrical and Computer Engineering and the NSF MRSEC for Technology Enabling Heterostructures, Purde University, West Lafayette, Indiana*, 47907, 1 – 43.

Luque, A. and Hedegus, S., (2003), Handbook of PV Science and Engineering, *West Sussex: Wiley*, 1 – 52.

Meinel, A. and Meinel, M., (1976), Applied Solar Energy, *Addison Wesley Publishing Company*, 10 – 78.

Martinot, E., Ramankutty, R., Rittner, F., (2000), The GEF Solar PV Portfolio: Emerging Experiences and Lessons, Monitoring and Evaluation Working Paper 2, Global Environmental Facility (GEF), Washington, DC, USA, 5 - 15.

Masters, G., (2004), Renewable and Efficient Power Systems, John Wiley and Sons, 1 - 20.

Martin, A., (2003), General Temperature Dependence of Solar Cell Performance and General Implications for Device Modelling, *Progress in Photovoltaics: Research and Applications*, 11, 333 - 340.

Meng, F., Sun, T. and Cui, R., (2000), Recombination Properties of Grain Boundaries in Polycrystalline Silicon under Illumination, *Semiconductor Science and Technology*, 15 (9), 926.

Menesses-Rodriguez, D., (2005), Photovoltaic Solar Cells Performance at Elevated Temperatures, *Solar Cells*, 78, 243 - 250.

Millman, J. and Halkins, C., (1972), Integrated Electronics: Analog and Digital Circuits and Systems, *ISE ed., Tokyo: McGraw-Hill Kogakosha Ltd*, 1 - 58.

Ministry of Energy (MOE), (2010), Solar Energy, *Ministry of Energy (MOE)*, [accessed online at http://www.energy.go.ke, June 4, 2010].

Mulvaney, D., Bolam, V., Cendejas, M., Davis, S., Orueias, L., Kim, S., Man, S., Rowan, W. Sanz, E., Satre, P., Sridhar, A. and Young, D., (2009), Towards a Just and Sustainable Solar Industry, *Silicon Valley Toxics Coalition*, 1 - 48.

Muoghalu, J. (2003), Priority Parameters: Abiotic and Biotic components, *In Environmental Monitoring (edited by Inyang, H. and Daniels, J.), Encyclopedia of Life Support Systems (EOLSS)*, 1 - 8.

Murray, J. and King, D., (2012), Climate Policy: Oil's tipping point has passed, *Nature* 481, 433 - 435.

Mwabora, J., (1999), Copper Indium Diselenide Based Solar Cells: Effect of Preparation Conditions & Thickness on Performance, *Ph.D. Thesis, University of Dar es Salaam*, 51 - 67.

Naghavi, N., Spiering, S., Powalla, M., Cavana, B. and Lincot, D., (2003), High Efficiency Copper Indium Gallium Diselenide (CIGS) Solar Cells with Indium Sulphide Buffer Layers Deposited by Atomic Layer Chemical Vapour Deposition (ALCVD), *Progress in Photovoltaics: Research and Applications,* 11 (7), 437 – 414.

National Instruments, (2009), Part II – photovoltaic cell *I-V* characterization theory and LabVIEW analysis code, *National Instruments (NI),* [retrieved from http://zoneni.com/devzone/tut/p/id/7230 on 20 March, 2012], 1 – 5.

Nayaab, M., Karayel, M., Neeman, E. and Selkowitz, S., (1983), Analysis of Atmospheric Turbidity for Daylight Calculations, *International Daylighting Conference, Phoenix AZ, February, 16 – 18,* 1 – 23.

Neaman, D., (1997), Semiconductor Physics and Devices: Basic principles, 2nd edition, *Homewood, IL: Irwin,* 5 – 28.

Nelson, J., (2010), Physics of Solar cells, *Lecture Notes for Winter College on Optics and Energy, International Centre for Theoretical Physics (ICTP),* 2132 (2), 1 – 32.

Newport Corporation, (2011), The Challenge of Making Reliable Solar Cell Measurements, *Technology and Applications Centre – Newport Corporation,* 1 – 6.

Nikos, K., Benkstein, K., Lagemaat, J., Frank, A., Yuan, Q. and Schiff, A., (2006), Temperature Dependence of the Electron Diffusion Coefficient in Electrolyte-Filled TiO_2 Nanoparticle Films: Evidence against Multiple Trapping in Exponential Conduction Band Tails, *Physical Review,* B, **73,** 045326, 1 – 8.

Nwanya, A., Ezema, F. and Ejikeme, P., (2011), Dye-Sensitized Solar Cells: A Technically and Economically Alternative Concept to *p-n* Junction Photovoltaic Devices, *International Journal of Physical Sciences,* **6,** (22), 5190 – 5201.

Ogacho, A., (2010), A Study of TiO_2 Dye-Sensitized Solar Cells with a Hole Transport Material, *Ph.D thesis for the Department of Physics, University of Nairobi.*

Olwendo, J., (2008), A Theoretical Approach to Studies of Temperature Effect on Mobility of Photo Injected Electrons in Dye-Sensitized Solar Cells, *M.Sc. thesis for the Department of Physics, University of Nairobi.*

O'Regan, B. and Grätzel, M., (1991), A Low-Cost, High Efficiency Solar Cell Based on Dye-Sensitised Colloidal TiO$_2$ Films, *Nature*, **353**, 737 - 739.

Ozone Processing Team – NASA/GSFC Code 613.3, (2012), Total Ozone Mapping Spectrometer, *http://www.jwocky.gsf.nasa.gov/teacher/latlon.html* [Accessed on 4/3/2012].

Ozuomba, J., Ekpunobi, A. and Ekwo, P., (2011), The Photovoltaic Performance of Dye-Sensitized Solar Cells Based on Chlorine Local Dye, *Chalcogenide Letters*, **8** (3), 155 - 161.

Papageorgion, N., Athanassov, Y., Armand, M., Bonhote, P. and Petterson, H., (1996), The Performance and Stability of Ambient Temperature Molten Salts for Solar Cell Applications, *Journal of Electrochemical Society*, **143** (10), 3099 - 3108.

Patel, K., Jani, M., Pathak, V. and Srivastava, R., (2009), Deposition of CdSe Thin Films by Thermal Evaporation and their Structural and Optical Properties, *Chalcogenide Letters*, **6** (6), 279 – 286.

Pizzini, S., Acciarri, A. and Binetti, S., (2005), From Electronic Grade to Solar Grade Silicon: Chances and Challenges in Photovoltaics, *Physica Status Solid (A) Applications and Materials*, **202** (15) 2928 – 2942.

Pota, H., (2004), A New Derivation of the Law of the Junctions, *Institute of Electrical and Electronics Engineers (IEEE) Transactions in Education*, **47** (4), 1 – 3.

Proulx, T., (2011), Experimental Mechanics on Emerging Energy Systems and Materials, volume 5, *The Society for Experimental Mechanics, Inc.*, 205.

Pulka, H., (1984), Coatings on Glasses, *Thin Film Science and Technology*, 6, 254.

Purnima, T., Ruberu, A. and Vela, J., (2011), Expanding the One-Dimensional CdS-CdSe Composition Landscape: Axially Anisotropic CdS$_{1-x}$Se$_x$ Nanorods, *ACS Nano*, 5 (7), 5775 – 5784.

Quaschning, V., (2005), Understanding Renewable Energy Systems, *Earthscan Canada*, 1 - 3.

Qingjiang, Y., Cuiling, Y., Fengyun, G., Jinzhong, W., Shujie, J., Shiyong, and Liancheng, Z., (2012), A Stable and Efficient Quasi-Solid State DSSC with a Low

Molecular Weight Organic Gelator, *Energy and Environmental Science*, DOI: 10.1039/c2ee03128k.

Rabah, K., Ndjeli, L. and Raturi, A., (1995), Review of PV Energy Development in Kenya for Rural Electrification, *International Centre for Theoretical Physics (ICTP)*, 95, 4817.

Resnick Institute (RI), (2011), Critical Materials for Sustainable Energy Applications, *California Institute of Technology*, 1 – 46.

Rijnberg, (1998), Long Term Stability of Nanocrystalline DSC, *2nd World Conference and Exhibition on PV Solar Energy Conversion, 6 – 10, July, Vienna, Australia,* 1 – 24.

Rotman, D., (2012), Alta Devices: Finding a Solar Solution, *In Technology Review – Massechussets Institute of Technology,* [Accessed on 26th March, 2012 at http://m.technologyreview.com/energy/39649/].

Ruby, D., (2011), Major Cost Components of PV Cells and Current Efforts to Reduce them, *PV Expert,* 1 – 134.

Saga, T., (2010), Advances in Crystalline Silicon Solar Cell Technology for Industrial Mass Production, *NPG Asia Materials*, 2, 96 – 102.

Sawant, S. and Biliga, B., (2000), Current Saturation Control in Silicon Emmiter Switched Thyristors, *Solid State Electronics,* 44 (1), 133 – 142.

Shockley, W., (1949), The Theory of *p-n* Junctions in Semiconductors and *p-n* Junction Transistors, *Bell Systems Technology,* 28, 435.

Shockley, W. and Queisser, H., (1961), Detailed Balance Limit of Efficiency of *p-n* Junction Solar Cells, *Journal of Applied Physics,* 32 (3), 510.

Sigrist, M., (2010), Solid State Theory, *Institute für Theoretische Physik HIT K23.8,* 1 – 134.

Simiyu, J., (2010), Characterization of Anthocyanin Dyes and Investigation of Charge Transport in TiO_2 DSSCs, *Ph.D. thesis for the University of Nairobi,* 1 - 13.

Snaith, H., Schmidt-Mende, L., Grátzel, M. and Chieza, M., (2006), Light Intensity, Temperature and Thickness Dependence of the Open Circuit Voltage in Solid-State DSSCs, *Journal of physical chemistry,* 74 (4), 1-6.

Streetman, B., (1993), Solid State Electronic Devices, *Prentice Hall of India, New Delhi, India,* 5 – 20.

Sze, S., (1981), Physics of Semiconductor Devices, *New York: Wiley International Publishers Inc.,* 122 - 124.

Tada, A., Geng, Y., Wei, Q., Hashimoto, K. and Tajima, K., (2011), Tailoring Organic Heterojunction Interfaces in Bilayer Polymer PV Devices, *Nature Materials,* 10, 450 – 455.

Thavasi, V., Renugopalakrishnan, V., Jose, R. and Ramakrishna, S., (2009), Controlled Electron Injection and Transport in Material Interfaces in DSSCs, *Materials Science and Engineering: Reports,* 63, 81 – 99.

Thiyangu, S., Pei, Z. and Jhong, M., (2012), Amorphous Silicon Nanocone Array Solar Cell, *Nanoscale Research Letters,* 7, 172.

Thompson, B. and Fr□chet, J., (2008), Polymer-Fullerene Composite Solar Cells, *Angewandle Chemie,* 47, 58 – 77.

Tiedje, T., Yablonovitch, E., Cody, G. and Brooks, B., (1984), Limiting Efficiency of Silicon Solar Cells, *Institute of Electrical and Electronics Engineers (IEEE) Trans. Electron Devices,* 31, 711 – 716.

Timmer, J., (2012), We've Hit 'Peak Oil'; Now Comes Permanent Price Volatility, *Arstechnica.com* [accessed on 14 March 2012 at http://arstechnica.com/science/news/2012/01].

Tolman, R., (1938), Principles of Statistical Mechanics, *Oxford University Press,* 71 – 84.

Torcellini, P., Pless, S. and Deru, M., (2006), Zero Energy Buildings: A Critical Look at the Definition, *In conference paper NREL/CP – 550 – 39833, National Renewable Energy Laboratory (NREL),* 1 – 15.

Toyoda, T., Sano, T., Nakajima, J., Doi, S., Fukumoto, S., Ito, A., Tohyama, T., Yoshida, M., Kanagawa, T., Motohiro, T. and Shiozawa, M., (2004). Outdoor

Performance of Large-Scale DSSMs. *Journal of Photochemistry and Photobiology A: Chemistry*, 164, 203 – 207.

Tributsch, H., (1971), Application of Electrochemical Kinetics to Photosynthesis and Oxidative Phosphorylation: The Redox Element Hypothesis and the Principle of Parametric Energy Coupling, *Bioenergetics*, **2**, 249.

Ugwoke, P., (2012), Performance Assessment of Three Different Photovoltaic Modules as a Function of Solar Insolation in South Eastern Nigeria, *International Journal of Applied Science and Technology*, 2 (3), 319 – 327.

Vogel, H., (1873), On the Sensitiveness of Bromide of Silver to the So-called Chemically Inactive Colors, *Photographische Mittheilungen*, **10** (117), 233-237.

Wafula, H., (2006), Effects of Nitration on Pressed TiO_2 Photoelectrodes for DSSCs, *M.Sc. thesis for the Department of Physics, University of Nairobi.*

Waita, S., (2008), DSSCs Fabricated from Obliquely Sputtered Nanoporous TiO₂ Thin Films: Characterization, Electron Transport and Lifetime Studies, *Ph.D thesis for the Department of Physics, University of Nairobi.*

Waita, S., Aduda, B., Mwabora, J., Granqvist, C., Lindquist, S., Niklasson, G., Hagfeldt, A. and Boschloo, G., (2007), Electron Transport and Recombinations in DSSCs Fabricated from Obliquely Sputtered and Thermally Annealed TiO₂ Films, *Journal of Electroanalytical Chemistry*, **605** (2), 151 – 156.

Walton, J., (2010), Thin Film Group II-VI Solar Cells Based on Band–Offsets, *M.Sc. Thesis (Physics) for the Portland State University*, 1 – 58.

Wenham, S., Green, M., Watt, M. and Corkish, R., (2007), Applied Photovoltaics, *T J International Ltd.*, 6.

Whitney, Jr., (2010), Significant Sustainable Energy Systems, *In clean energy action project. Solar PV Energy*, 1 – 36.

Williams, R., (1960), Becquerel Photovoltaic Effect in Binary Compounds, *Journal of physical chemistry*, 32 (5), 1505.

Wolf, M. and Rauschenbach, H., (1963), Series Resistance Rffects on Solar Cell Measurements, *Advanced Energy Conversion*, 3, 455 – 479.

World Bank, (2010), *World Development Report 2010: Development and Climate Change*, The World Bank, Washington, DC, USA, 11-24.

Wrosnki, C., Pearce, J., Koval, R., Ferlauto, A. and Collins, R., (2002), Progress in Amorphous Silicon Based Solar Cell Technology, *Centre for Thin Film Devices and Materials Research Laboratory (NREL), The Pennyslvania State University*, 1 – 6.

Yastrebova, N., (2007), High Efficiency Multi-Junction Solar Cells: Current Status and Future Potential, *Centre for Research in Photovoltaics, University of Ottawa*, 1 – 22.

Young, A., (1994), Air Mass and Refraction, *Applied Optics*, **33**, 1108 – 1110.

Yu, Q., Yu, C., Guo, F., Wang, J., Jioa, S., Gao, S., Li, H. and Zhao, L., (2012), A Stable and Efficient Quasi-Solid-State DSSC with a Low Molecular Weight Organic Galetor, *Energy and Environmental Science*, 1 – 5.

Appendices

A1. The CM3 Pyranometer Calibration Data

Voltage (mV)	Voltage (V)	Radiation Intensity Based on the KIPP & ZONEN Pyranometer Sensitivity of 22.36×10^{-2} Volts/Wm^{-2}	Radiation Intensity Based on the Haenni Solar 130 Radiation Meter (Wm^{-2})	Variation of the KIPP & ZONEN and Haenni Solar 130 Radiation Meters (Wm^{-2})	Radiation Obtained from the Extrapolation of the Curves to the y-axis (Wm^{-2})
[± 0.1]	[± 0.0001]	[± 0.001]	[± 1]	[± 0.001]	[± 0.01]
-	-	-	-	-	0012.75
00.0	-	-	-	-	
12.3	0.0123	550.089	560	± 09.911	-
12.4	0.0124	554.562	-	-	-
12.5	0.0125	559.034	-	-	-
12.6	0.0126	563.506	576	± 12.494	-
12.7	0.0127	567.979	579	± 11.021	-
12.9	0.0129	576.923	580	± 03.077	-
13.0	0.0130	581.395	590	± 08.605	0588.73
13.1	0.0131	585.868	600	± 14.132	-
13.2	0.0132	590.340	600	± 09.660	-
14.0	0.0140	626.112	629	± 02.882	-
15.0	0.0150	670.841	663	± 07.841	0677.34
16.4	0.0164	733.453	740	± 06.547	-
17.0	0.0170	760.286	763	± 02.714	-
18.0	0.0180	805.009	802	± 03.001	-
19.0	0.0190	849.732	860	± 10.268	-
20.0	0.0200	894.454	900	± 05.546	0898.87
21.0	0.0210	939.177	945	± 05.823	-
22.0	0.0220	983.900	991	± 07.100	-
25.0	-	-	-	-	1120.40

A2. The LabVIEW™ Application.

Introduction

The development of the automated *J-V* characterization using Laboratory Virtual Instruments Electronic Workbench (LabVIEW™) is presented in this section because this system was used during data collection in this work. LabVIEW™ is a virtual instruments application that provides a graphical environment for signal acquisition, data analysis and presentation of analyzed data. It is an application from National Instruments Inc. (USA) and operates by means of an interface between physical devices and mimics physical instruments. LabVIEW™ contains tools for data acquisition, analysis, display and storage. It has a user interface that has knobs, push buttons, etc as controls and indicators like graphs, which are controlled by a block diagram that directs the codes.

Communication protocol

LabVIEW™ application as used in this work communicated with the Keithley 2400 source meter through GPIB hardware via an interface card. The application was used in the measurement of current-density and voltage; and to plot the *J-V* characteristics. Performance parameters like the efficiency, fill factor and maximum power were then extracted from the *J-V* curves. The Keithley 2400 source meter drivers were used as part of the communication with LabVIEW™ application in acquiring and measuring the output from the DSSC module for *J-V* characterization.

J-V characterization system automation

Figure 7-1 presents a flow chart to illustrate how events stream during use of the LabVIEW™ application in *J-V* characteristics acquisition.

```
Start  →  Initialize the Source
          Meter
              ↓
          Set Parameters
              ↓
          Switch on Output
              ↓
Is V = 0?
          Read V
          Measure J          No?
          Plot V vs J
          Next V
              ↓
          Yes?
          Output Off
              ↓
          Save Data
              ↓
          Exit
```
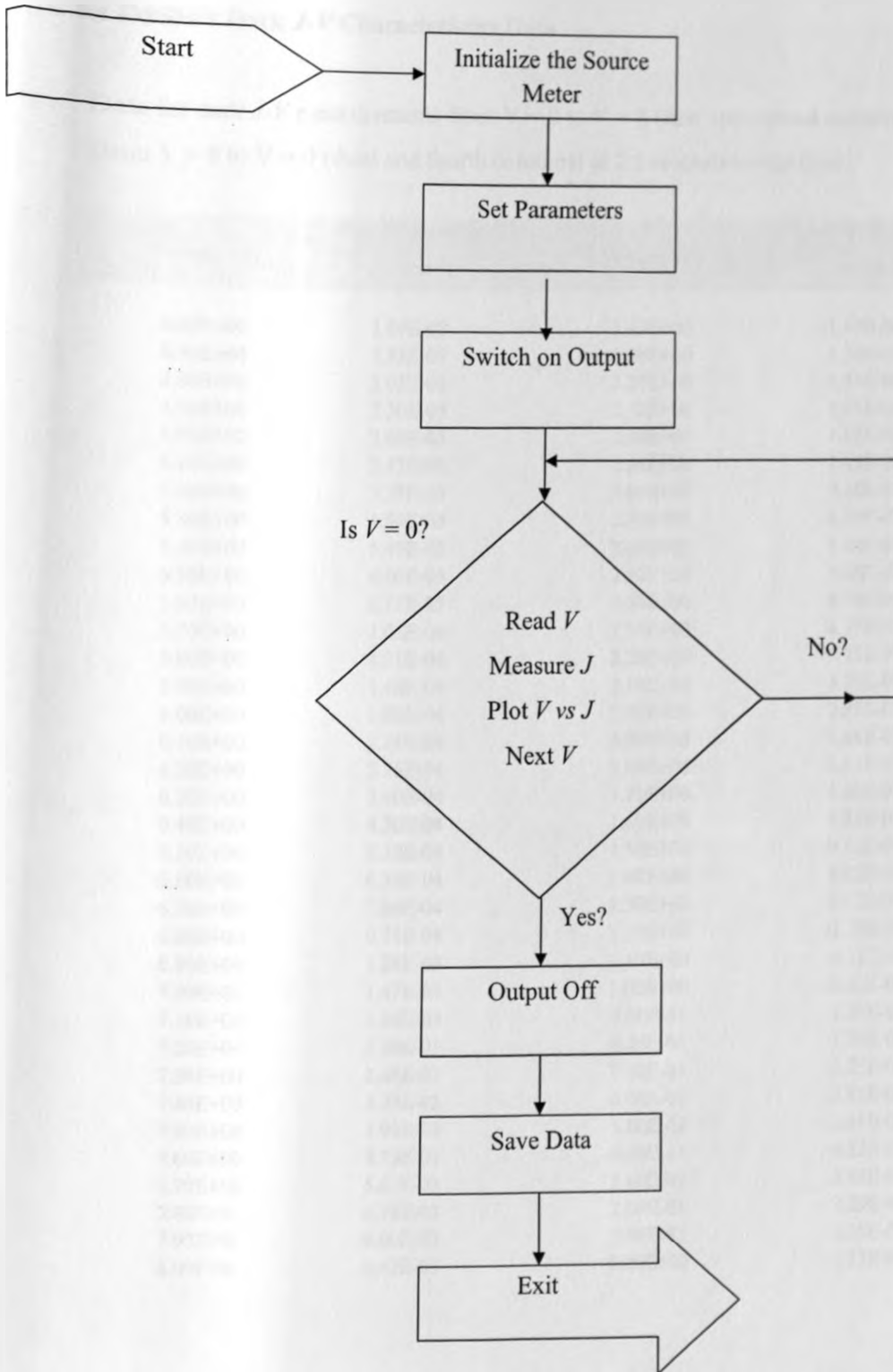
Figure 7.1: The events in the process of measuring and plotting J-V characteristics using LabVIEW^{TM}.

A3. The DSSM's Dark J-V Characteristics Data

a. Data for dark J-V measurements from V = 0 to V = 8 (first and second columns) and from V = 8 to V = 0 (third and fourth columns) at 2.5 seconds sweep time.

Voltage (V)	Current Density, J (Acm^{-2})	Voltage (V)	Current Density, J (Acm^{-2})
4.60E+00	1.69E-05	3.40E+00	1.47E-06
4.70E+00	1.82E-05	3.30E+00	1.28E-06
4.80E+00	2.02E-05	3.20E+00	1.14E-06
4.90E+00	2.30E-05	3.10E+00	1.01E-06
5.00E+00	2.68E-05	3.00E+00	1.12E-06
5.10E+00	3.17E-05	2.90E+00	1.03E-06
5.20E+00	3.78E-05	2.80E+00	9.28E-07
5.30E+00	4.54E-05	2.70E+00	6.35E-07
5.40E+00	5.49E-05	2.60E+00	6.04E-07
5.50E+00	6.66E-05	2.50E+00	5.36E-07
5.60E+00	8.11E-05	2.40E+00	4.78E-07
5.70E+00	1.05E-04	2.30E+00	4.19E-07
5.80E+00	1.21E-04	2.20E+00	3.75E-07
5.90E+00	1.48E-04	2.10E+00	3.31E-07
6.00E+00	1.82E-04	2.00E+00	2.87E-07
6.10E+00	2.24E-04	1.90E+00	2.48E-07
6.20E+00	2.76E-04	1.80E+00	2.11E-07
6.30E+00	3.40E-04	1.70E+00	1.68E-07
6.40E+00	4.20E-04	1.60E+00	1.31E-07
6.50E+00	5.18E-04	1.50E+00	9.13E-08
6.60E+00	6.39E-04	1.40E+00	6.03E-08
6.70E+00	7.88E-04	1.30E+00	2.17E-08
6.80E+00	9.71E-04	1.20E+00	-1.39E-08
6.90E+00	1.28E-03	1.10E+00	-4.71E-08
7.00E+00	1.47E-03	1.00E+00	-8.62E-08
7.10E+00	1.80E-03	9.00E-01	-1.29E-07
7.20E+00	2.20E-03	8.00E-01	-1.74E-07
7.30E+00	2.68E-03	7.00E-01	-2.25E-07
7.40E+00	3.25E-03	6.00E-01	-2.85E-07
7.50E+00	3.93E-03	5.00E-01	-3.61E-07
7.60E+00	4.73E-03	4.00E-01	-4.52E-07
7.70E+00	5.67E-03	3.00E-01	-5.68E-07
7.80E+00	6.75E-03	2.00E-01	-7.29E-07
7.90E+00	8.00E-03	1.00E-01	-1.26E-06
8.00E+00	9.42E-03	0.00E+00	-1.13E-06

e (V)	Current Density, J (Acm⁻²)	Voltage (V)	Current Density, J (Acm⁻²)
;+00	-7.02E-07	8.00E+00	9.20E-05
E-01	-2.91E-07	7.90E+00	7.81E-05
E-01	-3.59E-08	7.80E+00	6.56E-05
)E-01	1.47E-07	7.70E+00	5.47E-05
)E-01	2.93E-07	7.60E+00	4.54E-05
)E-01	4.09E-07	7.50E+00	3.75E-05
)E-01	5.06E-07	7.40E+00	3.09E-05
0E-01	5.80E-07	7.30E+00	2.54E-05
0E-01	6.47E-07	7.20E+00	2.07E-05
0E-01	7.10E-07	7.10E+00	1.69E-05
0E+00	7.74E-07	7.00E+00	1.34E-05
0E+00	8.35E-07	6.90E+00	1.12E-05
:0E+00	1.06E-06	6.80E+00	9.41E-04
30E+00	9.97E-07	6.70E+00	7.35E-04
40E+00	1.13E-06	6.60E+00	5.96E-04
50E+00	1.01E-06	6.50E+00	4.83E-04
60E+00	1.07E-06	6.40E+00	3.91E-04
70E+00	1.12E-06	6.30E+00	3.17E-04
.80E+00	1.18E-06	6.20E+00	2.57E-04
.90E+00	1.25E-06	6.10E+00	2.08E-04
.00E+00	1.31E-06	6.00E+00	1.69E-04
:.10E+00	1.39E-06	5.90E+00	1.34E-04
2.20E+00	1.48E-06	5.80E+00	1.12E-04
2.30E+00	1.58E-06	5.70E+00	1.02E-04
2.40E+00	1.68E-06	5.60E+00	7.46E-05
2.50E+00	1.79E-06	5.50E+00	6.12E-05
2.60E+00	1.93E-06	5.40E+00	5.02E-05
2.70E+00	2.07E-06	5.30E+00	4.14E-05
2.80E+00	2.23E-06	5.20E+00	3.43E-05
2.90E+00	2.41E-06	5.10E+00	2.85E-05
3.00E+00	2.61E-06	5.00E+00	2.31E-05
3.10E+00	2.83E-06	4.90E+00	2.00E-05
3.20E+00	3.09E-06	4.80E+00	1.69E-05
3.30E+00	3.38E-06	4.70E+00	1.41E-05
3.40E+00	3.73E-06	4.60E+00	1.21E-05
3.50E+00	4.13E-06	4.50E+00	1.03E-05
3.60E+00	4.61E-06	4.40E+00	1.04E-05
3.70E+00	5.17E-06	4.30E+00	7.49E-06
3.80E+00	5.83E-06	4.20E+00	6.39E-06
3.90E+00	6.60E-06	4.10E+00	5.43E-06
4.00E+00	7.50E-06	4.00E+00	4.71E-06
4.10E+00	8.55E-06	3.90E+00	4.01E-06
4.20E+00	1.00E-05	3.80E+00	3.56E-06
4.30E+00	1.56E-05	3.70E+00	3.12E-06
4.40E+00	1.16E-05	3.60E+00	2.74E-06
4.50E+00	1.24E-05	3.50E+00	2.44E-06
4.60E+00	1.37E-05	3.40E+00	2.17E-06

b. Data for dark *J-V* measurements from V = 0 to V = 8 (first and second columns) and from V = 8 to V = 0 (third and fourth columns) at 5 seconds sweep time.

Voltage (*V*)	Current Density, *J* (Acm^{-2})	Voltage (*V*)	Current Density, *J* (Acm^{-2})
0.00E+00	-7.02E-07	8.00E+00	9.26E-03
1.00E-01	-2.91E-07	7.90E+00	7.81E-03
2.00E-01	-3.59E-08	7.80E+00	6.56E-03
3.00E-01	1.47E-07	7.70E+00	5.47E-03
4.00E-01	2.93E-07	7.60E+00	4.54E-03
5.00E-01	4.09E-07	7.50E+00	3.75E-03
6.00E-01	5.06E-07	7.40E+00	3.09E-03
7.00E-01	5.80E-07	7.30E+00	2.54E-03
8.00E-01	6.47E-07	7.20E+00	2.07E-03
9.00E-01	7.10E-07	7.10E+00	1.69E-03
1.00E+00	7.74E-07	7.00E+00	1.38E-03
1.10E+00	8.35E-07	6.90E+00	1.12E-03
1.20E+00	1.06E-06	6.80E+00	9.41E-04
1.30E+00	9.97E-07	6.70E+00	7.35E-04
1.40E+00	1.13E-06	6.60E+00	5.96E-04
1.50E+00	1.01E-06	6.50E+00	4.83E-04
1.60E+00	1.07E-06	6.40E+00	3.91E-04
1.70E+00	1.12E-06	6.30E+00	3.17E-04
1.80E+00	1.18E-06	6.20E+00	2.57E-04
1.90E+00	1.25E-06	6.10E+00	2.08E-04
2.00E+00	1.31E-06	6.00E+00	1.69E-04
2.10E+00	1.39E-06	5.90E+00	1.38E-04
2.20E+00	1.48E-06	5.80E+00	1.12E-04
2.30E+00	1.58E-06	5.70E+00	1.02E-04
2.40E+00	1.68E-06	5.60E+00	7.46E-05
2.50E+00	1.79E-06	5.50E+00	6.12E-05
2.60E+00	1.93E-06	5.40E+00	5.02E-05
2.70E+00	2.07E-06	5.30E+00	4.14E-05
2.80E+00	2.23E-06	5.20E+00	3.43E-05
2.90E+00	2.41E-06	5.10E+00	2.85E-05
3.00E+00	2.61E-06	5.00E+00	2.38E-05
3.10E+00	2.83E-06	4.90E+00	2.00E-05
3.20E+00	3.09E-06	4.80E+00	1.69E-05
3.30E+00	3.38E-06	4.70E+00	1.43E-05
3.40E+00	3.73E-06	4.60E+00	1.21E-05
3.50E+00	4.13E-06	4.50E+00	1.03E-05
3.60E+00	4.61E-06	4.40E+00	1.04E-05
3.70E+00	5.17E-06	4.30E+00	7.49E-06
3.80E+00	5.83E-06	4.20E+00	6.39E-06
3.90E+00	6.60E-06	4.10E+00	5.48E-06
4.00E+00	7.50E-06	4.00E+00	4.71E-06
4.10E+00	8.55E-06	3.90E+00	4.08E-06
4.20E+00	1.00E-05	3.80E+00	3.56E-06
4.30E+00	1.56E-05	3.70E+00	3.12E-06
4.40E+00	1.16E-05	3.60E+00	2.74E-06
4.50E+00	1.24E-05	3.50E+00	2.44E-06
4.60E+00	1.37E-05	3.40E+00	2.17E-06

4.70E+00	1.56E-05	3.30E+00	1.94E-06
4.80E+00	1.80E-05	3.20E+00	1.75E-06
4.90E+00	2.11E-05	3.10E+00	1.59E-06
5.00E+00	2.50E-05	3.00E+00	1.45E-06
5.10E+00	2.98E-05	2.90E+00	1.32E-06
5.20E+00	3.57E-05	2.80E+00	1.21E-06
5.30E+00	4.30E-05	2.70E+00	1.11E-06
5.40E+00	5.20E-05	2.60E+00	1.03E-06
5.50E+00	6.31E-05	2.50E+00	1.12E-06
5.60E+00	7.70E-05	2.40E+00	1.05E-06
5.70E+00	9.42E-05	2.30E+00	9.59E-07
5.80E+00	1.81E-04	2.20E+00	7.26E-07
5.90E+00	1.41E-04	2.10E+00	6.93E-07
6.00E+00	1.74E-04	2.00E+00	6.45E-07
6.10E+00	2.14E-04	1.90E+00	6.00E-07
6.20E+00	2.63E-04	1.80E+00	5.54E-07
6.30E+00	3.25E-04	1.70E+00	5.12E-07
6.40E+00	4.01E-04	1.60E+00	4.69E-07
6.50E+00	4.95E-04	1.50E+00	4.32E-07
6.60E+00	6.12E-04	1.40E+00	3.95E-07
6.70E+00	7.55E-04	1.30E+00	3.62E-07
6.80E+00	9.31E-04	1.20E+00	3.25E-07
6.90E+00	1.21E-03	1.10E+00	2.92E-07
7.00E+00	1.41E-03	1.00E+00	2.46E-07
7.10E+00	1.73E-03	9.00E-01	2.13E-07
7.20E+00	2.12E-03	8.00E-01	1.75E-07
7.30E+00	2.59E-03	7.00E-01	1.22E-07
7.40E+00	3.15E-03	6.00E-01	6.29E-08
7.50E+00	3.82E-03	5.00E-01	-3.69E-09
7.60E+00	4.61E-03	4.00E-01	-7.97E-08
7.70E+00	5.53E-03	3.00E-01	-1.87E-07
7.80E+00	6.61E-03	2.00E-01	-3.24E-07
7.90E+00	7.85E-03	1.00E-01	-5.04E-07
8.00E+00	9.27E-03	0.00E+00	-7.48E-07

c. Data for dark J-V measurements from V = 0 to V = 8 (first and second columns) and from V = 8 to V = 0 (third and fourth columns) at 12.5 seconds sweep time.

Voltage (V)	Current Density, J (Acm^{-2})	Voltage (V)	Current Density, J (Acm^{-2})
0.00E+00	-3.23E-07	8.00E+00	9.12E-03
1.00E-01	-3.22E-08	7.90E+00	7.68E-03
2.00E-01	1.73E-07	7.80E+00	6.44E-03
3.00E-01	3.23E-07	7.70E+00	5.37E-03
4.00E-01	4.46E-07	7.60E+00	4.45E-03
5.00E-01	5.38E-07	7.50E+00	3.68E-03
6.00E-01	6.10E-07	7.40E+00	3.02E-03
7.00E-01	6.66E-07	7.30E+00	2.48E-03
8.00E-01	7.22E-07	7.20E+00	2.03E-03
9.00E-01	7.65E-07	7.10E+00	1.65E-03
1.00E+00	8.14E-07	7.00E+00	1.35E-03
1.10E+00	8.52E-07	6.90E+00	1.09E-03

1.20E+00	8.95E-07	6.80E+00	9.22E-04
1.30E+00	9.36E-07	6.70E+00	7.20E-04
1.40E+00	1.21E-06	6.60E+00	5.84E-04
1.50E+00	1.04E-06	6.50E+00	4.73E-04
1.60E+00	1.08E-06	6.40E+00	3.84E-04
1.70E+00	1.13E-06	6.30E+00	3.11E-04
1.80E+00	1.18E-06	6.20E+00	2.53E-04
1.90E+00	1.25E-06	6.10E+00	2.05E-04
2.00E+00	1.30E-06	6.00E+00	1.67E-04
2.10E+00	1.39E-06	5.90E+00	1.36E-04
2.20E+00	1.46E-06	5.80E+00	1.11E-04
2.30E+00	1.53E-06	5.70E+00	1.01E-04
2.40E+00	1.63E-06	5.60E+00	7.41E-05
2.50E+00	1.73E-06	5.50E+00	6.08E-05
2.60E+00	1.83E-06	5.40E+00	5.00E-05
2.70E+00	1.95E-06	5.30E+00	4.13E-05
2.80E+00	2.08E-06	5.20E+00	3.43E-05
2.90E+00	2.23E-06	5.10E+00	2.85E-05
3.00E+00	2.40E-06	5.00E+00	2.39E-05
3.10E+00	2.60E-06	4.90E+00	2.01E-05
3.20E+00	2.82E-06	4.80E+00	1.71E-05
3.30E+00	3.08E-06	4.70E+00	1.45E-05
3.40E+00	3.38E-06	4.60E+00	1.24E-05
3.50E+00	3.74E-06	4.50E+00	1.07E-05
3.60E+00	4.14E-06	4.40E+00	1.05E-05
3.70E+00	4.62E-06	4.30E+00	8.06E-06
3.80E+00	5.16E-06	4.20E+00	7.01E-06
3.90E+00	5.78E-06	4.10E+00	6.13E-06
4.00E+00	6.44E-06	4.00E+00	5.36E-06
4.10E+00	7.07E-06	3.90E+00	4.72E-06
4.20E+00	7.77E-06	3.80E+00	4.16E-06
4.30E+00	8.66E-06	3.70E+00	3.68E-06
4.40E+00	9.91E-06	3.60E+00	3.28E-06
4.50E+00	1.99E-05	3.50E+00	2.92E-06
4.60E+00	1.29E-05	3.40E+00	2.63E-06
4.70E+00	1.49E-05	3.30E+00	2.37E-06
4.80E+00	1.75E-05	3.20E+00	2.15E-06
4.90E+00	2.06E-05	3.10E+00	1.96E-06
5.00E+00	2.44E-05	3.00E+00	1.79E-06
5.10E+00	2.91E-05	2.90E+00	1.64E-06
5.20E+00	3.50E-05	2.80E+00	1.51E-06
5.30E+00	4.22E-05	2.70E+00	1.40E-06
5.40E+00	5.10E-05	2.60E+00	1.31E-06
5.50E+00	6.20E-05	2.50E+00	1.21E-06
5.60E+00	7.56E-05	2.40E+00	1.12E-06
5.70E+00	9.24E-05	2.30E+00	1.05E-06
5.80E+00	1.62E-04	2.20E+00	1.16E-06
5.90E+00	1.39E-04	2.10E+00	1.09E-06
6.00E+00	1.71E-04	2.00E+00	1.03E-06
6.10E+00	2.10E-04	1.90E+00	9.50E-07
6.20E+00	2.59E-04	1.80E+00	7.55E-07
6.30E+00	3.19E-04	1.70E+00	7.30E-07
6.40E+00	3.94E-04	1.60E+00	6.92E-07
6.50E+00	4.86E-04	1.50E+00	6.48E-07
6.60E+00	6.00E-04	1.40E+00	6.16E-07

Voltage	Current Density	Voltage	Current Density
6.70E+00	7.41E-04	1.30E+00	5.77E-07
6.80E+00	9.13E-04	1.20E+00	5.41E-07
6.90E+00	1.17E-03	1.10E+00	5.06E-07
7.00E+00	1.38E-03	1.00E+00	4.75E-07
7.10E+00	1.70E-03	9.00E-01	4.38E-07
7.20E+00	2.08E-03	8.00E-01	3.98E-07
7.30E+00	2.54E-03	7.00E-01	3.53E-07
7.40E+00	3.09E-03	6.00E-01	3.06E-07
7.50E+00	3.75E-03	5.00E-01	2.42E-07
7.60E+00	4.53E-03	4.00E-01	1.67E-07
7.70E+00	5.44E-03	3.00E-01	6.65E-08
7.80E+00	6.50E-03	2.00E-01	-6.34E-08
7.90E+00	7.73E-03	1.00E-01	-2.35E-07
8.00E+00	9.13E-03	0.00E+00	-4.69E-07

d. Data for dark J-V measurements from V = 0 to V = 8 (first and second columns) and from V = 8 to V = 0 (third and fourth columns) at 25 seconds sweep time.

Voltage (V)	Current Density, J (Acm^{-2})	Voltage (V)	Current Density, J (Acm^{-2})
0.00E+00	-1.57E-07	8.00E+00	8.94E-03
1.00E-01	9.91E-08	7.90E+00	7.52E-03
2.00E-01	2.82E-07	7.80E+00	6.29E-03
3.00E-01	4.22E-07	7.70E+00	5.24E-03
4.00E-01	5.31E-07	7.60E+00	4.34E-03
5.00E-01	6.29E-07	7.50E+00	3.58E-03
6.00E-01	6.69E-07	7.40E+00	2.94E-03
7.00E-01	7.15E-07	7.30E+00	2.41E-03
8.00E-01	7.56E-07	7.20E+00	1.97E-03
9.00E-01	7.89E-07	7.10E+00	1.61E-03
1.00E+00	8.30E-07	7.00E+00	1.31E-03
1.10E+00	8.61E-07	6.90E+00	1.06E-03
1.20E+00	8.97E-07	6.80E+00	8.97E-04
1.30E+00	9.34E-07	6.70E+00	7.01E-04
1.40E+00	9.71E-07	6.60E+00	5.69E-04
1.50E+00	1.05E-06	6.50E+00	4.62E-04
1.60E+00	1.87E-06	6.40E+00	3.75E-04
1.70E+00	1.09E-06	6.30E+00	3.05E-04
1.80E+00	1.15E-06	6.20E+00	2.47E-04
1.90E+00	1.20E-06	6.10E+00	2.01E-04
2.00E+00	1.25E-06	6.00E+00	1.64E-04
2.10E+00	1.31E-06	5.90E+00	1.34E-04
2.20E+00	1.38E-06	5.80E+00	1.09E-04
2.30E+00	1.45E-06	5.70E+00	1.00E-04
2.40E+00	1.54E-06	5.60E+00	7.31E-05
2.50E+00	1.64E-06	5.50E+00	6.01E-05
2.60E+00	1.73E-06	5.40E+00	4.95E-05
2.70E+00	1.84E-06	5.30E+00	4.09E-05
2.80E+00	1.95E-06	5.20E+00	3.40E-05
2.90E+00	2.11E-06	5.10E+00	2.83E-05

3.00E+00	2.27E-06	5.00E+00	2.38E-05
3.10E+00	2.45E-06	4.90E+00	2.00E-05
3.20E+00	2.67E-06	4.80E+00	1.70E-05
3.30E+00	2.91E-06	4.70E+00	1.45E-05
3.40E+00	3.18E-06	4.60E+00	1.25E-05
3.50E+00	3.52E-06	4.50E+00	1.08E-05
3.60E+00	3.89E-06	4.40E+00	1.05E-05
3.70E+00	4.32E-06	4.30E+00	8.16E-06
3.80E+00	4.79E-06	4.20E+00	7.16E-06
3.90E+00	5.30E-06	4.10E+00	6.30E-06
4.00E+00	5.84E-06	4.00E+00	5.56E-06
4.10E+00	6.49E-06	3.90E+00	4.92E-06
4.20E+00	7.30E-06	3.80E+00	4.36E-06
4.30E+00	8.27E-06	3.70E+00	3.90E-06
4.40E+00	9.45E-06	3.60E+00	3.48E-06
4.50E+00	1.55E-05	3.50E+00	3.13E-06
4.60E+00	1.26E-05	3.40E+00	2.83E-06
4.70E+00	1.46E-05	3.30E+00	2.58E-06
4.80E+00	1.71E-05	3.20E+00	2.33E-06
4.90E+00	2.02E-05	3.10E+00	2.13E-06
5.00E+00	2.40E-05	3.00E+00	1.96E-06
5.10E+00	2.86E-05	2.90E+00	1.80E-06
5.20E+00	3.43E-05	2.80E+00	1.67E-06
5.30E+00	4.14E-05	2.70E+00	1.55E-06
5.40E+00	5.01E-05	2.60E+00	1.44E-06
5.50E+00	6.10E-05	2.50E+00	1.36E-06
5.60E+00	7.43E-05	2.40E+00	1.26E-06
5.70E+00	9.07E-05	2.30E+00	1.18E-06
5.80E+00	1.48E-04	2.20E+00	1.12E-06
5.90E+00	1.36E-04	2.10E+00	1.05E-06
6.00E+00	1.67E-04	2.00E+00	1.13E-06
6.10E+00	2.06E-04	1.90E+00	1.08E-06
6.20E+00	2.53E-04	1.80E+00	1.00E-06
6.30E+00	3.12E-04	1.70E+00	9.46E-07
6.40E+00	3.85E-04	1.60E+00	8.94E-07
6.50E+00	4.75E-04	1.50E+00	7.74E-07
6.60E+00	5.86E-04	1.40E+00	7.50E-07
6.70E+00	7.22E-04	1.30E+00	7.24E-07
6.80E+00	8.90E-04	1.20E+00	6.92E-07
6.90E+00	1.12E-03	1.10E+00	6.52E-07
7.00E+00	1.35E-03	1.00E+00	6.25E-07
7.10E+00	1.65E-03	9.00E-01	5.86E-07
7.20E+00	2.03E-03	8.00E-01	5.49E-07
7.30E+00	2.47E-03	7.00E-01	5.10E-07
7.40E+00	3.01E-03	6.00E-01	4.66E-07
7.50E+00	3.65E-03	5.00E-01	4.12E-07
7.60E+00	4.42E-03	4.00E-01	3.37E-07
7.70E+00	5.31E-03	3.00E-01	2.42E-07
7.80E+00	6.36E-03	2.00E-01	1.15E-07
7.90E+00	7.57E-03	1.00E-01	-5.79E-08
8.00E+00	8.95E-03	0.00E+00	-2.90E-07

Shadow Length (cm) (Day One) [±0.1]	Shadow Length (cm) (Day Two) [±0.1]	Shadow Length (cm) (Day Three) [±0.01]	Mean Shadow Length (cm) [±0.1]	Optical Air Mass (AM) [±0.01]	Zenith Angle (Degrees) [±0.001]
62.4	61.8	58.8	61.0	1.15	0.290
56.2	56.8	62.1	58.4	1.14	0.28?
48.0	51.2	53.4	50.9	1.10	0.25?
40.0	40.2	51.7	44.0	1.08	0.233
33.6	32.8	30.8	32.4	1.04	0.17?
23.1	22.8	24.6	23.5	1.02	0.10?
-	-	00.0	00.0	1.00	0
00.0	02.2	-	00.7	1.00	0
-	00.0	-	00.0	1.00	0
18.2	20.1	18.0	18.8	1.01	0.0?1
33.6	35.3	34.0	34.3	1.05	0.170
47.2	45.6	46.7	46.5	1.09	0.235
53.8	54.7	52.8	53.8	1.12	0.260
61.8	62.8	62.0	62.2	1.15	0.29?
65.6	64.6	65.2	65.1	1.17	0.313

A4. Data on the Optical Air Mass (AM)

Time of the Day (Hours) [±0.01]	Shadow Length (cm) (Day One) [±0.1]	Shadow Length (cm) (Day Two) [±0.1]	Shadow Length (cm) (Day Three) [±0.01]	Mean Shadow Length (cm) [±0.1]	Optical Air Mass (AM) [±0.01]	Zenith Angle (Degrees) [±0.001]
0700	62.4	61.8	58.8	61.0	1.15	0.296
0800	56.2	56.8	62.1	58.4	1.14	0.287
0900	48.0	51.2	53.4	50.9	1.10	0.257
1000	40.0	40.2	51.7	44.0	1.08	0.255
1100	33.6	32.8	30.8	32.4	1.04	0.251
1200	23.1	22.8	24.6	23.5	1.02	0.249
1243	-	-	00.0	00.0	1.00	0
1246	00.0	02.2	-	00.7	1.00	0
1250	-	00.0	-	00.0	1.00	0
1300	18.2	20.1	18.0	18.8	1.01	0.081
1400	33.6	35.3	34.0	34.3	1.05	0.178
1500	47.2	45.6	46.7	46.5	1.09	0.235
1600	53.8	54.7	52.8	53.8	1.12	0.268
1700	61.8	62.8	62.0	62.2	1.15	0.296
1800	65.6	64.6	65.2	65.1	1.17	0.313

A5. Data for the *J-V* Characterization under different Irradiance Intensities.

a. Data for the *J-V* characterization under 653 Wm^{-2} light intensity.

Voltage (*V*)	Current Density, *J* (Acm^{-2})
7.12E+00	-3.43E-04
7.02E+00	-3.57E-04
6.92E+00	-3.75E-04
6.82E+00	-3.93E-04
6.72E+00	-4.12E-04
6.62E+00	-4.28E-04
6.52E+00	-4.44E-04
6.42E+00	-4.59E-04
6.32E+00	-4.73E-04
6.22E+00	-4.86E-04
6.12E+00	-4.98E-04
6.02E+00	-5.08E-04
5.92E+00	-5.17E-04
5.82E+00	-5.26E-04
5.72E+00	-5.34E-04
5.62E+00	-5.41E-04
5.52E+00	-5.47E-04
5.42E+00	-5.52E-04
5.32E+00	-5.57E-04
5.22E+00	-5.60E-04
5.12E+00	-5.62E-04
5.02E+00	-5.66E-04
4.92E+00	-5.68E-04
4.82E+00	-5.70E-04
4.72E+00	-5.71E-04
4.62E+00	-5.72E-04
4.52E+00	-5.73E-04
4.42E+00	-5.73E-04
4.32E+00	-5.73E-04
4.22E+00	-5.73E-04
4.12E+00	-5.74E-04
4.02E+00	-5.73E-04
3.92E+00	-5.73E-04
3.82E+00	-5.73E-04
3.72E+00	-5.72E-04
3.62E+00	-5.72E-04
3.52E+00	-5.73E-04
3.42E+00	-5.72E-04
3.32E+00	-5.73E-04
3.22E+00	-5.74E-04
3.12E+00	-5.76E-04
3.02E+00	-5.77E-04
2.92E+00	-5.79E-04
2.82E+00	-5.81E-04
2.72E+00	-5.82E-04
2.62E+00	-5.83E-04
2.52E+00	-5.84E-04
2.42E+00	-5.84E-04
2.32E+00	-5.85E-04
2.22E+00	-5.85E-04
2.12E+00	-5.85E-04
2.02E+00	-5.87E-04

1.92E+00	-5.88E-04
1.82E+00	-5.89E-04
1.72E+00	-5.89E-04
1.62E+00	-5.89E-04
1.52E+00	-5.90E-04
1.42E+00	-5.91E-04
1.32E+00	-5.91E-04
1.22E+00	-5.91E-04
1.12E+00	-5.91E-04
1.02E+00	-5.91E-04
9.23E-01	-5.92E-04
8.23E-01	-5.91E-04
7.23E-01	-5.92E-04
6.23E-01	-5.92E-04
5.23E-01	-5.92E-04
4.23E-01	-5.92E-04
3.23E-01	-5.92E-04
2.23E-01	-5.93E-04
1.23E-01	-5.92E-04
2.25E-02	-5.92E-04

b. Data for the J-V characterization under 703 Wm^{-2} light intensity.

Voltage (V)	Current Density, J (Acm^{-2})
7.50E+00	-2.40E-04
7.40E+00	-2.73E-04
7.30E+00	-3.03E-04
7.20E+00	-3.30E-04
7.10E+00	-3.55E-04
7.00E+00	-3.78E-04
6.90E+00	-4.01E-04
6.80E+00	-4.22E-04
6.70E+00	-4.41E-04
6.60E+00	-4.60E-04
6.50E+00	-4.77E-04
6.40E+00	-4.94E-04
6.30E+00	-5.09E-04
6.20E+00	-5.22E-04
6.10E+00	-5.35E-04
6.00E+00	-5.47E-04
5.90E+00	-5.58E-04
5.80E+00	-5.68E-04
5.70E+00	-5.76E-04
5.60E+00	-5.84E-04
5.50E+00	-5.91E-04
5.40E+00	-5.97E-04
5.30E+00	-6.41E-04
5.20E+00	-6.07E-04
5.10E+00	-6.11E-04
5.00E+00	-6.13E-04
4.90E+00	-6.16E-04
4.80E+00	-6.18E-04
4.70E+00	-6.20E-04
4.60E+00	-6.22E-04
4.50E+00	-6.22E-04

Voltage (V)	Current Density, J (Acm^{-2})
4.40E+00	-6.23E-04
4.30E+00	-6.22E-04
4.20E+00	-6.22E-04
4.10E+00	-6.23E-04
4.00E+00	-6.22E-04
3.90E+00	-6.25E-04
3.80E+00	-6.23E-04
3.70E+00	-6.23E-04
3.60E+00	-6.25E-04
3.50E+00	-6.26E-04
3.40E+00	-6.27E-04
3.30E+00	-6.25E-04
3.20E+00	-6.26E-04
3.10E+00	-6.27E-04
3.00E+00	-6.28E-04
2.90E+00	-6.31E-04
2.80E+00	-6.31E-04
2.70E+00	-6.33E-04
2.60E+00	-6.33E-04
2.50E+00	-6.32E-04
2.40E+00	-6.32E-04
2.30E+00	-6.35E-04
2.20E+00	-6.35E-04
2.10E+00	-6.37E-04
2.00E+00	-6.39E-04
1.90E+00	-6.40E-04
1.80E+00	-6.41E-04
1.70E+00	-6.42E-04
1.60E+00	-6.42E-04
1.50E+00	-6.42E-04
1.40E+00	-6.43E-04
1.30E+00	-6.42E-04
1.20E+00	-6.44E-04
1.10E+00	-6.43E-04
1.00E+00	-6.43E-04
9.03E-01	-6.43E-04
8.03E-01	-6.44E-04
7.03E-01	-6.45E-04
6.03E-01	-6.45E-04
5.03E-01	-6.47E-04
4.03E-01	-6.54E-04
3.03E-01	-6.51E-04
2.03E-01	-6.48E-04
1.03E-01	-6.49E-04
2.50E-03	-6.50E-04

c. Data on the J-V characterization under 747 Wm^{-2} light intensity.

Voltage (V)	Current Density, J (Acm^{-2})
	-1.95E-04
7.65E+00	-2.34E-04
7.55E+00	-2.68E-04
7.45E+00	-2.99E-04
7.35E+00	-3.28E-04
7.25E+00	-3.55E-04
7.15E+00	-3.81E-04
7.05E+00	-4.06E-04
6.95E+00	

6.85E+00	-4.29E-04
6.75E+00	-4.52E-04
6.65E+00	-4.73E-04
6.55E+00	-4.92E-04
6.45E+00	-5.11E-04
6.35E+00	-5.28E-04
6.25E+00	-5.44E-04
6.15E+00	-5.59E-04
6.05E+00	-5.73E-04
5.95E+00	-5.85E-04
5.85E+00	-5.96E-04
5.75E+00	-6.45E-04
5.65E+00	-6.16E-04
5.55E+00	-6.24E-04
5.45E+00	-6.31E-04
5.35E+00	-6.38E-04
5.25E+00	-6.42E-04
5.15E+00	-6.46E-04
5.05E+00	-6.50E-04
4.95E+00	-6.53E-04
4.85E+00	-6.55E-04
4.75E+00	-6.55E-04
4.65E+00	-6.56E-04
4.55E+00	-6.56E-04
4.45E+00	-6.57E-04
4.35E+00	-6.57E-04
4.25E+00	-6.57E-04
4.15E+00	-6.57E-04
4.05E+00	-6.58E-04
3.95E+00	-6.58E-04
3.85E+00	-6.58E-04
3.75E+00	-6.58E-04
3.65E+00	-6.59E-04
3.55E+00	-6.58E-04
3.45E+00	-6.60E-04
3.35E+00	-6.60E-04
3.25E+00	-6.62E-04
3.15E+00	-6.65E-04
3.05E+00	-6.69E-04
2.95E+00	-6.72E-04
2.85E+00	-6.75E-04
2.75E+00	-6.76E-04
2.65E+00	-6.77E-04
2.55E+00	-6.78E-04
2.45E+00	-6.79E-04
2.35E+00	-6.80E-04
2.25E+00	-6.81E-04
2.15E+00	-6.82E-04
2.05E+00	-6.84E-04
1.95E+00	-6.85E-04
1.85E+00	-6.87E-04
1.75E+00	-6.89E-04
1.65E+00	-6.88E-04
1.55E+00	-6.89E-04
1.45E+00	-6.91E-04
1.35E+00	-6.90E-04
1.25E+00	-6.91E-04
1.15E+00	-6.91E-04
1.05E+00	-6.92E-04
9.55E-01	-6.92E-04
8.55E-01	-6.93E-04

7.55E-01	-6.94E-04
6.55E-01	-6.93E-04
5.55E-01	-6.91E-04
4.55E-01	-6.91E-04
3.55E-01	-6.93E-04
2.55E-01	-6.93E-04
1.55E-01	-6.93E-04
5.45E-02	-6.94E-04
-4.55E-02	-6.93E-04

d. Data on the I-V characterization under 805 Wm^{-2} light intensity.

Voltage (V)	Current Density, J (Acm^{-2})
8.07E+00	-4.57E-05
7.97E+00	-8.54E-05
7.87E+00	-1.21E-04
7.77E+00	-1.57E-04
7.67E+00	-1.92E-04
7.57E+00	-2.27E-04
7.47E+00	-2.60E-04
7.37E+00	-2.93E-04
7.27E+00	-3.24E-04
7.17E+00	-3.54E-04
7.07E+00	-3.84E-04
6.97E+00	-4.12E-04
6.87E+00	-4.39E-04
6.77E+00	-4.64E-04
6.67E+00	-4.89E-04
6.57E+00	-5.12E-04
6.47E+00	-5.34E-04
6.37E+00	-5.54E-04
6.27E+00	-5.73E-04
6.17E+00	-5.91E-04
6.07E+00	-6.38E-04
5.97E+00	-6.23E-04
5.87E+00	-6.37E-04
5.77E+00	-6.50E-04
5.67E+00	-6.61E-04
5.57E+00	-6.72E-04
5.47E+00	-6.81E-04
5.37E+00	-6.90E-04
5.27E+00	-6.98E-04
5.17E+00	-7.04E-04
5.07E+00	-7.10E-04
4.97E+00	-7.15E-04
4.87E+00	-7.19E-04
4.77E+00	-7.23E-04
4.67E+00	-7.26E-04
4.57E+00	-7.29E-04
4.47E+00	-7.29E-04
4.37E+00	-7.31E-04
4.27E+00	-7.32E-04
4.17E+00	-7.32E-04
4.07E+00	-7.33E-04
3.97E+00	-7.33E-04
3.87E+00	-7.35E-04

Voltage	Current Density
3.77E+00	-7.35E-04
3.67E+00	-7.35E-04
3.57E+00	-7.35E-04
3.47E+00	-7.36E-04
3.37E+00	-7.37E-04
3.27E+00	-7.37E-04
3.17E+00	-7.38E-04
3.07E+00	-7.40E-04
2.97E+00	-7.42E-04
2.87E+00	-7.44E-04
2.77E+00	-7.46E-04
2.67E+00	-7.49E-04
2.57E+00	-7.51E-04
2.47E+00	-7.53E-04
2.37E+00	-7.53E-04
2.27E+00	-7.54E-04
2.17E+00	-7.55E-04
2.07E+00	-7.57E-04
1.97E+00	-7.57E-04
1.87E+00	-7.59E-04
1.77E+00	-7.60E-04
1.67E+00	-7.62E-04
1.57E+00	-7.64E-04
1.47E+00	-7.64E-04
1.37E+00	-7.65E-04
1.27E+00	-7.66E-04
1.17E+00	-7.66E-04
1.07E+00	-7.66E-04
9.72E-01	-7.67E-04
8.72E-01	-7.66E-04
7.72E-01	-7.66E-04
6.72E-01	-7.67E-04
5.72E-01	-7.68E-04
4.72E-01	-7.68E-04
3.72E-01	-7.68E-04
2.72E-01	-7.67E-04
1.72E-01	-7.68E-04
7.20E-02	-7.68E-04
-2.80E-02	-7.69E-04

e.   Data on the J-V characterization under 864 Wm^{-2} light intensity.

Voltage (V)	Current Density, J (Acm^{-2})
8.14E+00	-1.95E-05
8.04E+00	-7.72E-05
7.94E+00	-1.17E-04
7.84E+00	-1.56E-04
7.74E+00	-1.92E-04
7.64E+00	-2.27E-04
7.54E+00	-2.62E-04
7.44E+00	-2.95E-04
7.34E+00	-3.27E-04
7.24E+00	-3.59E-04
7.14E+00	-3.89E-04
7.04E+00	-4.18E-04
6.94E+00	-4.46E-04
6.84E+00	-4.74E-04

6.74E+00	-5.00E-04
6.64E+00	-5.24E-04
6.54E+00	-5.48E-04
6.44E+00	-5.70E-04
6.34E+00	-5.91E-04
6.24E+00	-6.39E-04
6.14E+00	-6.29E-04
6.04E+00	-6.46E-04
5.94E+00	-6.62E-04
5.84E+00	-6.77E-04
5.74E+00	-6.90E-04
5.64E+00	-7.03E-04
5.54E+00	-7.14E-04
5.44E+00	-7.24E-04
5.34E+00	-7.32E-04
5.24E+00	-7.40E-04
5.14E+00	-7.48E-04
5.04E+00	-7.53E-04
4.94E+00	-7.59E-04
4.84E+00	-7.62E-04
4.74E+00	-7.68E-04
4.64E+00	-7.70E-04
4.54E+00	-7.72E-04
4.44E+00	-7.74E-04
4.34E+00	-7.75E-04
4.24E+00	-7.76E-04
4.14E+00	-7.76E-04
4.04E+00	-7.77E-04
3.94E+00	-7.77E-04
3.84E+00	-7.77E-04
3.74E+00	-7.77E-04
3.64E+00	-7.80E-04
3.54E+00	-7.80E-04
3.44E+00	-7.81E-04
3.34E+00	-7.81E-04
3.24E+00	-7.81E-04
3.14E+00	-7.83E-04
3.04E+00	-7.83E-04
2.94E+00	-7.86E-04
2.84E+00	-7.89E-04
2.74E+00	-7.91E-04
2.64E+00	-7.93E-04
2.54E+00	-7.95E-04
2.44E+00	-7.97E-04
2.34E+00	-7.98E-04
2.24E+00	-7.99E-04
2.14E+00	-8.00E-04
2.04E+00	-8.01E-04
1.94E+00	-8.02E-04
1.84E+00	-8.04E-04
1.74E+00	-8.06E-04
1.64E+00	-8.07E-04
1.54E+00	-8.08E-04
1.44E+00	-8.10E-04
1.34E+00	-8.11E-04
1.24E+00	-8.11E-04
1.14E+00	-8.12E-04
1.04E+00	-8.12E-04
9.43E-01	-8.12E-04
8.43E-01	-8.12E-04
7.43E-01	-8.13E-04

3E-01	-8.13E-04
3E-01	-8.13E-04
43E-01	-8.14E-04
43E-01	-8.15E-04
43E-01	-8.14E-04
43E-01	-8.14E-04
30E-02	-8.14E-04

erization under 917 Wm^{-2} light intensity.

oltage (V)	Current Density, J (Acm^{-2})
8.17E+00	-5.58E-05
8.07E+00	-1.08E-04
7.97E+00	-1.45E-04
7.87E+00	-1.82E-04
7.77E+00	-2.17E-04
7.67E+00	-2.51E-04
7.57E+00	-2.85E-04
7.47E+00	-3.17E-04
7.37E+00	-3.48E-04
7.27E+00	-3.79E-04
7.17E+00	-4.09E-04
7.07E+00	-4.37E-04
6.97E+00	-4.65E-04
6.87E+00	-4.92E-04
6.77E+00	-5.18E-04
6.67E+00	-5.42E-04
6.57E+00	-5.66E-04
6.47E+00	-5.89E-04
6.37E+00	-6.35E-04
6.27E+00	-6.31E-04
6.17E+00	-6.51E-04
6.07E+00	-6.69E-04
5.97E+00	-6.86E-04
5.87E+00	-7.02E-04
5.77E+00	-7.16E-04
5.67E+00	-7.31E-04
5.57E+00	-7.42E-04
5.47E+00	-7.53E-04
5.37E+00	-7.63E-04
5.27E+00	-7.73E-04
5.17E+00	-7.81E-04
5.07E+00	-7.89E-04
4.97E+00	-7.96E-04
4.87E+00	-8.01E-04
4.77E+00	-8.06E-04
4.67E+00	-8.10E-04
4.57E+00	-8.13E-04
4.47E+00	-8.18E-04
4.37E+00	-8.19E-04
4.27E+00	-8.21E-04
4.17E+00	-8.22E-04
4.07E+00	-8.22E-04
3.97E+00	-8.23E-04
3.87E+00	-8.23E-04
3.77E+00	-8.24E-04

Voltage	Current Density
3.67E+00	-8.24E-04
3.57E+00	-8.25E-04
3.47E+00	-8.24E-04
3.37E+00	-8.25E-04
3.27E+00	-8.26E-04
3.17E+00	-8.25E-04
3.07E+00	-8.27E-04
2.97E+00	-8.28E-04
2.87E+00	-8.30E-04
2.77E+00	-8.33E-04
2.67E+00	-8.36E-04
2.57E+00	-8.38E-04
2.47E+00	-8.41E-04
2.37E+00	-8.43E-04
2.27E+00	-8.44E-04
2.17E+00	-8.47E-04
2.07E+00	-8.49E-04
1.97E+00	-8.48E-04
1.87E+00	-8.51E-04
1.77E+00	-8.53E-04
1.67E+00	-8.56E-04
1.57E+00	-8.57E-04
1.47E+00	-8.58E-04
1.37E+00	-8.59E-04
1.27E+00	-8.60E-04
1.17E+00	-8.60E-04
1.07E+00	-8.60E-04
9.65E-01	-8.60E-04
8.65E-01	-8.61E-04
7.65E-01	-8.61E-04
6.65E-01	-8.61E-04
5.65E-01	-8.63E-04
4.65E-01	-8.63E-04
3.65E-01	-8.63E-04
2.65E-01	-8.64E-04
1.65E-01	-8.64E-04
6.50E-02	-8.64E-04
-3.50E-02	-8.66E-04

g. Data on the J-V characterization under 997.32 Wm^{-2} light intensity.

Voltage (V)	Current Density, J (Acm^{-2})
8.14E+00	-5.71E-05
8.04E+00	-1.15E-04
7.94E+00	-1.54E-04
7.84E+00	-1.93E-04
7.74E+00	-2.31E-04
7.64E+00	-2.67E-04
7.54E+00	-3.04E-04
7.44E+00	-3.38E-04
7.34E+00	-3.73E-04
7.24E+00	-4.06E-04
7.14E+00	-4.39E-04
7.04E+00	-4.70E-04
6.94E+00	-5.01E-04
6.84E+00	-5.31E-04

6.74E+00	
6.64E+00	-5.59E-04
6.54E+00	-5.88E-04
6.44E+00	-6.35E-04
6.34E+00	-6.40E-04
6.24E+00	-6.64E-04
6.14E+00	-6.88E-04
6.04E+00	-7.10E-04
5.94E+00	-7.31E-04
5.84E+00	-7.50E-04
5.74E+00	-7.69E-04
5.64E+00	-7.86E-04
5.54E+00	-8.01E-04
5.44E+00	-8.17E-04
5.34E+00	-8.30E-04
5.24E+00	-8.43E-04
5.14E+00	-8.55E-04
5.04E+00	-8.65E-04
4.94E+00	-8.74E-04
4.84E+00	-8.82E-04
4.74E+00	-8.89E-04
4.64E+00	-8.95E-04
4.54E+00	-9.00E-04
4.44E+00	-9.06E-04
4.34E+00	-9.08E-04
4.24E+00	-9.09E-04
4.14E+00	-9.12E-04
4.04E+00	-9.14E-04
3.94E+00	-9.15E-04
3.84E+00	-9.16E-04
3.74E+00	-9.17E-04
3.64E+00	-9.16E-04
3.54E+00	-9.17E-04
3.44E+00	-9.19E-04
3.34E+00	-9.19E-04
3.24E+00	-9.20E-04
3.14E+00	-9.21E-04
3.04E+00	-9.20E-04
2.94E+00	-9.24E-04
2.84E+00	-9.25E-04
2.74E+00	-9.27E-04
2.64E+00	-9.30E-04
2.54E+00	-9.31E-04
2.44E+00	-9.33E-04
2.34E+00	-9.34E-04
2.24E+00	-9.36E-04
2.14E+00	-9.37E-04
2.04E+00	-9.38E-04
1.94E+00	-9.38E-04
1.84E+00	-9.40E-04
1.74E+00	-9.42E-04
1.64E+00	-9.45E-04
1.54E+00	-9.49E-04
1.44E+00	-9.51E-04
1.34E+00	-9.51E-04
1.24E+00	-9.54E-04
1.14E+00	-9.55E-04
1.04E+00	-9.58E-04
9.38E-01	-9.59E-04
8.38E-01	-9.59E-04
7.38E-01	-9.59E-04
	-9.60E-04

6.38E-01	-9.61E-04
5.38E-01	-9.61E-04
4.38E-01	-9.62E-04
3.38E-01	-9.64E-04
2.38E-01	-9.65E-04
1.38E-01	-9.67E-04
3.75E-02	-9.66E-04

A6. Data on the Effect of Temperature on the DSSM's *J-V* Characteristics.

a. Data for 31.6°C module temperature

Current Density, J (Acm^{-2})	Voltage (V)
-7.98E-04	1.24E+00
-7.88E-04	1.78E+00
-7.78E-04	2.21E+00
-7.68E-04	2.60E+00
-7.58E-04	2.96E+00
-7.48E-04	3.31E+00
-7.38E-04	3.65E+00
-7.28E-04	3.98E+00
-7.18E-04	4.30E+00
-7.08E-04	4.61E+00
-6.98E-04	4.91E+00
-6.88E-04	5.20E+00
-6.78E-04	5.49E+00
-6.68E-04	5.77E+00
-6.58E-04	6.20E+00
-6.48E-04	6.29E+00
-6.38E-04	6.54E+00
-6.28E-04	6.77E+00
-6.18E-04	7.00E+00
-6.08E-04	7.22E+00
-5.98E-04	7.41E+00
-5.88E-04	7.61E+00
-5.78E-04	7.80E+00
-5.68E-04	7.96E+00
-5.58E-04	8.12E+00
-5.48E-04	8.27E+00
-5.38E-04	8.41E+00
-5.28E-04	8.54E+00
-5.18E-04	8.65E+00
-5.08E-04	8.75E+00
-4.98E-04	8.84E+00

-4.88E-04	8.93E+00
-4.78E-04	9.00E+00
-4.68E-04	9.06E+00
-4.58E-04	9.12E+00
-4.48E-04	9.16E+00
-4.38E-04	9.20E+00
-4.28E-04	9.22E+00
-4.18E-04	9.24E+00
-4.08E-04	9.25E+00
-3.98E-04	9.26E+00
-3.88E-04	9.26E+00
-3.78E-04	9.27E+00
-3.68E-04	9.28E+00
-3.58E-04	9.27E+00
-3.48E-04	9.27E+00
-3.38E-04	9.27E+00
-3.28E-04	9.29E+00
-3.18E-04	9.29E+00
-3.08E-04	9.29E+00
-2.98E-04	9.29E+00
-2.88E-04	9.31E+00
-2.78E-04	9.33E+00
-2.68E-04	9.37E+00
-2.58E-04	9.40E+00
-2.48E-04	9.44E+00
-2.38E-04	9.48E+00
-2.28E-04	9.50E+00
-2.18E-04	9.51E+00
-2.08E-04	-9.53E-04
-1.98E-04	-9.54E-04
-1.88E-04	-9.57E-04
-1.78E-04	-9.60E-04
-1.68E-04	9.63E+00
-1.58E-04	9.66E+00
-1.48E-04	9.67E+00
-1.38E-04	9.68E+00
-1.28E-04	9.70E+00
-1.18E-04	9.71E+00
-1.08E-04	9.72E+00
-9.85E-05	9.73E+00
-8.85E-05	9.73E+00
-7.85E-05	9.74E+00
-6.85E-05	9.74E+00
-5.85E-05	9.75E+00
-4.85E-05	9.76E+00
-3.85E-05	9.77E+00
-2.85E-05	9.78E+00

-1.85E-05	9.79E+00
-8.45E-06	9.80E+00

b. Data for 32.8°C module temperature

Current Density, J (Acm^{-2})	Voltage (V)
-8.26E-04	3.48E+00
-8.16E-04	7.66E+00
-8.06E-04	1.15E+00
-7.96E-04	1.54E+00
-7.86E-04	1.91E+00
-7.76E-04	2.28E+00
-7.66E-08	2.64E+00
-7.56E-04	3.00E+00
-7.46E-04	3.34E+00
-7.36E-04	3.68E+00
-7.26E-04	4.01E+00
-7.16E-04	4.33E+00
-7.06E-04	4.64E+00
-6.96E-04	4.94E+00
-6.86E-04	5.23E+00
-6.76E-04	5.52E+00
-6.66E-04	5.79E+00
-6.56E-04	6.23E+00
-6.46E-04	6.31E+00
-6.36E-04	6.55E+00
-6.26E-04	6.79E+00
-6.16E-04	7.01E+00
-6.06E-04	7.21E+00
-5.96E-04	7.41E+00
-5.86E-04	7.59E+00
-5.76E-04	7.76E+00
-5.66E-04	7.92E+00
-5.56E-04	8.07E+00
-5.46E-04	8.19E+00
-5.36E-04	8.32E+00
-5.26E-04	8.43E+00
-5.16E-04	8.54E+00
-5.06E-04	8.63E+00
-4.96E-04	8.72E+00
-4.86E-04	8.79E+00
-4.76E-04	8.86E+00
-4.66E-04	8.92E+00
-4.56E-04	8.97E+00

-4.46E-04	8.99E+00
-4.36E-04	9.02E+00
-4.26E-04	9.05E+00
-4.16E-04	9.06E+00
-4.06E-04	9.07E+00
-3.96E-04	9.09E+00
-3.86E-04	9.09E+00
-3.76E-04	9.10E+00
-3.66E-04	9.09E+00
-3.56E-04	9.11E+00
-3.46E-04	9.10E+00
-3.36E-04	9.10E+00
-3.26E-04	9.11E+00
-3.16E-04	9.11E+00
-3.06E-04	9.12E+00
-2.96E-04	9.13E+00
-2.86E-04	9.15E+00
-2.76E-04	9.17E+00
-2.66E-04	9.19E+00
-2.56E-04	9.22E+00
-2.46E-04	9.25E+00
-2.36E-04	9.26E+00
-2.26E-04	9.27E+00
-2.16E-04	9.29E+00
-2.06E-04	9.29E+00
-1.96E-04	9.30E+00
-1.86E-04	9.32E+00
-1.76E-04	9.34E+00
-1.66E-04	9.37E+00
-1.56E-04	9.39E+00
-1.46E-04	9.40E+00
-1.36E-04	9.42E+00
-1.26E-04	9.43E+00
-1.16E-04	9.44E+00
-1.06E-04	9.44E+00
-9.57E-05	9.45E+00
-8.57E-05	9.45E+00
-7.57E-05	9.45E+00
-6.57E-05	9.45E+00
-5.57E-05	9.47E+00
-4.57E-05	9.47E+00
-3.57E-05	9.47E+00
-2.57E-05	9.47E+00
-1.57E-05	9.48E+00
-5.70E-06	9.48E+00

c. **Data** for 34.2 °C module temperature

Current Density, J (Acm^{-2})	Voltage (V)
-8.00E-04	1.20E+00
-7.90E-04	1.55E+00
-7.80E-04	1.92E+00
-7.70E-04	2.28E+00
-7.60E-04	2.64E+00
-7.50E-04	2.98E+00
-7.40E-04	3.32E+00
-7.30E-04	3.65E+00
-7.20E-04	3.97E+00
-7.10E-04	4.28E+00
-7.00E-04	4.58E+00
-6.90E-04	4.88E+00
-6.80E-04	5.16E+00
-6.70E-04	5.43E+00
-6.60E-04	5.68E+00
-6.00E-45	5.93E+00
-6.40E-04	6.43E+00
-6.30E-04	6.40E+00
-6.20E-04	6.60E+00
-6.10E-04	6.80E+00
-6.00E-04	6.99E+00
-5.90E-04	7.16E+00
-5.80E-04	7.32E+00
-5.70E-04	7.48E+00
-5.60E-04	7.62E+00
-5.50E-04	7.73E+00
-5.40E-04	7.85E+00
-5.30E-04	7.96E+00
-5.20E-04	8.06E+00
-5.10E-04	8.14E+00
-5.00E-04	8.22E+00
-4.90E-04	8.28E+00
-4.80E-04	8.34E+00
-4.70E-04	8.38E+00
-4.60E-04	8.42E+00
-4.50E-04	8.45E+00
-4.40E-04	8.47E+00
-4.30E-04	8.49E+00
-4.20E-04	8.49E+00
-4.10E-04	8.51E+00
-4.00E-04	8.52E+00
-3.90E-04	8.51E+00

-3.80E-04	8.53E+00
-3.70E-04	8.53E+00
-3.60E-04	8.52E+00
-3.50E-04	8.53E+00
-3.40E-04	8.52E+00
-3.30E-04	8.52E+00
-3.20E-04	8.53E+00
-3.10E-04	8.54E+00
-3.00E-04	8.57E+00
-2.90E-04	8.58E+00
-2.80E-04	8.60E+00
-2.70E-04	8.63E+00
-2.60E-04	8.65E+00
-2.50E-04	8.67E+00
-2.40E-04	8.68E+00
-2.30E-04	8.70E+00
-2.20E-04	8.71E+00
-2.10E-04	8.72E+00
-2.00E-04	8.72E+00
-1.90E-04	8.74E+00
-1.80E-04	8.77E+00
-1.70E-04	8.80E+00
-1.60E-04	8.81E+00
-1.50E-04	8.82E+00
-1.40E-04	8.83E+00
-1.30E-04	8.84E+00
-1.20E-04	8.84E+00
-1.10E-04	8.85E+00
-9.98E-05	8.84E+00
-8.98E-05	8.84E+00
-7.98E-05	8.85E+00
-6.98E-05	8.86E+00
-5.98E-05	8.85E+00
-4.98E-05	8.86E+00
-3.98E-05	8.84E+00
-2.98E-05	8.86E+00
-1.98E-05	8.86E+00
-9.75E-06	8.86E+00

d. Data for 36.8°C module temperature

Current Density, J (Acm^{-2})	Voltage (V)
-7.87E-04	1.45E+00
-7.77E-04	1.78E+00

-7.67E-04	2.12E+00
-7.57E-04	2.46E+00
-7.47E-04	2.79E+00
-7.37E-04	3.11E+00
-7.27E-04	3.43E+00
-7.17E-04	3.73E+00
-7.07E-04	4.02E+00
-6.97E-04	4.30E+00
-6.87E-04	4.57E+00
-6.77E-04	4.83E+00
-6.67E-04	5.08E+00
-6.57E-04	5.32E+00
-6.47E-04	5.54E+00
-6.37E-04	5.75E+00
-6.27E-04	5.94E+00
-6.17E-04	6.45E+00
-6.07E-04	6.30E+00
-5.97E-04	6.45E+00
-5.87E-04	6.60E+00
-5.77E-04	6.73E+00
-5.67E-04	6.85E+00
-5.57E-04	6.97E+00
-5.47E-04	7.07E+00
-5.37E-04	7.15E+00
-5.27E-04	7.23E+00
-5.17E-04	7.30E+00
-5.07E-04	7.37E+00
-4.97E-04	7.42E+00
-4.87E-04	7.46E+00
-4.77E-04	7.51E+00
-4.67E-04	7.54E+00
-4.57E-04	7.55E+00
-4.47E-04	7.57E+00
-4.37E-04	7.59E+00
-4.27E-04	7.61E+00
-4.17E-04	7.61E+00
-4.07E-04	7.61E+00
-3.97E-04	7.62E+00
-3.87E-04	7.63E+00
-3.77E-04	7.63E+00
-3.67E-04	7.64E+00
-3.57E-04	7.63E+00
-3.47E-04	7.66E+00
-3.37E-04	7.64E+00
-3.27E-04	7.65E+00
-3.17E-04	7.66E+00
-3.07E-04	7.68E+00

-2.97E-04	7.70E+00
-2.87E-04	7.72E+00
-2.77E-04	7.74E+00
-2.67E-04	7.77E+00
-2.57E-04	7.78E+00
-2.47E-04	7.81E+00
-2.37E-04	7.81E+00
-2.27E-04	7.83E+00
-2.17E-04	7.84E+00
-2.07E-04	7.85E+00
-1.97E-04	7.87E+00
-1.87E-04	7.90E+00
-1.77E-04	7.92E+00
-1.67E-04	7.93E+00
-1.57E-04	7.93E+00
-1.47E-04	7.94E+00
-1.37E-04	7.96E+00
-1.27E-04	7.95E+00
-1.17E-04	7.96E+00
-1.07E-04	7.96E+00
-9.75E-05	7.98E+00
-8.75E-05	7.97E+00
-7.75E-05	7.97E+00
-6.75E-05	7.97E+00
-5.75E-05	7.98E+00
-4.75E-05	7.98E+00
-3.75E-05	7.98E+00
-2.75E-05	7.98E+00
-1.75E-05	7.98E+00
-7.45E-06	7.99E+00
-9.75E-06	8.86E+00

e. Data for 37.4°C module temperature

Current Density, J (Acm^{-2})	Voltage (V)
-8.00E-04	4.57E+00
-7.97E-04	8.54E+00
-7.87E-04	1.21E+00
-7.77E-04	1.57E+00
-7.67E-04	1.92E+00
-7.57E-04	2.27E+00
-7.47E-04	2.60E+00
-7.37E-04	2.93E+00
-7.27E-04	3.24E+00
-7.17E-04	3.54E+00

-7.07E-04	3.84E+00
-6.97E-04	4.12E+00
-6.87E-04	4.39E+00
-6.77E-04	4.64E+00
-6.67E-04	4.89E+00
-6.57E-04	5.12E+00
-6.47E-04	5.34E+00
-6.37E-04	5.54E+00
-6.27E-04	5.73E+00
-6.17E-04	5.91E+00
-6.07E-04	6.38E+00
-5.97E-04	6.23E+00
-5.87E-04	6.37E+00
-5.77E-04	6.50E+00
-5.67E-04	6.61E+00
-5.57E-04	6.72E+00
-5.47E-04	6.81E+00
-5.37E-04	6.90E+00
-5.27E-04	6.98E+00
-5.17E-04	7.04E+00
-5.07E-04	7.10E+00
-4.97E-04	7.15E+00
-4.87E-04	7.19E+00
-4.77E-04	7.23E+00
-4.67E-04	7.26E+00
-4.57E-04	7.29E+00
-4.47E-04	7.29E+00
-4.37E-04	7.31E+00
-4.27E-04	7.32E+00
-4.17E-04	7.32E+00
-4.07E-04	7.33E+00
-3.97E-04	7.33E+00
-3.87E-04	7.35E+00
-3.77E-04	7.35E+00
-3.67E-04	7.35E+00
-3.57E-04	7.35E+00
-3.47E-04	7.36E+00
-3.37E-04	7.37E+00
-3.27E-04	7.37E+00
-3.17E-04	7.38E+00
-3.07E-04	7.40E+00
-2.97E-04	7.42E+00
-2.87E-04	7.44E+00
-2.77E-04	7.46E+00
-2.67E-04	7.49E+00
-2.57E-04	7.51E+00
-2.47E-04	7.53E+00

-2.37E-04	7.53E+00
-2.27E-04	7.54E+00
-2.17E-04	7.55E+00
-2.07E-04	7.57E+00
-1.97E-04	7.57E+00
-1.87E-04	7.59E+00
-1.77E-04	7.60E+00
-1.67E-04	7.62E+00
-1.57E-04	7.64E+00
-1.47E-04	7.64E+00
-1.37E-04	7.65E+00
-1.27E-04	7.66E+00
-1.17E-04	7.66E+00
-1.07E-04	7.66E+00
-9.72E-05	7.67E+00
-8.72E-05	7.66E+00
-7.72E-05	7.66E+00
-6.72E-05	7.67E+00
-5.72E-05	7.68E+00
-4.72E-05	7.68E+00
-3.72E-05	7.68E+00
-2.72E-05	7.67E+00
-1.72E-05	7.68E+00
-7.20E-06	7.68E+00

f. Data at 39.5°C module temperature

Current Density, J (Acm^{-2})	Voltage (V)
-7.72E-04	1.80E+00
-7.62E-04	2.20E+00
-7.52E-04	2.56E+00
-7.42E-04	2.87E+00
-7.32E-04	3.17E+00
-7.22E-04	3.45E+00
-7.12E-04	3.72E+00
-7.02E-04	3.98E+00
-6.92E-04	4.22E+00
-6.82E-04	4.45E+00
-6.72E-04	4.67E+00
-6.62E-04	4.88E+00
-6.52E-04	5.08E+00
-6.42E-04	5.26E+00
-6.32E-04	5.43E+00
-6.22E-04	5.59E+00
-6.12E-04	5.74E+00
-6.02E-04	5.87E+00

-5.92E-04	5.99E+00
-5.82E-04	6.52E+00
-5.72E-04	6.20E+00
-5.62E-04	6.29E+00
-5.52E-04	6.38E+00
-5.42E-04	6.44E+00
-5.32E-04	6.51E+00
-5.22E-04	6.57E+00
-5.12E-04	6.62E+00
-5.02E-04	6.66E+00
-4.92E-04	6.70E+00
-4.82E-04	6.73E+00
-4.72E-04	6.75E+00
-4.62E-04	6.77E+00
-4.52E-04	6.78E+00
-4.42E-04	6.79E+00
-4.32E-04	6.81E+00
-4.22E-04	6.81E+00
-4.12E-04	6.82E+00
-4.02E-04	6.83E+00
-3.92E-04	6.83E+00
-3.82E-04	6.84E+00
-3.72E-04	6.84E+00
-3.62E-04	6.84E+00
-3.52E-04	6.84E+00
-3.42E-04	6.85E+00
-3.32E-04	6.86E+00
-3.22E-04	6.86E+00
-3.12E-04	6.87E+00
-3.02E-04	6.89E+00
-2.92E-04	6.91E+00
-2.82E-04	6.93E+00
-2.72E-04	6.94E+00
-2.62E-04	6.96E+00
-2.52E-04	6.98E+00
-2.42E-04	6.97E+00
-2.32E-04	6.97E+00
-2.22E-04	6.98E+00
-2.12E-04	6.98E+00
-2.02E-04	6.99E+00
-1.92E-04	6.99E+00
-1.82E-04	7.00E+00
-1.72E-04	7.02E+00
-1.62E-04	7.02E+00
-1.52E-04	7.03E+00
-1.42E-04	7.03E+00
-1.32E-04	7.03E+00

Current Density	Voltage
-1.22E-04	7.03E+00
-1.12E-04	7.04E+00
-1.02E-04	7.05E+00
-9.24E-05	7.04E+00
-8.24E-05	7.05E+00
-7.24E-05	7.04E+00
-6.24E-05	7.04E+00
-5.24E-05	7.05E+00
-4.24E-05	7.04E+00
-3.24E-05	7.05E+00
-2.24E-05	7.05E+00
-1.24E-05	7.05E+00

g. Data at 43.8°C module temperature

Current Density, J (Acm^{-2})	Voltage (V)
-7.92E-04	1.26E+00
-7.82E-04	1.53E+00
-7.72E-04	1.80E+00
-7.62E-04	2.07E+00
-7.52E-04	2.33E+00
-7.42E-04	2.57E+00
-7.32E-04	2.81E+00
-7.22E-04	4.04E+00
-7.12E-04	3.27E+00
-7.02E-04	3.47E+00
-6.92E-04	3.67E+00
-6.82E-04	3.86E+00
-6.72E-04	4.03E+00
-6.62E-04	4.19E+00
-6.52E-04	4.35E+00
-6.42E-04	4.49E+00
-6.32E-04	4.61E+00
-6.22E-04	4.73E+00
-6.12E-04	4.84E+00
-6.02E-04	4.93E+00
-5.92E-04	5.02E+00
-5.82E-04	5.11E+00
-5.72E-04	5.18E+00
-5.62E-04	5.24E+00
-5.52E-04	5.29E+00
-5.42E-04	5.36E+00
-5.32E-04	5.40E+00
-5.22E-04	5.43E+00
-5.12E-04	5.45E+00
-5.02E-04	5.48E+00

-4.92E-04	5.51E+00
-4.82E-04	5.51E+00
-4.72E-04	5.52E+00
-4.62E-04	5.53E+00
-4.52E-04	5.54E+00
-4.42E-04	5.55E+00
-4.32E-04	5.56E+00
-4.22E-04	5.56E+00
-4.12E-04	5.57E+00
-4.02E-04	5.58E+00
-3.92E-04	5.58E+00
-3.82E-04	5.58E+00
-3.72E-04	5.58E+00
-3.62E-04	5.59E+00
-3.52E-04	5.59E+00
-3.42E-04	5.59E+00
-3.32E-04	5.60E+00
-3.22E-04	5.62E+00
-3.12E-04	5.63E+00
-3.02E-04	5.64E+00
-2.92E-04	5.65E+00
-2.82E-04	5.67E+00
-2.72E-04	5.67E+00
-2.62E-04	5.68E+00
-2.52E-04	5.68E+00
-2.42E-04	5.69E+00
-2.32E-04	5.69E+00
-2.22E-04	5.70E+00
-2.12E-04	5.70E+00
-2.02E-04	5.71E+00
-1.92E-04	5.73E+00
-1.82E-04	5.73E+00
-1.72E-04	5.74E+00
-1.62E-04	5.75E+00
-1.52E-04	5.75E+00
-1.42E-04	5.75E+00
-1.32E-04	5.75E+00
-1.22E-04	5.75E+00
-1.12E-04	5.74E+00
-1.02E-04	5.75E+00
-9.18E-05	5.75E+00
-8.18E-05	5.75E+00
-7.18E-05	5.76E+00
-6.18E-05	5.75E+00
-5.18E-05	5.75E+00

G24i

Dye Sensitised Outdoor Photovoltaic Module

FLEXIBLE

Omny
data sheet
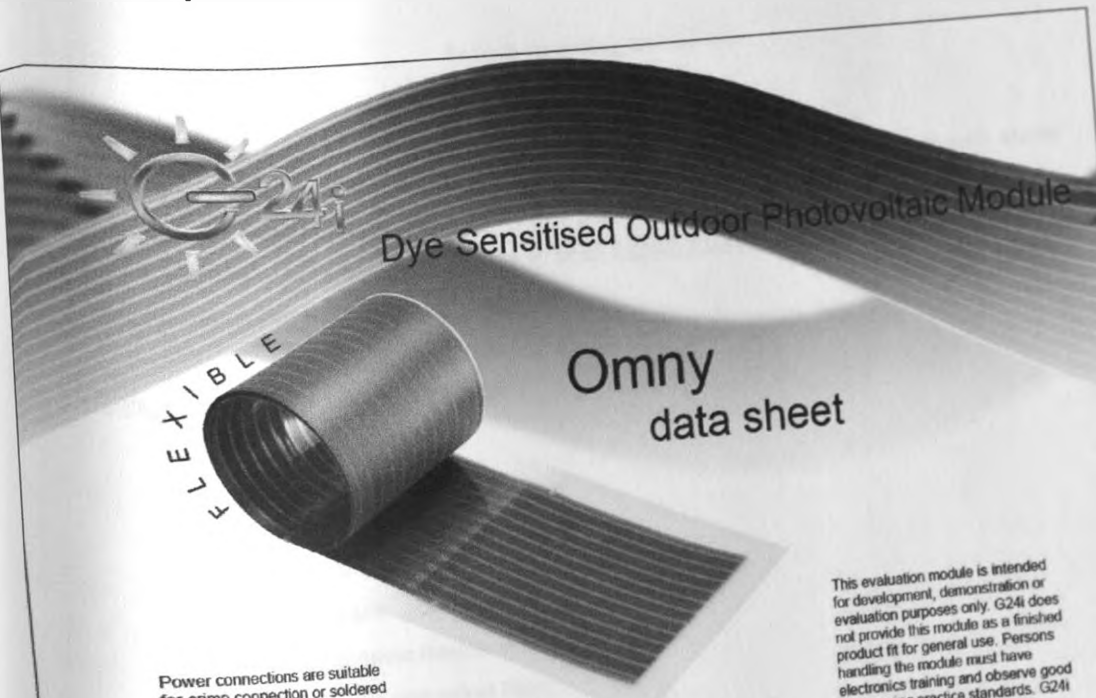
Power connections are suitable for crimp connection or soldered connection with the appropriate use of heat-shunt tweezers to ensure minimal heating of the polymer material.

This evaluation module is intended for development, demonstration or evaluation purposes only. G24i does not provide this module as a finished product fit for general use. Persons handling the module must have electronics training and observe good engineering practice standards. G24i reserves the right to change the module specification at any time.
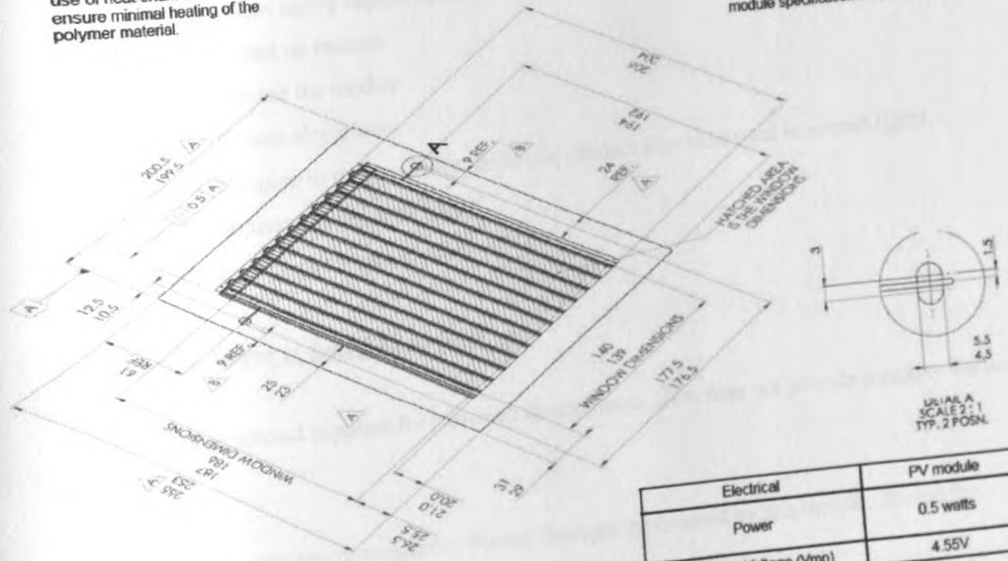
Electrical	PV module
Power	0.5 watts
Operating Voltage (Vmp)	4.55V
Operating current (Imp)	110mA
Typical Open Circuit Voltage (Voc)	8.0V
Typical Short Circuit Current (Isc)	140mA

G24 Innovations Ltd, Wentloog Environmental Centre, Cardiff, UK, CF3 2GH Tel:+44 (0) 2920 837 340
www.g24i.com
For all prototype samples e-mail: sales@g24i.com
G0117, Iss01

48. The Omny 11200 DSSM Prototype Operating Instructions from G24i

Sample Operating Instructions
Instructions

This DSC solar panel sample is for the customer to trial in different applications. Simply attache connections to the terminals and place the solar panel in a sunny location to provide electricity. Please call G24 Innovations on 02920837 340 or email info@24i.com to discuss wiring, electronics and incorporation into different assemblies.

Important System Care Instructions

- DO NOT pierce module
- DO NOT cut the module
- DO NOT put the module in mouth
- DO NOT ingest
- DO NOT immerse module in liquid
- DO NOT place near naked flame
- DO NOT place heavy objects on module
- DO NOT stand on module
- DO NOT crease the module
- DO NOT shade along lanes
- DO NOT expose to intense light sources (the product should be used in normal light)
- Avoid temperatures above 65 Deg C
- If module damaged return to G24i

Terms & Conditions of supply of samples

This is a sample product supplied for prototype development. G24i does not provide warranty for this sample.

G24i does not assume any responsibility for any damages occasioned by this sample. Should the sample prove defective, please return to:

Address: G24 Innovations Ltd
                  Wentloog Environmental Centre
                  Wentloog Ave
                  United Kingdom
                  CF3 2EE

Web: www.g24i.com

Application of Dye-Sensitized Solar Cell Technology in the Tropics: Effects of Radiation Intensity and Temperature on DSSC Performance

Otakwa R. V. M*; Simiyu, J.; Waita, S. M. and Mwabora J. M

Department of Physics, College of Physical and Biological Sciences, University of Nairobi,
PO Box 30197 – 00100 GPO, Nairobi, KENYA
*Corresponding author: raphael.makokha@yahoo.com

Abstract - effects of radiation intensity and temperature on the performance of a dye-sensitized solar module (DSSM) have been investigated in a tropical area in Nairobi, Kenya. Outdoor measurements were performed on cloudless days at normal incidence of the incoming solar beam radiation to the module. A series of current-voltage (I-V) characterizations were carried out at different solar radiation intensities and module temperatures. The module performance parameters: Short circuit current density, (I_{sc}), Open circuit voltage, (V_{oc}), Fill factor, (FF) and solar-to-electricity conversion efficiency, (η) were extracted from the I-V curves. Better efficiencies were observed at lower than higher radiation intensities. There was also an overall improved performance at elevated temperatures. The results may be useful during fabrication of dye-sensitized solar cells meant for use in the tropics.

Index Terms— Dye-sensitized, performance, radiation, temperature, tropics

I. INTRODUCTION

The need to switch to the use of renewable energy is ever increasing. Fossil fuel reserves that have been depended upon to provide the world's energy are quickly diminishing [1][2]. This decline has amplified costs of fossil fuel exploration and mining [1]. The sensitive geopolitical issues experienced by countries with fossil fuel reserves [3] make the situation worse. These matters have contributed to the escalation of energy costs that have pushed energy out of reach for many people. Those at the bottom of the economic pyramid are the worst affected [4].

The over-reliance upon fossil fuels by the world [5] has also been linked to the increase in acid rains, greenhouse gases and depletion of the ozone layer [6]. Impacts of greenhouse gases, e.g., global warming have been widespread [7][8].They have adversely affected life on earth [9]. Adoption of energy sources that are alternative to fossil fuels and renewable in nature is imperative. These renewable energy sources include biomass, geothermal, tidal, water cycle or

hydro, atmospheric movements and solar radiation [10]. They are consequences of the earth's inherent heat, gravitational perturbations by the moon and sun, and solar radiation [11].

The most abundant and fairly distributed of these is solar radiation with about 3.9×10^{24} joules of solar energy reaching the earth annually [12]. This impressive supply of solar energy is complemented by its vast resourcefulness – it can be converted into electricity by exciting electrons in a solar cell and can also yield chemical fuel through natural photosynthesis in green plants or artificial photosynthesis in human-engineered systems. Solar energy can also be used to produce heat for direct use or for further conversion to electricity [12].

Though the prices of solar photovoltaic (PV) systems are currently high [14], investing in solar power assures free energy after a reasonable payback period. This makes solar electricity both cost effective and economical [15] in the long run. Solar energy is also environmentally friendly [16] and can be availed even to the remotest parts of the world. [17] has attributed this to the minimal incidences of wear and tear by solar energy systems since they do not comprise of heavy moving parts. Solar energy is also free, abundant, readily available, and does not interfere with people's ways of life. Generation of electricity from solar energy is therefore a socially, politically, economically, environmentally and culturally (SPEEC) attractive method of directly generating electrical power.

Reduction in solar energy cost will enhance its penetration, especially among the poor. This in turn will improve the ecological footprint of communities, nations and the world. Though first generation silicon solar devices dominate the PV market currently, their fabrication costs are high, which calls for high efficiencies [18]. This translates to high prices, hence choking their penetration to the poor. Second generation

solar devices are also expensive to fabricate. Third generation solar cells, the dye-sensitized solar cell are cheaper alternatives to the conventional silicon solar cells as well as the second generation solar cells, and can be fabricated under less stringent conditions [19]. They are therefore favorable in taking up the huge energy opportunities that exist in the tropics. They have however not been field-tested in the tropics, which is the focus of this study.

II. MATERIALS AND METHODS

A. Basic Theory

1) J-V characterization

The response of a PV device is determined by its J-V characteristics both in the dark and under illumination. The J-V characteristics are in practical cases modeled according to the ideal diode equation (1), which for accounts for the shunt and series resistances [20],

$$J = J_L - J_s \exp\left[\frac{V + R_S J}{m V_T}\right] - \sigma V \qquad (1)$$

where J, J_L, J_s, V, m, V_T, R_s, J, and σ are the ideal current density, the current density from the source (in this work, it is the photo-generated current density, J_{ph} and will be referred to as such), the saturation current density, voltage across the PV terminals, the ideality factor, series resistance and shunt conductance respectively.

In the dark, an applied voltage, known also as the bias voltage generates current density in the opposite direction to the one generated by light. This current density is known as the dark current density and is computed from the equation [21] [20],

$$J_{dark} = -J_s \exp\left[\frac{V + R_s J}{m V_T}\right] - \sigma V \qquad (2)$$

where J, J_{dark}, J_s, V, m, V_T, R_s, J, and σ are the ideal current density, the dark current density, the saturation current density, voltage across the PV terminals of the PV device, the ideality factor (=1 for an ideal PV device or ≠1 for a non-ideal PV device), series resistance and shunt conductance respectively.

Under illumination, the J-V characteristics are described by the equation [22] [20],

$$J = J_{ph} - J_s \exp\left[\frac{V + R_s J}{m V_T}\right] - \sigma V \qquad (3)$$

where J, J_{ph}, J_s, V, m, V_T, R_s, and σ are the ideal current density, the photo-generated current density, the saturation current density, voltage across the PV device terminals, the ideality factor (=1 for an ideal device or ≠1 for a non-ideal device), the thermal voltage, series resistance and shunt conductance respectively.

Setting of the ideality factor in equation (1) to one is the ideal case that assumes that all recombinations in the PV device occur via the band to band or the bulk areas of the PV device – not in the junction. The ideality factor describes how closely the PV device follows the ideal case scenario. In practical cases, PV devices are non-ideal since recombinations occur in other ways and areas of the devices other than only via band to band or in the bulk area of the devices. These devices yield ideality factors that deviate from the ideal.

From equations (2) and (3), the dark current density and photo-generated current density (respectively) can be plotted as functions of the applied bias voltage. This results in a curve typically known as the current density-voltage (J-V) characteristic curve. From the J-V curve, key parameters; V_{oc}, J_{sc}, J_s, FF, R_s, R_{sh} can be extracted and, m and η computed. V_{oc} is the voltage measured when the terminals of a PV device are isolated. It relates to the condition when the potential difference is at its maximum value. At this point, dark current density and short circuit photo-current densities exactly cancel out and no flow of current is observed between the PV terminals. Setting J to zero in equation (3) and rearranging yields equation (4) that can be used to compute the photo-generated current, J_{ph}.

$$J_{ph} = J_s \exp\left[\frac{V}{m V_T}\right] \qquad (4)$$

where J_{ph}, J_s, V m, and V_T are the photo-generated current density, the saturation current density, voltage across the PV device's terminals, the ideality factor and the thermal voltage respectively.

When V is maximum, i.e., V=V_{oc}, equation (4) leads to,

$$J_{ph} = J_s \exp\left[\frac{V_{oc}}{m V_T}\right] \qquad (5)$$

where J_{ph}, J_s, V_{oc}, m, V_T and σ are the photo-generated current density, the saturation current density, the open circuit voltage, the ideality factor, thermal voltage and shunt conductance respectively.

Making V_{oc} the subject in equation (5) yields (6), which describes the voltage at zero current. This is the open circuit voltage,

$$V_{oc} = mV_T \ln \frac{J_{ph}}{J_s} \qquad (6)$$

where J_{ph}, J_s, V_{oc}, m and V_T are the photo-generated current density, the saturation current density, the open circuit voltage and the ideality factor and the thermal voltage respectively.

J_{sc} describes the photo-generated charge carriers, which in the case of exposure of the PV device to light is the light-generated current density. It is measured at the condition when the applied voltage is zero. Essentially, this is the current measured when the circuit is shorted and both the load and power are zero. If we set the applied voltage, V to zero and J to J_{sc} in equation (3), we obtain,

$$J_{sc} = J_{ph} - J_s \qquad (7)$$

where J_{sc}, J_{ph}, and J_s are the short circuit current density, the photo-generated current density and the saturation current respectively.
This implies that,

$$J_{sc} \equiv J_{ph} \qquad (8)$$

where J_{sc} and J_{ph} are the short circuit current density and the photo-generated current density respectively.

The actual current that flows out of a solar PV device is the ideal current, i.e., the short-circuit current density, minus the current that flows through the diode or dark current density, J_{dark},

$$J = J_{sc} - J_{dark} \qquad (9)$$

where J, J_{sc} and J_{dark} are the ideal current density, the short circuit current density and the dark current density respectively.

FF is generally influenced by the series and shunt resistances. It is a measure of the squareness of the J-V curve and hence the quality of the solar PV device. It is defined as the ratio. It is determined from equation [22],

$$FF = \frac{P_m}{V_{oc}J_{sc}} = \frac{J_{mp}V_{mp}}{V_{oc}J_{sc}} \qquad (10)$$

where FF, P_m, V_{oc}, J_{sc}, J_{mp} and V_{mp} are the fill factor, maximum power, the open circuit voltage, the short circuit current density, the maximum power current density and the maximum power voltage respectively.
A PV device's maximum power (P_m), maximum power current density (J_{mp}) and maximum power voltage (V_{mp}) are be extracted from a P-V curve. There exists a certain potential between the J_{sc} and V_{oc} on the J-V curve where P_m is found.

At this point, the solar PV device delivers the highest power output (P_m). Voltage at this point is known as the maximum power voltage, while the current density is known as the maximum power current density. P_m, V_{mp}, J_{mp} can also be computed as shown in equations (11), (12) and (13),

$$P_m = FFV_{oc}J_{sc} \qquad (11)$$

$$V_{mp} = \frac{FFV_{oc}J_{sc}}{J_{mp}} \qquad (12)$$

$$J_{mp} = \frac{FFV_{oc}J_{sc}}{V_{mp}} \qquad (13)$$

where P_m, FF, V_{oc}, J_{sc}, J_{mp} and V_{mp} are the maximum power, the fill factor, the open circuit voltage, the short circuit current density, the current density at maximum power and the voltage at maximum power respectively.

η is associated with the overall performance of the PV device. It is defined as the ratio of P_m to the power of incident radiation (P_{in}), which is given by the equation [20],

$$\eta = \frac{P_m}{P_{in}} = \frac{J_{mp}V_{mp}}{P_{in}} = \frac{V_{oc}J_{sc}FF}{P_{in}} x100\% \qquad (14)$$

where η, P_m, J_{mp}, V_{mp}, V_{oc}, J_{sc} FF, and P_{in} are the efficiency, the maximum power, the maximum power current density, the maximum power voltage, the open circuit voltage, the short circuit current density, the fill factor and the power of the light that is incident on the PV device respectively.

B. Experimental

1) Materials

One functional dye-sensitized solar module was used in this study. The module; Omny 11200 outdoor module - model number HS Code 85414090 was used as supplied by G24 Innovations Limited (UK). It was made up of 11 cells, rated 0.5 Watts peak and 8 Volts. The cells were 1.5 inches thick and of a 15.92 cm^2 active area each; bringing the total active area of the module to 175.12 cm^2. The other apparatus used in the study were a tilt-able metal rack supplied by Solargent Limited, Kenya, 6 cm immersion thermometer supplied by Griffin & George Limited, UK, a GTH 1160 NiCr-Ni digital thermocouple supplied by TC limited, UK, a Raytek* Plus laser beam thermometer supplied by Raytek, USA, a CM3 pyranometer supplied by Kipp & Zonen, Delft/Holland, a Haenni solar 130 radiation meter supplied by Jenensfort, Switzerland, a DT9205A* digital multimeter supplied by Taurus Electronics Limited, Kenya, a Tektronix TDS 3032 digital phosphor oscilloscope supplied by

Tektronix inc., USA, a Keithley 2400 digital source meter supplied by Keithley inc., USA and a Laboratory Virtual Engineering Workbench (LabVIEW™) application software supplied by National Instruments inc., USA, a desktop computer supplied by Hewlett-Packard (HP), Kenya and an IEEE-488 GPIB cable supplied by National Instruments inc., USA.

2) J-V characterization under illumination

The module sample was fixed on the tilt-able metal rack and the CM3-pyranometer positioned in the plane of array with the module as shown in figure 4.3. The set-up was positioned on the roof-top of the Department of Physics, University of Nairobi at a suitable place where shadows could not be cast on either the module or the pyranometer. The module was connected to the Keithley 2400 Source Meter using alligator clips The Keithley source meter was connected to the HP desktop computer via an IEEE-488 GPIB interface. The computer was installed with LabVIEW™ application software. To the pyranometer, the DT9205A* digital multimeter was connected to facilitate acquisition of irradiance data. Figure 2 illustrates how the experiment was set up.

Figure 1: Picture of the module and pyranometer set-up

Fig .2 I-V characterization experimental set-up

Current-voltage readings were first acquired at normal incidence to the incoming solar beam radiation by varying the tilt to coincide with the optimum tilt angle at the period. Optimum tilt angle was obtained from the air mass versus optimum tilt angle curve.

Both the ambient and module temperatures at the time of the I-V measurement acquisition were recorded. Ambient temperatures were measured using the 6 cm immersion thermometer – measurements that were corroborated with those from the Kenya Meteorological department and NASA. Module temperatures were obtained by attaching the GTH 1160 NiCr-Ni digital thermocouple sensor to the back side of the module recording the reading. Readings from the thermocouple sensor were checked by simultaneously point a laser beam from the Raytek* Plus laser beam thermometer at about one meter perpendicular to the module and obtaining the temperature reading on top of the module.

III. RESULTS AND DISCUSSION

Current density, J was observed to increase with radiation intensity. This behavior can be linked to the increasing number of photons that led to an increase in the number of excited electrons with more energy than the work function of the dye upon sensitization. These photo-excited electrons then escape into the semiconductor's conduction band and are collected at the load as current.
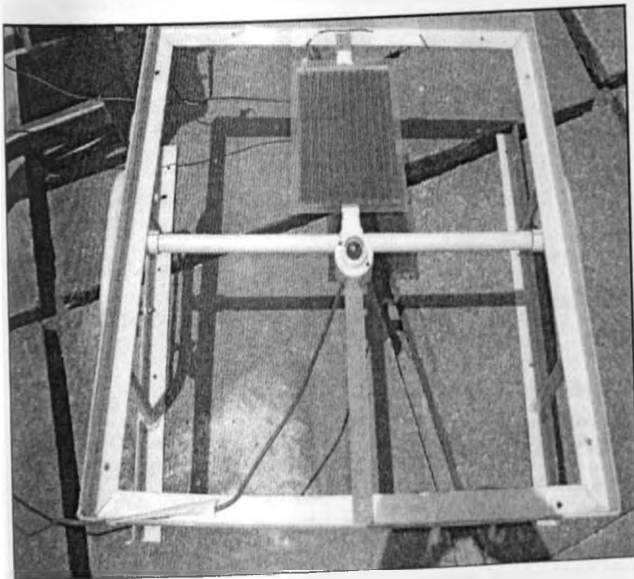
Fig .3 *I-V* characteristics for the module at different radiation intensities

Fig .4 Relationship of V_{oc}, J_{sc}, FF and η as functions of irradiance intensity

Figure 6 shows how *FF*, V_{oc}, J_{sc} and η were affected by the variations in the irradiance intensity. it is observed that the module's short circuit current density, J_{sc} and the irradiance intensity are correlated. This is in agreement with with equation 9 and shows that the actual current flowing out of the solar PV device is the ideal current. However, J_{sc} values were very low for the module, which may imply that the electron recombinations through the electrolyte and during collection at the transparent conducting oxide (TCO) are high in the module. Reduction in *FF* has been observed at high irradiance levels. This shows the large series resistance (R_s) of the module.

Better relative efficiencies are observed at lower irradiance intensities as compared to the higher irradiance intensities. V_{oc} increased exponentially with irradiance intensity up to about 850 Wm^{-2} after which it remained constant upon further increase in irradiance intensity. This may be linked to the thin film nature of the module's cells, where the electron density in the conduction band of the semiconductor is high due to the high injection levels owing to the closeness of the injection to the collection - leading to a quick build-up of charges that exponentially raise V_{oc}. The constant V_{oc} after 850 Wm^{-2} may be linked to a state of equilibrium that arises after some period of time between photo-generation and recombination processes.

Figure 7 shows how the module performed at various module temperatures. As temperature increased, Rs→0. This shows that the module had an overall benefit from elevated temperatures as P_{max} is higher at higher module temperatures.
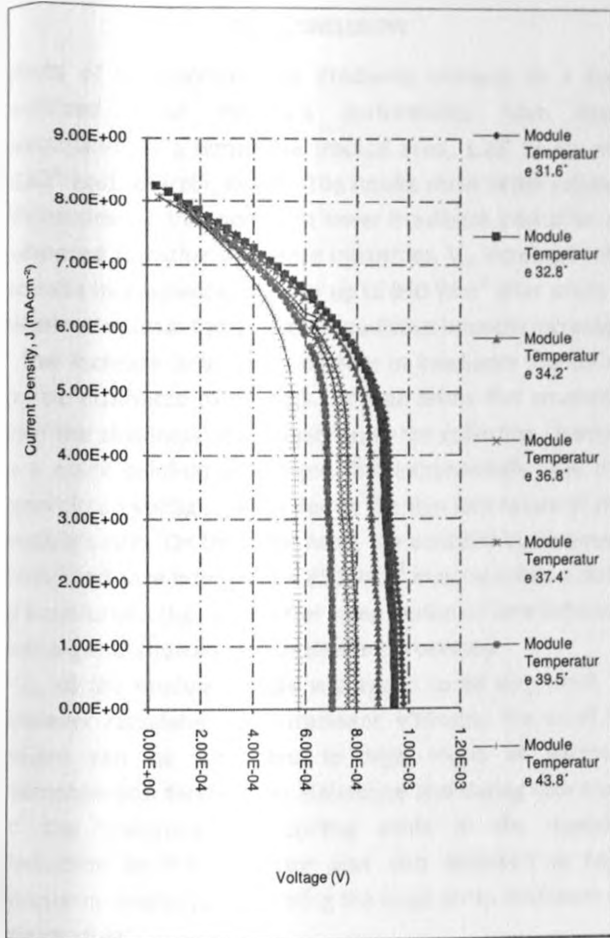
113

Fig .5 *I-V* characteristics of the DSSC module at different module temperatures.

Fig .6 Relationship of J_{sc} and P_{max} as functions of module temperature.

Figure 8 shows how the fill factor, *FF*, *Voc* and η varied with temperature changes. There is a monotonic decrease in V_{oc} with increase in cell temperature that leads to a monotonic decrease in the solar-to-electricity conversion efficiency, η. The relative temperature dependence of V_{oc} and *FF* is however smaller. It can therefore be stated that the temperature dependence of η is dominated by the factors that affect J_{sc}. The trend of the results on η and module temperature may be linked to the limiting process of the tri-iodide diffusion, which limits J_{sc}.

J_{sc} increases with increasing temperature up to some point before starting to decrease. This J_{sc} increase behavior of the module at low module temperatures can be attributed to the diffusion of the tri-iodide which limits J_{sc}, while at increased cell temperatures, according to Arrhenius law according to which the diffusion coefficient exponentially increases with increasing temperature there is an observed increase in short circuit current density, J_{sc}. Nonetheless, the decrease that is observed after about 40°C module temperature can be attributed to the possibility of recombinations at higher temperatures leading to reduction in current collection.

These limiting processes are linked to type and concentration of electrolyte components as is evident from the experiment by [23], which showed that when I_2 and consequently the tri-iodide concentration is low in the measured temperature window of 5-50°C firstly, J_{sc} increases with temperature, reaches a maximum but later, further increase in temperature leads to decrease in J_{sc} [23].

IV. CONCLUSION

Effects of temperature and irradiance intensity on a dye-sensitized solar module's performance have been investigated in a temperate tropical area, 1.28° South and 35.82° East, Nairobi, Kenya. The results show better relative efficiencies for the module at lower irradiance intensities as compared to higher irradiance intensities. V_{oc} increased with increase in irradiance intensity up to 850 Wm^{-2} after which it remained constant with further irradiance intensity increase.

The increase in V_{oc} with increase in irradiance intensities can be attributed to the high injection levels that emanates from the closeness of the injection to the collection - leading to a quick build-up of charged that exponentially raise the open circuit voltage. This is due to the thin film nature of the module's cells. On the other hand, the constant V_{oc} observed from irradiance intensities > 850 Wm^{-2} may be linked a state of equilibrium that arises after some period of time between photo-generation and recombination processes.

J_{sc} of the module sample was found to be very small. It however correlated with irradiance intensity. The small J_{sc} values can be attributed to high levels of electron recombination through the electrolyte and during collection at the transparent conducting oxide in the module. Reduction in the fill factor was also observed at high irradiance intensities, indicating the large series resistance of the module.

An overall benefit from elevated module temperatures was observed as the maximum power increased with increasing module temperatures and irradiance intensity. V_{oc} for the module showed a monotonic decrease with increase in temperature leading to a monotonic decrease in efficiency. The temperature dependence of V_{oc} and fill factor were however very small, which implies that the temperature-dependence of efficiency for the module was dominated by factors that affect the J_{sc}. These include the diffusion of the tri-iodide that limits J_{sc} at low temperatures but leads to increases in J_{sc} at higher temperatures in accordance with Arrhenius law. The decrease in J_{sc} after about 40°C module temperature can be attributed to the possibility of recombinations at higher temperatures.

The relatively better efficiencies observed for the dye-sensitized solar module at low irradiance intensities together with its ability to benefit from elevated temperatures under high illumination place dye-sensitized solar modules in a remarkable position for use in the temperate tropics. The design of energy efficient building facades for the temperate tropics stands to benefit immensely from these findings.

REFERENCES

[1] Leng, R., (2005). Implications of the decline in world oil reserves for future world livestock production. *School of Rural Science and Agriculture, University of New England*, p. 95 – 105.

[2] Aleklett, K., (2007). Reserve driven forecasts for oil, gas and coal and limits in carbon dioxide emissions. *In discussion paper number 2007-18. Joint Transport Research Centre*, p. 1 – 20.

[3] Hahn, R., Litan, R. and Singer, H., (2007). The economics of 'wireless net neutrality'. *American Enterprise Institute (AEI) – Brookings Joint Centre for Regulatory Studies*, p. 1 – 54.

[4] Barnes, D. and Toman, M., (2006). Energy, equity and economic development. *In economic development and environmental sustainability. Oxford University Press*, p. 1 – 52.

[5] Heymann, E. (2011). Carbon capture and storage for climate protection – important, tedious and costly. *Deutsche Bank*, p. 1 – 5.

[6] Dincar, I., (2003). The role of energy in energy policy making. *Energy Policy*, 30, p. 137 – 149.

[7] IPCC. 2007., (2007) "Climate change 2007: The physical science basis: Summary of policy makers". *Intergovernmental Panel on Climate Change Secretariat*.

[8] IEA, (2007). Key world energy statistics 2007. *International Energy Agency, 2007.*

[9] Muoghalu, J. (2003). Priority parameters: Abiotic and biotic components. *In environmental monitoring (edited by Inyang, H. and Daniels, J.) Encyclopaedia of Life Support Systems (EOLSS)*, p. 1 – 8.

[10] Richards, B. and Schäfer, A. (2009). Renewable energy to power water treatment systems. *Elsevier*, p. 353 – 374.

[11] Kuhlbrodt, T., Griesel, A., Montoya, M., Levermann, A., Hofmann, M. and Rahmstorf, S., (2006). On the driving processes of atlantic meridional overtuning circulation. *Potsdam Institute for Climate Research*, p. 1 – 69.

[12] Quaschning, V., (2005). "Understanding Renewable Energy Systems". *Earthscan Canada*. 1-3.

[13] Lewis, N. and Crabtree, G., (2007). Solar energy conversion. *Physics Today*, 60, p. 37 - 42.

[14] Bakas, I., (2011). Solar energy/photovoltaics. *In solar energy and housing – Corpus. Copenhagen Resource Institute (CRI)*, p. 1 – 6.

[15] Krugmann, P., (2011). That's right: Solar power is now cost-effective. *The Seattle Times*, [retrieved on 23rd March, 2012 at http://seattletimes.nwsource.com/html/opinion].

[16] Gunerhan, H., Hepbasli, A. and Giresunlu, U., (2009). Environmental impacts from solar energy systems. *Energy Sources*, A, 31, p. 131 – 138.

[17] Whitney, Jr., (2010). Significant sustainable energy systems. *In clean energy action project. Solar PV Energy*, p. 1 – 36.

[18] Saga, T., (2010). Advances in crystalline silicon solar cell technology for industrial mass production. *NPG Asia Materials*, 2, p. 96 – 102.

[19] O'Regan, B. and Grätzel, M., (1991). A low cost, high efficiency solar cell based on dye sensitised colloidal TiO$_2$ films. *Nature*, 353, p. 737 - 739.

[20] Hedegus, S. and Shafarman, N., (2004). Thin film solar cells: Device Measurement and Analysis. *Progress in Photovoltaic Research and Application*, 12, 155-176.

[21] Sze, S. M., (1981). "Physics of semiconductor devices". *New York: Wiley International Publishers Inc.*122 - 124.

[22] Simiyu, J., (2010). "Characterization of Anthocyanin Dyes and

[24] Berginc, M., Krašovec, U. O., Hočevar, M. and Topič, M., (2008). Performance of dye-sensitized solar cells based on ionic liquids:

[23] Investigation of Charge Transport in TiO$_2$ Dye Sensitized Solar Cells". Ph.D thesis for the University of Nairobi. 1 - 13.

Effect of temperature and iodine concentration. *Thin Solid Films*, 516, p. 7155 – 7159.

Raphael **Venson Makokha Otakwa** is a postgraduate student (Physics) at the University of Nairobi, Kenya. He is a registered solar energy applications practitioner in Kenya and holds a Master of Science (M.Sc.) in Physics (condensed matter and solar energy) from the University of Nairobi. His research interests are in solar energy materials and applications.

EDUCATION

Dark current density-voltage (J-V) characteristics of a commercialized dye-sensitized solar module ideal for use in the Tropics

Otakwa R. V. M.[*], Simiyu, J.[1], Waita, S. M.[1] & Mwabora J. M.[1]

[1]Department of Physics, College of Physical and Biological Sciences, University of Nairobi.
PO Box 30197 – 00100 GPO, Nairobi, Kenya
[*]Corresponding email: raphael.makokha@yahoo.com

Abstract

The performance of a commercialized dye-sensitized solar module (DSSM) has been investigated in the dark to clarify how to accurately determine its performance. Accurate characterization of a DSSM requires consideration of its temporal response obtained during dark J-V characterization. A series of J-V measurements were obtained by applying a bias voltage to the module and measuring the generated current automatically using a Keithley 2400 digital source meter. The J-V curves for the module were not dependent on the voltage sweep direction even when the sweep time was in the order of seconds. This makes it ideal for use in weather conditions characterized by fluctuations in daily solar radiation availability.

Index Terms - Dye-sensitized, dark, performance, characterization

I. Introduction

Research in dye-sensitized solar cells (DSSCs) has been enormous [1]. This is because they promise to be cheaper alternatives to the conventional silicon solar cells and can be fabricated under less stringent conditions [2]. A number of application studies on DSSCs are currently underway, including their use for energy efficient glazing and Building Integrated Photovoltaics (BIPV) [3].

G24 Innovations Limited, Dyesol and Solaronix are among the companies that have pioneered the commercialization of the DSSC technology. Accurate investigation of these products, just as in the case of other PV devices commercialized for use under various field operating conditions requires consideration of their dark J-V characterization [4]. Dark J-V characterization is used to observe the temporal response in PV devices, the parasitic resistances (series and shunt), the ideality factor and the saturation current. This study investigates the dark J-V characteristics of the DSSC module supplied for outdoor use by G24 Innovations Limited, UK.

II. Materials and Methods

Basic Theory

Current density-voltage (J-V) characterization

The response of a PV device is determined by its J-V characteristics obtained both in the dark and under illumination. In practical cases, J-V characteristics are modeled according to equation (1), which accounts for shunt resistances (R_{sh}) and series resistances (R_s) [5] [6],

$$J = J_L - J_s \exp\left[\frac{V+R_sJ}{mV_T}\right] - \sigma V \qquad (1)$$

where J, J_L, J_s, V, m, V_T, R_s, J, and σ are the ideal current density, the current density from the source (in this work, it is the photo-generated current density, J_{ph} and will be referred to as such), the saturation current density, voltage across the PV terminals, the ideality factor, series resistance and shunt conductance respectively.

Dark J-V characterization is preferred in analyzing the electrical characteristics of PV devices because

it is more sensitive than light J-V measurements in determining R_{sh}, R_s, m and J_s that dictate the electrical performance of a PV device. In the dark, a bias voltage generates current density in the direction opposite to the one generated under illumination. Dark current density (J_{dark}) is computed from the equation [7] [5],

$$J_{dark} = -J_s \, exp \left[\frac{V + R_s J}{m V_T} \right] - \sigma V \qquad (2)$$

where J, J_{dark}, J_s, V, m, V_T, R_s, J_s and σ are the ideal current density, the dark current density, the saturation current density, voltage across the PV terminals of the PV device, the ideality factor ($=1$ for an ideal PV device or $\neq1$ for a non-ideal PV device), series resistance and shunt conductance respectively.

Setting m in equation (1) to one yields the ideal diode case that assumes that all recombinations in the PV device occur via band to band or the bulk areas of the PV device – not in the junction. m describes how closely the PV device follows the ideal case scenario. In practical cases, PV devices are non-ideal since recombinations occur in other ways and areas of the devices than band to band or the bulk area of the devices. These devices yield m that deviates from the ideal. From equation (2), the dark current density can be plotted as a function of the applied bias voltage. This results in a curve typically known as the dark current density-voltage (J-V) characteristic curve. From the J-V curve, key parameters; J_s, FF, R_s, R_{sh} can be extracted and, m and η computed.

The slope of the linear region of the J-V curve in the third quadrant (reverse bias) is a continuation of the linear region in the first quadrant – which is the same linear region used to calculate R_{sh}. It follows that R_{sh} can be derived from the J-V curve obtained as the inverse of slope of the J-V curve at the maximum current density point (or J_{sc}) while R_s are identified as the inverse of the slope of the J-V curve at the maximum voltage point (or V_{oc}). In most solar cells, it is imperative that $R_{sh} > R_s$. In an ideal solar cell, $R_{sh} = \infty$ and $R_s = 0$ [8]. J_s is normally proportional to the thermally induced recombination or generation processes of charge carriers. It exponentially increases with temperature. By measuring the dark J-V curve of a PV device, an idea of J_s can be obtained.

As $V \rightarrow 0$, current is mainly determined by the shunt resistance. After this section on the J-V curve, follows the section that describes the ideal diode behavior of the PV device. Once the internal electrical field diminishes, current now gets determined by the sum of all series resistances of the cells that constitute the PV module. Plotting the J-V curve in a semi-logarithmic scale, the exponential part becomes a straight line, which upon extrapolation to the interception with the y-axis, gives J_s. J_s is controlled by the exchange current at the semiconductor/electrolyte interface. It depends on the rate of reduction of the triiodide. The ideality factor, which is a measure of how closely the PV device follows the ideal diode equation, is derived from the slope of the J-V curve. It is influenced by the fabrication process and the semiconductor material used. FF on the other hand is generally influenced by the series and shunt resistances. It is a measure of the squareness of the J-V curve and hence the quality of the solar PV device. It is defined as a ratio and determined from equation [9]:

$$FF = \frac{P_m}{V_{oc} J_{sc}} = \frac{J_{mp} V_{mp}}{V_{oc} J_{sc}} \qquad (3)$$

where FF, P_m, V_{oc}, J_{sc}, J_{mp} and V_{mp} are the fill factor, maximum power, the open circuit voltage, the short circuit current density, the maximum power current density and the maximum power voltage respectively.

Experimental

Materials

One functional dye-sensitized solar module was used in this study. The module; Omny 11200 outdoor module - model number HS Code 85414090 was used as supplied by G24 Innovations Limited (UK). It was made up of 11 cells, rated 0.5 Watts peak and 8 Volts. The cells were 1.5 inches thick and of a 15.92 cm² active area each; bringing the total active area of the module to 175.12 cm². Other apparatus used in the study were a DT9205A* digital multimeter supplied by Taurus Electronics Limited, Kenya, a Keithley 2400 digital source meter supplied by Keithley inc., USA and a Laboratory Virtual Engineering Workbench (LabVIEW™) application software supplied by National Instruments inc., USA, a

desktop computer supplied by Hewlett-Packard (HP), Kenya and an IEEE-488 GPIB cable supplied by National Instruments inc., USA.

Dark J-V characterization

The module's terminals were tested for polarity using the DT9205A⁺ digital multimeter. It was then appropriately connected to the positive and negative terminals of the Keithley 2400 source meter using alligator clips. The Keithely 2400 source meter was connected via the IEE-488 GPIB interface to the HP desktop computer that was installed with the LabVIEW™ application software. The LabVIEW™ communication protocol is presented figure 3. Dark J-V measurements were obtained by applying a bias voltage to the module and measuring the generated current automatically using a Keithley 2400 digital source meter.
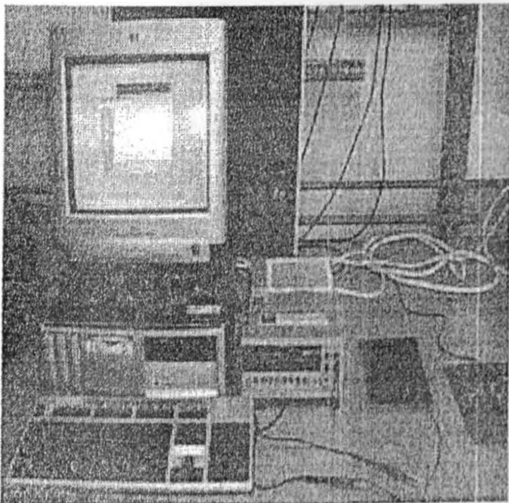
Figure 1: Photograph of the experiment set-up.
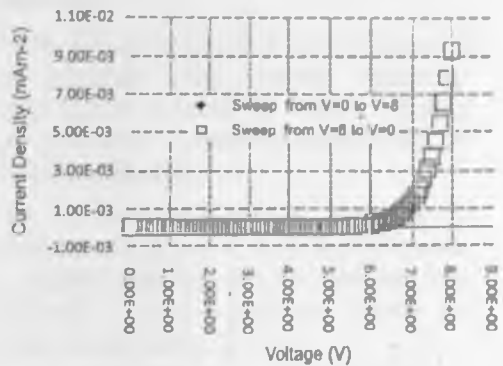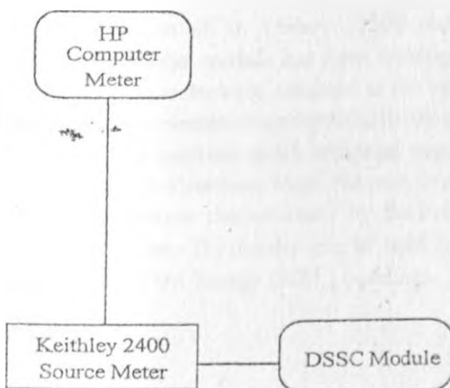
Figure 2: Dark J-V characterization set-up block diagram.

Results

Figures 3, 4, 5 and 6 are the dark J-V characteristics for the module acquired by applying voltage from V = 0 to V = 8 and from V = 8 to V = 0 sweep directions at 2.5, 5, 12.5 and 25 seconds sweep times.
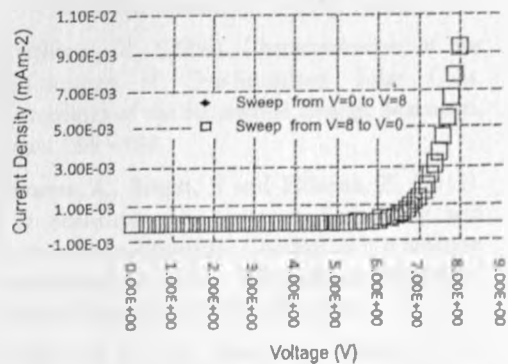

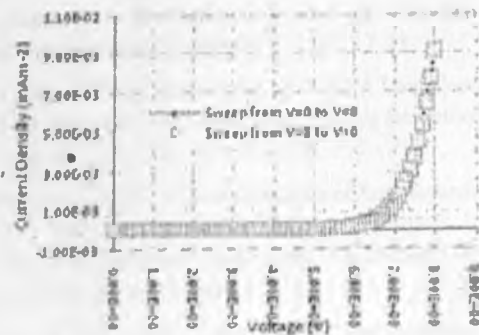Figure 3: Dark J-V curves for sweep times from V = 0 to V = 8 and vice versa at 2.5 seconds.

Figure 4: Dark J-V curves for sweep times from V = 0 to V = 8 and vice versa at 5 seconds.

Figure 5: Dark *J-V* curves for sweep times from V=0 to V=8 and vice versa at 12.5 seconds.
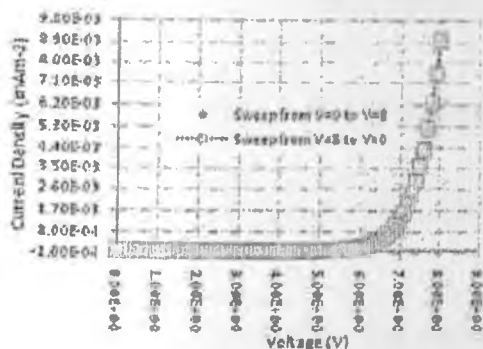

Figure 6: Dark *J-V* curves for sweep times from V=0 to V=8 and vice versa at 25 seconds.

Discussion

In the paper by Hishikawa [4], the DSSC samples used (prepared by Pioneer Corporation) showed a temporal response, which was much slower than for conventional solar cells such as silicon *p-n* junction structures. Using the same methodology, this study reports that the *J-V* curves at the different sweep directions perfectly mapped onto each other. This shows the reproducibility of results irrespective of the sweep direction chosen. The results point to a quick temporal response. This contradicts the findings by Hishikawa [10] and Hishikawa [4]. The performance of the module under this study may be attributed to the thinness of the TiO_2 nanoparticles and the adsorbed sensitizing dye layers, which reduce the optical path length taken by the incident photons, hence leading to a quicker photo-excitation and a faster response.

Conclusion

The performance of an Omny 11200 outdoor dye-sensitized solar module has been investigated. The J_{dark} *J-V* characteristics obtained at the various sweep directions demonstrate reproducibility of the results and the module's quick temporal response. The product is therefore ideal for use even in weather conditions characterized by fluctuations in solar radiation. The results can be used in the design of Net Zero Energy (NZE) buildings.

References

Binions and Dunn, (2012). School of engineering and materials science research studentship. Queen Mary University of London [Accessed on 27/03/2010 at http://www.semsqmul.ac.uk/research/studentship].

Han, L., Islam, A., Chen, H., Malapaka, C., Chiranjeevi, B., Zhang, S., Yang, X. and Yanagida, M., (2012). High Efficiency Dye Sensitized Solar Cell with a Novel Co-adsorbent. Energy and Environmental Science, 2, 149.

Hedegus, S. and Shafarman, N., (2004). Thin film solar cells: Device Measurement and Analysis. Progress in Photovoltaic Research and Application, 12, 155-176.

Hishikawa, Y., (2008). Performance Measurement of Dye-Sensitized Solar Cells and Organic Polymer Solar Cells. Natural Institute of Advanced Industrial Science and Technology (AIST), Research Centre for Photovoltaics (RCPV), Central 2 Umezono, 1-1-1, Tsukuba, Ibaraki, 305 – 8568 Japan, 1 – 8.

Hishikawa, Y., (2006). Characterization of the Performance of Dye-Sensitized Solar Cells. Proceedings of the Renewable Energy, Makuhari, Japan, 184 – 188.

Nwanya, A., Ezema, F. and Ejikeme, P., (2011). Dye sensitized solar cells: A Technically and Economically Alternative Concept to p-n junction Photovoltaic Devices. International Journal of Physical Sciences, 6 (22), 5190 – 5201.

Otakwa, R. V. M., Simiyu, J., Waita, S. M., Mwabora, J. M., (2012). Application of dye-sensitized solar cell technology in the tropics: Effects of radiation intensity and temperature on DSSC performance. International Journal of Advanced Renewable Energy Research, 1, 2(4), 17-25

O'Regan, B. and Grätzel, M., (1991). A Low Cost, High Efficiency Solar cell based on Dye Sensitized Colloidal TiO_2 films. Nature, 353, 737 - 739.

Simiyu, J., (2010). Characterization of Anthocyanin Dyes and Investigation of Charge Transport in TiO_2 Dye Sensitized Solar Cells. Ph.D thesis for the University of Nairobi, 1 - 13.

Sze, S. M., (1981). Physics of Semiconductor Devices. New York: Wiley International Publishers Inc., Pp. 122 - 124.

Application of Dye-Sensitized Solar Cell Technology in the Tropics: Effects of Air Mass on Device Performance

Otakwa R. V. M.*, Simiyu, J.*, Waita, S. M.* ,Mwabora J. M.*

*Department of Physics, College of Physical and Biological Sciences, University of Nairobi

‡Corresponding Author: Otakwa R. V. M.,Department of Physics, College of Physical and Biological Sciences, University of Nairobi, PO Box 30197 – 00100 GPO, Nairobi, KENYA, raphael.makokha@yahoo.com

Abstract-Effects of air mass on the performance of a dye-sensitized solar module (DSSM) have been investigated in a tropical area in Nairobi, Kenya. Outdoor measurements were performed at different times on different days and a series of current-voltage (I-V) characterizations carried out at different air mass values and module tilt angles. The module performance parameters: Short circuit current density, (J_{sc}), Open circuit voltage, (V_{oc}), Fill factor, (FF) and solar-to-electricity conversion efficiency, (η) were extracted from the I-V curves. The module's η and FF increased with air mass while V_{oc} and J_{m} decreased with increase in AM. The module performed better in the afternoon hours than in the morning hours. The results may be useful in tuning dye-sensitized solar cells for use in the tropics as well as in the design of Net Zero Energy buildings.

Keywords-Dye-sensitized, Performance, Air mass, Net-zero-energy-buildings

1. Introduction

Dye-sensitized solar cells (DSSCs) are cheaper alternatives to the conventional silicon solar cells [1]. Their scalable, self-assembled and bottom-up fabrication processes are economical and ecological, making them attractive and credible alternatives to the conventional solar PV systems [2]. Remarkable advances have been in their fabrication [3-5].

In the tropics, a number of DSSC-related studies have been undertaken, including the effects of nitration on pressed TiO_2photo electrodes for DSSCs [6], DSSCs fabricated from obliquely DC sputtered TiO_2 films [7], theoretical approaches to the temperature effect on the mobility and transport of photo-injected electrons in DSSCs [8] and [9], effects of the concentration of dopant states in photo-activity in Niobium TiO_2 [10], TiO_2 DSSCs with a hole transport material Ogacho [11] and the Anthocyanin sensitized TiO_2photo electrochemical solar cells [12].

Lately in Nigeria, Ozuomba and co-workers [13] have fabricated DSSCs using dye extracted from local banana grass, whose performance compare with what has been reported by Law and co-workers [14] as well as Suri and co-workers (2007). Otakwa and co-workers [15] has investigated the effects of radiation intensity and temperature on the performance of DSSCs. These enormous research efforts point to the quest by people in the tropics to have access to cheaper electricity - a goal that has been elusive with the conventional silicon solar devices [16]. In this paper, the effect of air mass and tilt angle on the DSSC performance in the tropics is reported.

2. Materials and Methods

2.1. Basic Theory

The DSSC semiconductor electrochemistry

In DSSCs, the electronic excitation in the dye achieved through light absorption promotes dye molecule into a high energy state associated with the Lowest Unoccupied Molecular Orbital (LUMO). This simultaneously creates an electron deficiency in the low energy state - the Highest Occupied Molecular Orbital (HOMO). Electrons in the

LUMO and HOMO states are separated by a difference in enthalpy (h) [17],

$$\Delta h = \Delta E = E_{LUMO} - E_{HOMO} \qquad (1)$$

where,

Δh	=change in enthalpy,
ΔE	=difference in energy,
E_{LUMO}	=energy of the least unoccupiedmolecular orbital,
E_{HUMO}	=energy of the highest occupied molecular orbital.

This exodus of the population of the states from their thermal equilibrium values implies a difference in their chemical potentials (μ), which can be stated as follows:

$$\Delta\mu = \mu LUMO - \mu HOMO \qquad (2)$$

where,

$\Delta\mu$	=change in chemical potential,
μ_{LUMO}	=chemical potential of the least unoccupied molecular orbital,
μ_{HOMO}	=chemical potential of the highest occupied molecular orbital.

Efficient DSSC performance relies on the efficiency of electron injection and dye regeneration. Also, the LUMO energy of the dye should be well above that of the TiO_2 conduction band for efficiency in electron injection. For efficient dye regeneration and sustained photocurrent, the $\Delta\mu$ of the redox couple should be higher than the HOMO energy level of the dye molecules. The maximum voltage of a DSSC under illumination normally corresponds to the difference of the TiO_2 Fermi level (E_F) and the $\Delta\mu$ of the electrolyte.

Nonetheless, the basic operation principle of the DSSC relies on the photo-excitation of the dye molecules. Hence, anything that interferes with access to light for the DSSC affects its performance. The strength of the solar beam incident on the DSSC at a given point and time determines its efficiency in photo-exciting electrons from HOMO level of the dye molecules to the LUMO level as shown by equation (3),

$$TiO2|S + h\nu \leftrightarrow TiO_2|S^*{}_{LUMO} \qquad (3)$$

where,

TiO_2	=the titanium dioxide nanoparticles,
I	=the interface
S	=the ground state of the dye molecules,
$h\nu$	=the photon energy,
$S^*{}_{LUMO}$	=the excited state of the least unoccupied molecular orbital of the dye molecule.

Solar beams can be attenuated by absorption and scattering as they enter the earth's atmosphere in an effect known as extinction. Scattering is usually caused by suspended aerosols, which may be diverse in volume, size,

form and composition. Depletion of incoming solar irradiance by aerosol-laden atmospheres is referred to as atmospheric turbidity. Its effect on the DSSC device performance at the application sites requires to be considered. Absorption on the other hand is mainly caused by the Ozone layer (O_3), Oxygen (O_2), Nitrogen (N_2), precipitable water vapour (H_2O) and Carbon Dioxide (CO_2).

Apart from N_2 and O_2 which remain more or less constant, the amount of the ozone layer varies with latitude and season [18]. The amount of precipitable water vapour also varies instantaneously based on the local conditions [19]. Carbon dioxide has also been on an alarming increase due to the burning of fossil fuels. The atmospheric refraction of the solar beam by these atmospheric gases makes it take a longer path than is geometrically expected. Optical air mass or simply air mass (AM) plays a major role in determining atmospheric refraction [20]. AM is the path length traversed by the direct solar radiation as a ratio of the path traversed to a point at sea level when the sun is directly overhead. Studying how solar radiation is attenuated by the atmosphere in terms of the air mass, optical thickness and water vapour is important in understanding how solar devices would perform under different atmospheric settings.

To maximize collected energy, solar collectors are usually tilted to capture maximum radiation. Optimum tilt angle, and hence J_{ph} are influenced by the air mass at a particular place [21]. A number of formulae have been developed for computing AM. In this work, the method of erecting a vertical post at a place where the shadow of the post is cast on a flat surface has been used. Dividing the length of the hypotenuse of the triangle (length traversed by the ray of light) (figure 1) by the height of the post yields (geometrically expected path) [22, 23] and applying the Pythagoras theorem yields AM,

$$AM = \left[1 + \left(\frac{s}{h}\right)^2\right]^{1/2} \qquad (4)$$

where,

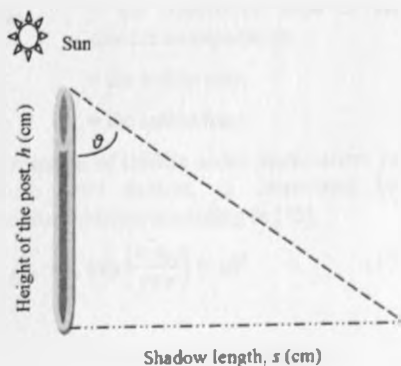|	
AM	=the air mass,
h	= the height of the post,
s	= the length of the shadow cast by the post.

Fig. 1.Illustration on how to determine air mass from the shadow of a vertical post.

From trigonometry, the cosine of θ is obtained by dividing the length adjacent to it by the hypotenuse; the inverse of which constitutes AM. This is used for small values of θ.

$$AM = 1/(Cos\ \theta) \tag{5}$$

where,

AM = the air mass,

θ = the angle from the vertical.

Equation (5) however assumes a homogenous atmosphere and ignores the earth's curvature. The earth is however not flat and the equation leads to an infinite air mass at the horizons. Kasten and Young [24] developed the equation:

$$AM = [Cos\theta + 0.50572\ (96.07995 - \theta)^{-1.6364}]^{-1} \tag{6}$$

where

AM = the air mass,

θ = the solar zenith angle.

The solar beam available for photo-generation depends on how it is attenuated through the atmosphere. On striking the surface of the DSSC cells, the solar beams eject electrons from the excited dye molecules. These get injected into the conduction band of the TiO_2 as demonstrated by equation (7),

$$S^{*}_{LUMO} + CB_{TiO_2} \rightarrow TiO_2|S^+ + e_{CB^-} \tag{7}$$

where,

S^{*}_{LUMO} = the excited state of the least unoccupied molecular orbital of the dye molecule,

CB_{TiO2} = the conduction band of the titanium dioxide semiconductor,

TiO_2 = titanium dioxide,

I = interface

S^+ = oxidized state of the dye molecules,

e_{CB^-} = the electron injected into the conduction band.

The electron then migrates through the TiO_2 nanoparticle network towards the transparent conducting oxide (TCO) substrate. Charge localization due to the polarization of the mediums and relaxation of the molecular ions dominates the physics of charge transfer and transport during these processes. The catalytic reaction at the counter electrode (courtesy of the platinum film) must guarantee fast re-generation of the redox couple as illustrated by [25],

$$Pt + I_3^- \rightarrow 3I^- \tag{8}$$
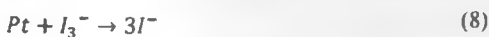
where,

P_t = the Platinum,

I_3^- = the iodide ions,

$3I^-$ = the iodine ions.

To achieve an efficient DSSC operation, the electron injection rate must be faster than the decay rate. The oxidized dye molecules must also be regenerated fast by the redox couple so as to kinetically compete in the uptake of the electrons from the counter electrode for the subsequent electron injection to prevent recombinations [26]. Also, the rate of reduction of the oxidized sensitizer (S^*) must be higher than the rate of back reaction of the injected electrons as well as the rate of injection of electrons in the electrolyte.

$$TiO_2|S^+ + 3I^- \rightarrow I_3^- + S \tag{9}$$

where,

TiO_2 = the titanium dioxide nanoparticles,

I = interface

S^* = the oxidized state of the dye molecules,

S = the ground state of the dye molecules,

I_3^- = the iodide ions,

$3I^-$ = the iodine ions.

During these processes, some electrons are not successfully injected into the TiO_2 conduction band due to inadequate energy. They as a result drop back into the HOMO level. The electrons already injected into the conduction band of the TiO_2 risk migrating back into the HOMO level of the dye molecules or into the electrolyte as illustrated by equations (7) and (8) respectively due to electron trapping defects. These result in recombinations that decrease the performance of the cell.

$$e_{CB^-} + S_{HOMO} \rightarrow S + CB_{TiO_2} \tag{10}$$

$$e_{CB^-} + I_3^- \rightarrow 3I^- + CB_{TiO_2} \tag{11}$$

where,

e_{CB^-} = the electron injected into the conduction band.

S_{HOMO} = the ground state of the least highest occupied molecular orbital of the dye molecules,

S = the ground state of the dye molecules,

CB_{TiO2} = the conduction band of the titanium dioxide nanoparticles,

I_3^- = the iodide ions,

$3I^-$ = the iodine ions.

The response of DSSCs under illumination; just as other photovoltaic (PV) devices, is determined by its J-V characteristics modelled according to [15],

$$J = J_{ph} - J_s \exp\left[\frac{V + R_s J}{mV_T}\right] - \sigma V \tag{12}$$

where

J = the ideal current density,

J_{ph} = the photo-generated current density,

J_s = the saturation current density,

V	= the voltage across the PV device terminals,
m	= the ideality factor,
V_T	= the thermal voltage,
R_s	=the series resistance,
σ	= the shunt conductance.

From equation (9) the photo-generated current density can be plotted as a function of the applied bias voltage. This results in a curve typically known as the current density-voltage (J-V) characteristic curve from which key device parameters; open circuit voltage (V_{oc}), short circuit current density (J_{sc}), fill factor (FF) can be extracted and efficiency (η) computed.

FF is a measure of the squareness of the J-V curve and hence the quality of the solar PV device. It is generally influenced by the series and shunt resistances. It is determined from equation [12],

$$FF = \frac{P_m}{V_{oc}J_{sc}} = \frac{J_{mp}V_{mp}}{V_{oc}J_{sc}} \qquad (13)$$

where,

FF	= the fill factor,
P_m	= the maximum power,
V_{oc}	= the open circuit voltage,
J_{sc}	= the short circuit current density,
J_{mp}	= the current density at maximum power point,
V_{mp}	= the voltage at maximum power point.

η describes the overall performance of the DSSC. It is defined as the ratio of P_m to the power of incident radiation (P_{in}), which is given by the equation [27],

$$\eta = \frac{P_m}{P_{in}} = \frac{J_{mp}V_{mp}}{P_{in}} = \frac{V_{oc}J_{sc}FF}{P_{in}} x100\% \qquad (14)$$

where,

η	= the efficiency,
P_m	= the maximum power,
J_{mp}	= the current density at maximum power point,
V_{mp}	= the voltage at maximum power point,
V_{oc}	= the open circuit voltage,
J_{sc}	= the short circuit current density,
FF	= the fill factor.

2.2. Experimental

Materials

One functional dye-sensitized solar module was used in this study. The module; Omny 11200 outdoor module -

model number HS Code 85414090 was used as supplied by G24 Innovations Limited (UK). It was made up of 11 cells, rated 0.5 Watts peak and 8 Volts. The cells were 1.5 inches thick and of a 15.92 cm^2 active area each; bringing the total active area of the module to 175.12 cm^2. The other apparatus used in the study were a tilt-able metal rack supplied by Solargent Limited, Kenya, a Keithley 2400 digital source meter supplied @Workbench (LabVIEW^{TM}) application software supplied by National Instruments Inc., USA, a desktop computer supplied by Hewlett-Packard (HP), Kenya and an IEEE-488 GPIB cable supplied by National Instruments Inc., USA. A protractor and a metre rule supplied by Textbook Centre, Kenya were also used in this work.

J-V characterization at different air mass values

The module was fixed on the tilt-able metal rack as shown in figure 2. The set-up was positioned on the roof-top of the Department of Physics, University of Nairobi at a suitable place where shadows could not be cast on either the module. The module was connected to the Keithley 2400 Source Meter using alligator clips The Keithley source meter was connected to the HP desktop computer via an IEEE-488 GPIB interface. The computer was installed with LabVIEW^{TM} application software.

To determine the air mass at different times, an upright post was erected at a suitable flat place next to the J-V characterization experiment. The post's height from the ground surface measured using a metre ruler. The length of the shadow cast by the post was measured simultaneously with the acquisition of the J-V characterization curves. J-V measurements were at tilts that were varied according to the zenith angles corresponding to the air mass at the different times. The module's performance parameters; V_{oc}, J_{sc}, FF and at the different air mass values were extracted from the J-V curves and η computed. The set-up was as is illustrated in figures 2 and 3.
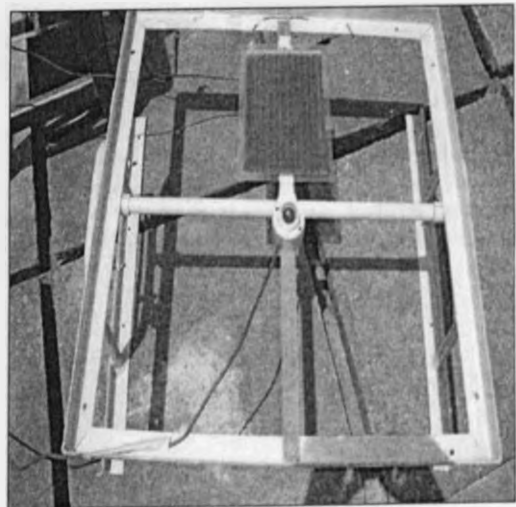

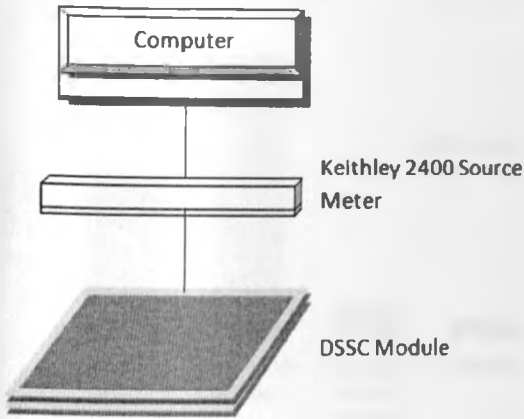Fig. 2. Picture of the set up of the module on the tilt-able metal rack.

Fig. 3.A simple illustration of the *J-V* characterization experimental set-up.

3. Results and Discussion

From figure 4, it is observed that Voc and Jsc reduced with increase in air mass. This can be attributed to reduction in radiation intensity as air mass increases, which agrees with the observation by Meinel and Meinel [28]. The points at which maximum power is attained (at the 'knee' of the *J-V* curves) increases with air mass. This corresponds to the battery charging region. The fill factor increases with tends to one as air mass increases. This implies that the quality of a DSSC module operating outdoors is best evaluated at higher than lower air mass.
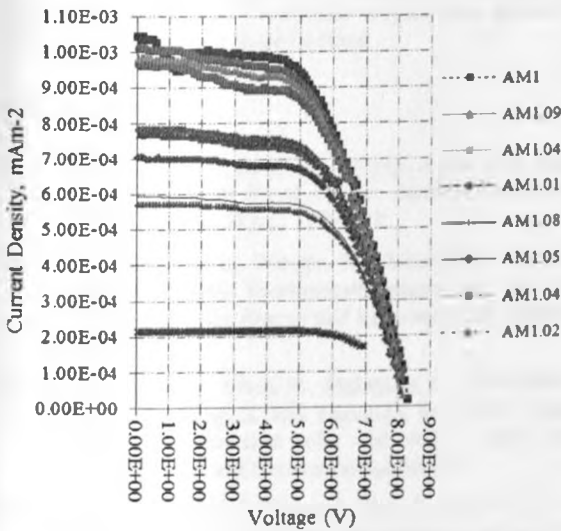

Fig. 4.*J-V* characteristic curves for the module at different air mass values

Air mass varied as shown in figure 5. Values for AM obtained between 700 hours to 1245 hours were slightly unstable compared to the values obtained between 1245 Hours to 1800 Hours. This can be attributed to the instantaneous variation in the atmospheric gaseous absorbers

like H_2O, O_2, O_3 and CO_2 as observed by Louche and co-workers [18]. Figure 5 also shows that air mass - and hence the intensity of the direct component of sunlight [28] was more stable in afternoon than in morning hours. V_{oc} and J_{sc} decreased with increase in *AM*.

This can be attributed to the atmospheric extinction of the solar beams due to the longer optical path that they travel through the atmosphere at higher *AM* values. With reduced amount of effective radiation reaching the surface of the module for photo-generation, the photo-generated electrons reduce and consequently, the photo-generated current. The behavior is in agreement with theory, which demonstrates equivalence between photo-generated current density and the corresponding short-circuit current density [15].

Figure 5 also shows how the module's efficiency increased marginally with *AM*. This can be attributed to greater effective radiation available for photo-generation by the module at higher *AM* than at lower *AM*.
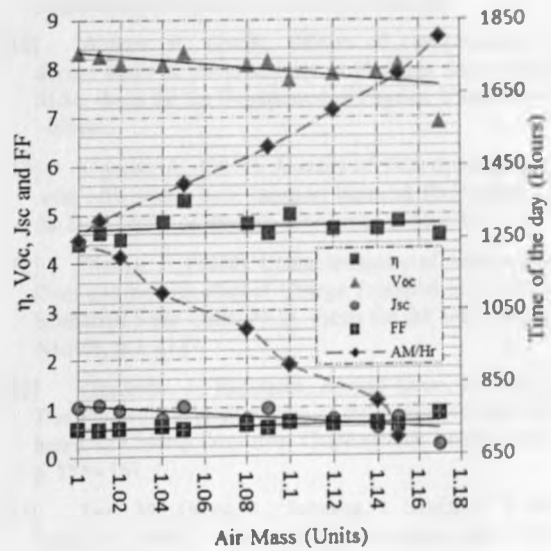

Fig. 5. Curve for Air Mass values at different times of the day.

A comparison of the module's performance in the morning hours and in the afternoon hours is given in figure 6. It is observed that the module performed relatively better in the afternoon hours than in the morning hours. This can be attributed to the more atmospheric turbidity and Railey scattering [24] in morning hours as compared to afternoon hours.
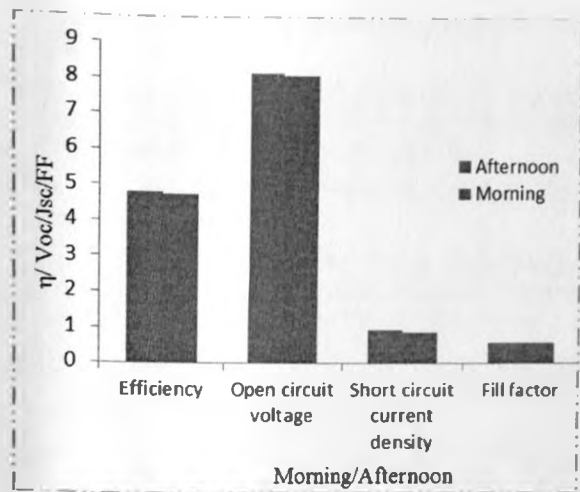
Fig. 6. A chart showing the comparative performance of the module in the morning and in the afternoon.

4. Conclusion

The effect of air mass on the performance of a dye-sensitized solar module has been investigated in a tropical area, 1.28° South and 35.82° East, Nairobi, Kenya. The results show better relative efficiencies for the module at higher air mass. V_{oc} and J_{sc} decreased with increase in air mass. An overall improved performance for the DSSC module was observed in the afternoon hours than in the morning hours. Tuning of DSSCs for use in the tropics may benefit from these finding. The design of energy efficient building facades for the temperate tropics also stands to benefit immensely from these findings.

References

[1] O'Regan, B. and Grätzel, M., (1991). A low cost, high efficiency solar cell based on dye sensitised colloidal TiO$_2$ films. Nature, 353, p. 737 - 739.

[2] Yum, J., Baranoff, E., Wenger, S., Nazeeruddin, Md. and Grätzel, M., (2010). Panchromatic engineering for dye sensitized solar cells. Energy and Environmental Science. 4 p. 842.

[3] Han, L., Islam, A., Chen, H., Malapaka, C., Chiranjeevi, B., Zhang, S., Yang, X. and Yanagida, M., (2012). High efficiency dye sensitized solar cell with a novel co-adsorbent. Energy and Environmental Science,

[4] Yu, Q., Yu, C., Guo, F., Wang, J., Jioa, S., Gao, S., Li, H. and Zhao, L., (2012). A stable and efficient quasi-solid-state dye-sensitized solar cell with a low molecular weight organic gelator. Energy and Environmental Science, DOI: 10.1039/c2ee03128k. p. 1-5.

[5] Qingjiang, Y., Cuiling, Y., Fengyun, G., Jinzhong, W., Shujie, J., Shiyong, G., Hongtao, L. and Liancheng, Z., (2012). Astable and efficient quasi-solid-state dye-sensitized solar cell with a low molecular weight organic

[6] Wafula, H., (2007). Effects of nitration on pressed TiO2photoelectrodes for dye-sensitized solar cells. M.Sc. thesis for the Department of Physics, University of Nairobi.

[7] Waita, S., (2008). Dye-sensitized solar cells fabricated from obliquely sputtered nanoporous TiO$_2$ thin films: characterization, electron transport and lifetime studies. Ph.D thesis for the Department of Physics, University of Nairobi.

[8] Kahuthu, S., (2008). Theoretical approach to the transport phenomenon of photo injected electrons in dye-sensitized solar cells. M.Sc. thesis for the University of Nairobi.

[9] Olwendo, J., (2008). A theoretical approach to studies of temperature effect on mobility of photo injected electrons in dye-sensitized solar cells. M.Sc. thesis for the Department of Physics, University of Nairobi.

[10]   Ajuoga, P., (2009). Effects of concentration on dopant states in photo activity in Niobium doped TiO2. M.Sc. thesis for the Department of Physics, University of Nairobi.

[11]   Ogacho, A., (2010). A study of TiO$_2$ dye-sensitized solar cells with a hole transport material. Ph.D thesis for the Department of Physics, University of Nairobi.

[12]   Simiyu, J., (2010). Characterization of Anthocyanin Dyes and Investigation of Charge Transport in TiO$_2$ Dye Sensitized Solar Cells. Ph.D. thesis for the University of Nairobi, p. 1 - 137.

[13]   Ozuomba, J., Ekpunobi, A. and Ekwo, P., (2011). The photovoltaic performance of dye-sensitized solar cell based on Chlorin local dye. Chalcogenide Letters. 8 (3), p. 155 - 161.

[14]   Law, M., Green, L., Johnson, J. Saykally, R. and Yang, P., (2005). Nanowire dye-sensitized solar cells. Nature Materilas, 4 (6) p. 455 - 459.

[15]   Otakwa, R. V. M., Simiyu, J., Waita, S. M. and Mwabora, J. M., (2012). Application of dye-sensitized solar cell technology in the tropics: Effects of radiation intensity and temperature on DSSC performance. International Journal of Advanced Renewable Energy Research (IJARER), 1 (2), p. 17 - 25.

[16]   Bakas, I., (2011). Solar energy/photovoltaics. In solar energy and housing - Corpus. Copenhagen Resource Institute (CRI), p. 1 - 6.

[17]   Bisquert, J., Cahen, D., Hodes, G., Rühle, S. and Zaban, A., (2004). Physical chemical principles of photovoltaic conversion with nanopartuculate, mesoporous dye-sensitized solar cells. Journal of Physical Chemistry, 108, p. 8106 - 8118.

[18]   Louche, A., Maurel, M., Simonnot, G., Peri, G. and Iqbal, M., (2000). Determination of □ngstr□m's turbidity coefficient from direct total solar irradiance

measurements. Laboratoired'Hélioénergétique. p. 1622 - 1630.

[19]   Iqba, M., (1987). Determination of Ångström's turbidity coefficient from direct total solar irradiance measurements. Solar Energy, 38, p. 89 - 96.

[20]   Young, A., (1994). Air mass and refraction. Applied optics. 33, p. 1108 - 1110.

[21]   Heinemann, D., (2000). Energy meteorology. In lecture notes for the postgraduate programme 'Renewable Energy'. Carl Von Ossietzky Universitat, p. 1 - 102.

[22]   Chambers, P., (1999). Teaching Pythagoras' theorem. In mathematics in school, The Mathematical Association, Leicester, 28 (4), p. 22 - 24.

[23]   Wenham, S., Green, M., Watt, M. and Corkish, R., (2007). Applied photovoltaics. T J International Ltd., p. 6.

[24]   Kasten, F. and Young, A., (1989). Revised optical air mass tables and approximation formula. Applied Optics, 28 (22), p. 4735 - 4738.

[25]   Kalagnan, G. and Kang, Y., (2006). A review on mass transport in dye-sensitized solar cells. Journal of Photochemistry and Photobiology C: Photochemistry Reviews, 7, p. 17 - 22.

[26]   Thavasi, V., Renugopalakrishnan, V., Jose, R. and Ramakrishna, S., (2009). Controlled electron injection and transport in material interfaces in dye-sensitized solar cells. Materials Science and Engineering: Reports, 63, p. 81 - 99.

[27]   Hedegus, S. and Shafarman, N., (2004). Thin film solar cells: Device Measurement and Analysis. Progress in Photovoltaic Research and Application, 12, 155-176.

[28]   Meinel, A. and Meinel, M., (1976). Applied solar energy. Addison Wesley Publishing Company,